Lisa Maria Mitterhuber, BSc

Structure function based evaluation of the thermal behavior of an LED

MASTER'S THESIS

to achieve the university degree of

Diplom-Ingenieurin

Master's degree programme: Technical Physics

submitted to

Graz University of Technology

Supervisor

O. Univ.-Prof. Ph. D. Peter Hadley

Institute of Solid State Physics

Graz, October 2015

In Kooperation mit:

Name des Firmenpartners

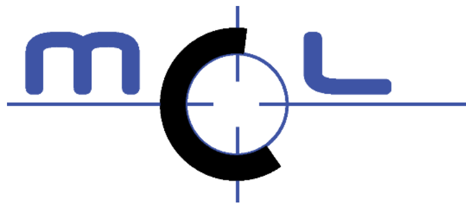

Der österreichischen Bundesregierung (insbesondere dem Bundesministerium für Verkehr, Innovation) vertreten durch die Österreichische Forschungsförderungsgesellschaft mbH (FFG wird für die Förderung im Rahmen des „4. Ausschreibung Produktion der Zukunft nat. Projekte“ Förderprogramms (Projektnummer: 843681, Projektname: TheLED) herzlich gedankt.

AFFIDAVIT

I declare that I have authored this thesis independently, that I have not used other than the declared sources/resources, and that I have explicitly indicated all material which has been quoted either literally or by content from the sources used. The text document uploaded to TUGRAZonline is identical to the present master‘s thesis dissertation.

______________________ ______________________

Date Signature

Abstract

Thermal management is one of the most important bottlenecks in LED lighting systems. Light output, light quality, lifetime and reliability are strongly related to thermal characteristics of LEDs. The heat as an unavoidable product of the LED's junction influences the performance of all its components. In order to ensure a good performance and reliability, it is essential to manage the heat generated by the device. Therefore the thermal characterization of a device is an important subject for LED testing. The JEDEC 51 standard offers a new in-situ and non-destructive method for the measurement of the thermal characteristic. The thermal characteristic is represented as a structure function which is extremely useful in the evaluation of the thermal behavior of LEDs. The structure function can be seen as a heat flow map of each layer beginning from the junction to the ambient. The structure function represents the 3D thermal distribution by a 1D $R_{th}C_{th}$ ladder model. This simplification offers an easier understanding of the heat flow path within the LED package. It contains detailed thermal information of each layer.

This master thesis deals with this type of thermal analysis. It is intended to create deeper understanding of the structure function. This is realized on the one hand by describing the mathematical path obtaining the structure function and on the other hand by discussing its containing information. The interpretation of the structure function can be done with the help of experiments and simulations. The principle of the interpretation is the development of a "validation-flow". In the "validation-flow" the simulated structure function will be adjusted iteratively to the measured one. This reverse engineering approach allows a verification of the thermal model against the real device. The result permits an interpretation of the structure function and furthermore it brings transparency to the thermal behavior of the structure of an LED.

Kurzfassung

Das Wärmemanagement in LED-Beleuchtungssystemen gewinnt immer mehr an Bedeutung, da Lichtausbeute, Lichtqualität, Lebensdauer und Zuverlässigkeit der LED entscheidend mit den thermischen Eigenschaften der LED zusammenhängen. Neben Licht erzeugt eine LED als unerwünschtes Nebenprodukt Wärme. Der Einfluss der Wärme wirkt sich dabei erheblich auf die Leistungsfähigkeit der LED aus. Aus diesem Grund ist es sehr wichtig, ein besseres Verständnis über die generierte Wärme zu erlangen. Dahingehend liefert eine thermische Charakterisierung der LED Einsicht. Ein Standard dieser Wärmecharakterisierung bietet die Serie des JEDEC 51- Standards. Dieser beschreibt eine neue Messmethode, die ein in-situ und zerstörfreies Messen erlaubt. Das Resultat der Wärmecharakterisierung wird in Form einer Strukturkurve dargestellt. Die Strukturkurve erweist sich als sehr nützlich für Auswertungen des thermischen Verhaltens der LED und bietet zudem eine bessere Einsicht in das Verhalten des Wärmeflusses in der LED. Die Strukturkurve beginnt bei der aktiven Schicht der LED und endet im Kühlkörper – sie stellt sozusagen eine Karte des Wärmepfades dar. Dieser Wärmepfad wird dabei als thermisches Netzwerk, das aus thermischen Widerständen R_{th} und thermischen Kapazitäten C_{th} besteht, beschrieben. Diese vereinfachte Darstellung beinhaltet nicht nur Informationen über den strukturellen Aufbau der LED, sondern bietet auch ein besseres Verständnis hinsichtlich des Wärmeflusses in der LED.

Diese wissenschaftliche Arbeit beschäftigt sich mit dieser Art der thermischen Analyse. Sie soll einen tieferen Einblick und Verständnis in den Aufbau der Strukturfunktion gewähren. Einerseits wird dies durch eine Beschreibung des mathematischen Weges – ausgehend von der Messung bis hin zu der Strukturkurve – realisiert, andererseits auch durch die Diskussion der Informationen, die die Strukturkurve beinhaltet, näher gebracht. Das Prinzip, auf das die Interpretation der Strukturkurve beruht, erfolgt hierbei mithilfe der Entwicklung eines „Validationflows“, bei dem Experiment und Struktursimulation in einem Reverse Engineering - Ansatz zu einem intrinsisch validierten Kalibrationsmodell führen.

Table of Content

Abstract I

Kurzfassung II

1 Introduction 1

2 Compact model theory 2

2.1 Thermal management 2

2.2 Reliability and lifetime of LEDs 3

2.3 Structure function 5

2.3.1 Thermal resistance 5

2.3.2 Thermal transfer 6

2.3.3 Thermal transient 10

2.3.4 Structure function 11

3 Measurement 16

3.1 Measurement setup 16

3.1.1 Temperature controlled environment 16

3.1.2 Power switching unit 18

3.1.3 Measurement unit 19

3.2 Temperature sensing 20

3.2.1 Temperature calibration 20

3.2.2 Measurement of temperature calibration and thermal transient 23

3.3 Electrical transient 27

4 Evaluation of the structure function 30

4.1 Introduction 30

4.2 Short overview of the calculation steps 31

4.3 Thermal impedance Curves - $Z_{th}(t)$ 32

4.4 Time constant spectrum 33

4.5 **N**etwork **I**dentification by **D**econvolution – method (NID-method) 36

4.5.1 Deconvolution 40

4.5.2 Discretization 44

4.6 Foster network 46

4.7 Cauer network 47

4.8 Foster to Cauer transformation 48
4.8.1 Fraction decomposition 49
4.8.2 Fast algorithm 50
4.9 Structure function 52
4.9.1 Computational effects 54
5 Simulation 60
5.1 Overview about FloTHERM 60
5.2 Geometries and Material parameters 61
5.3 Process of simulation 68
6 Calibrated system 70
6.1 Validation Flow 70
6.1.1 Experimental structure function 71
6.1.2 Simulated structure function 72
6.1.3 Correlation between measured and simulated structure function 73
6.1.4 Electrical transient correction based on the simulation 79
6.2 Results of the validation flow 81
7 Summary 83
8 References 85
9 Table of Figures 88
10 List of tables 92

1 Introduction

LEDs become more and more popular in lighting applications. They provide significant energy savings and a long lifetime (more than 50.000 hours). However, this can only be guaranteed when drive currents and operating temperatures are kept within certain limits. Every year the density of chips per area is increasing as well as the light output per chips. These progressions lead to higher temperatures in the devices and, as a consequence, produce a reliability loss. The challenge is to arrange the requirement of more reliability and long lifetime with the industry's progress. This leads to an increasing importance of the thermal management of LEDs. A key issue of the thermal management is the ability to obtain temperature data under operating conditions, so there is also a need for thermal testing. A good solution of thermal testing is the measurement of the thermal transient. This measurement contains information about the thermal characteristic (heat flow path) of the investigated device. The thermal transient is often hard to interpret but it serves as base of further evaluations. It can be converted into the so-called **structure function**. This function can be used as thermal characterization and thermal evaluation of the LED system. It describes the heat flow path like a map of the LED's structure.

Subsequently, the structure function will be discussed as a thermal analysis method – starting with the thermal transient measurement. The computation from the thermal transient to the structure function will also be considered more closely. With the help of experiments and simulations the structure function can be interpreted and hence a calibrated model of an LED module can be developed.

This thesis is structured in five chapters. The first chapter is an introduction of the thermal analysis of LED systems. The thermal dynamics and its opportunities of interpretation and further processing are discussed. Furthermore the main concept of thermal systems is analyzed and therefore the basic idea of the structure function is explained. In the second chapter, the measurement of the thermal transient and its setup are described. The third chapter is a summary of the theory of the calculation process of the structure function resulting from the thermal transient. Different methodologies of the calculation steps are discussed with their pros and cons. The fourth chapter presents another way of obtaining the thermal transient of one LED module. The thermal transient is simulated with the aid of a **C**omputational **F**luid **D**ynamics (**CFD**) software. Finally, the last chapter deals with a validation flow, where the measured and simulated thermal transients are compared to each other. This comparison offers the opportunity to develop a calibrated LED system. The calibrated system allows a better interpretation of the structure function.

2 Compact model theory

2.1 Thermal management

Nowadays light emitting diodes (LEDs) are highly energy-efficient light sources, where 2/3 of energy is converted into light. Only 1/3 of the energy is wasted and finally transferred into heat. The dissipative power (heat) is an unavoidable product of any electronic device. Therefore, the thermal management of LED systems is and will remain one of the most important bottlenecks. Thermal management is the effort to ensure that the generated heat is removed to minimize LED temperature and in order to maximize the LED's performance and lifetime [1].

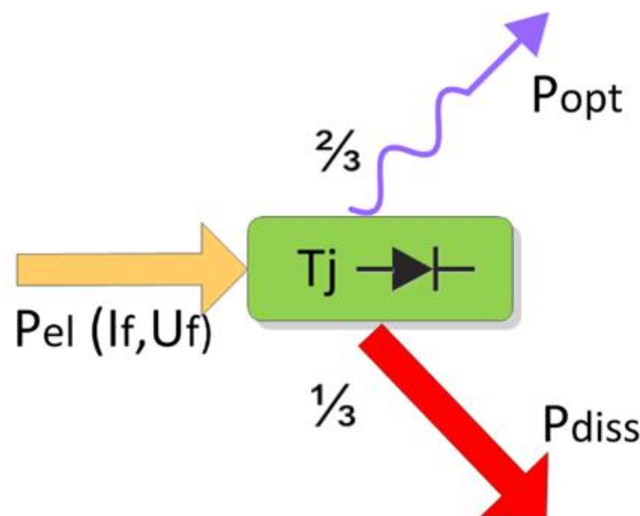

Figure 1: The electric energy (P_{el}) in a light emitting diode, which is a function of the induced current (I_f) and voltage (U_f), becomes rather heat (P_{diss}) than light (P_{opt})

In the thermal analysis of LEDs, the junction temperature T_j is an important parameter – it is the temperature of LED's active layer. The higher the junction temperature, the higher the reliability loss will be. In the LED's active layer, carrier injection and photon emission occur and thus directly affect LED's efficiency, reliability and lifetime. Regarding this, the measurement of the junction temperature is really important. An accurate value of the junction temperature can be determined, if its measurement is performed under working conditions, where the heat is dissipated. This creates difficulties as the LED chips are well protected in the package. Going around these difficulties, the industry has introduced a monitor point at the package. The thermal resistance from the junction to the reference point is given as critical device parameter. Since the temperature of this monitor point is measured, the junction temperature can be indirectly obtained. However, this is still an estimation and not accurate enough. Therefore a new method is introduced which offers a better monitoring of the junction temperature (see chapter 3). Within this new method, the recorded temperature can be additionally used to determine the thermal characteristic of a device enabling predictions about the reliability of the LED. The thermal analysis contains information not only about the allowed limits of the applied current and the environmental temperature,

but also about the “thermal” contribution of each layer in the device. This knowledge can help manage the heat and also to prevent failures in the device. Therefore thermal management becomes more and more an integral part of the system design of an LED-based lighting solution [2].

2.2 Reliability and lifetime of LEDs

There is only scarce information of the reliability and lifetime of LEDs. Customers are interested in the estimation of the duration of the life time. More knowledge about LEDs’ reliability and lifetime would reduce the barrier to the acceptance of this lighting alternative in traditional applications [1]. The reliability of a device is the property that states how the function assigned to the product is fulfilled within a certain period of time. If the device can no longer fulfill its functionality, there must be a failure. One failure criterion of LEDs is the L70 criterion. If there is a 30% reduction in lumens at room temperature, the time up to 70% light degradation is the lifetime of an LED light source.[2]

The reliability and lifetime of LEDs are dependent on various factors similar to other conventional lighting. The failures can be classified into extrinsic and intrinsic causes. Extrinsic failures are early, random and spontaneous failures [3]. They are generated by defective materials, poor assembly and deviations in the manufacturing process, but also by incorrect handling and operations by the customer like too high current. Extrinsic failures can be avoided by controlling the environmental conditions and improvement of the manufacturing process. Intrinsic failures occur at the end of the product cycle. Reducing these failures requires a full understanding of the cause of failures. This is challenging since the root of the failures cannot be seen clearly. The LED changes continuously over the whole operating time and there are correlations between different failures. Chang et al. have published a table summarizing the relationships between failure sites and their causes, effects, modes and mechanisms of LEDs (compare Table 1).

Table 1: Failure sites, causes, effects, modes and mechanisms of LEDs [2]

Failure Site	Failure Cause	Effect on Device	Failure Mode	Failure Mechanism
Semiconductor (Die)	• High Current–Induced Joule Heating	Thermomechanical Stress	Lumen Degradation, Increase in Reverse Leakage Current, Increase in Parasitic Series Resistance	Defect and Dislocation Generation and Movement
	• High Current–Induced Joule Heating • High Ambient Temperature • Poor Sawing and Grinding Process	Thermomechanical Stress	Lumen Degradation	Die Cracking
	• Poor Fabrication Process of p-n Junction • High Current–Induced Joule Heating • High Ambient Temperature	Thermal Stress	Lumen Degradation, Increase in Series Resistance and/or Forward Current	Dopant Diffusion
	• High Drive Current or High Current Density	Electrical Overstress	No Light, Short Circuit	Electromigration
Interconnects (Bond Wire, Ball, and Attachment)	• High Drive Current/ High Peak Transient Current	Electrical Overstress	No Light, Open Circuit	Electrical Overstress-Induced Bond Wire Fracture
	• Thermal Cycling Induced Deformation • Mismatch in Material Properties (e.g., CTEs, Young's Modulus)	Thermomechanical Stress	No Light, Open Circuit	Wire Ball Bond Fatigue
	• Moisture Ingress	Hygro-mechanical Stress		
	• High Drive Current or High Pulsed / Transient Current	Electrical Overstress	Lumen Degradation, Increase in Parasitic Series Resistance, Short Circuit	Electrical Contact Metallurgical Interdiffusion
	• High Temperature	Thermal Stress		
	• Poor Material Properties (e.g., poor thermal conductivity of substrate)	Thermal Resistance Increase	No Light, Open Circuit	Electrostatic Discharge
	• High Voltage (Reverse Biased Pulse)	Electrical Overstress		
Package (Encapsulant, Lens, Lead Frame, and Case)	• High Current–Induced Joule Heating • High Ambient Temperature	Electrical Overstress	Lumen Degradation	Carbonization of the Encapsulant
	• Mismatch in Material Properties (CTEs and CMEs) • Interface Contamination	Thermomechanical Stress	Lumen Degradation	Delamination
	• Moisture Ingress	Hygro-mechanical Stress		
	• Prolonged Exposure to UV	Photodegradation	Lumen Degradation, Color Change, Discoloration of the Encapsulant	Encapsulant Yellowing
	• High Drive Current Induced Joule Heating • High Ambient Temperature • Presence of Phosphor	Thermal Stress		
	• High Ambient Temperature • Poor Thermal Design	Thermomechanical Stress	Lumen Degradation	Lens Cracking
	• Moisture Ingress	Hygro-mechanical Stress		
	• High Current–Induced Joule Heating • High Ambient Temperature	Thermal Stress	Lumen Degradation, Broadening of Spectrum (Color Change)	Phosphor Thermal Quenching
	• Mismatch in Material Properties / Thermal Cycling Induced High Temperature Gradient	Mechanical Stress Cyclic Creep and Stress Relaxation Fracture of Brittle Intermetallic Compounds	Lumen Degradation, Forward Voltage Increase	Solder Joint Fatigue

Regarding this table, the most important physical influencing factors (failure cause) are temperature, humidity and current. E.g. an increase of the ambient temperature as well as an increase of the applied current results in an increase of the junction temperature and this leads to a decrease in lifetime. Generally, reliability of LEDs is strongly affected by thermal effects and it can be used as a predictor of LED life [2]. The higher the operating temperature, the shorter the LED-life will be. In this case, the thermal design of LEDs and hence the reduction of temperature within the LED package are gaining more and more importance for avoiding heat from harming the device [4].

2.3 Structure function

One method of laboratory testing of the thermal properties of an LED in reliability analysis and in quality assurance offers the representation of the heat flow path, the so-called **structure function**. The structure function provides a map of cumulative thermal capacitances of the heat flow path with respect to thermal resistances, starting from junction to the ambient. All essential structural changes in the LED are reflected in the structure function.

2.3.1 Thermal resistance

The reduction and control of the junction temperature of LEDs are an important issue in the thermal management. Beside the junction temperature there is another important parameter which describes the device's performance – "the junction-to-ambient thermal resistance" [5]. The junction temperature can be estimated with the aid of thermal resistance. It is a measure of the capability of the whole device to dissipate heat. This thermal resistance R_{thJX} is defined as

$$R_{thJX} = \frac{\mathrm{T_J} - T_X}{P_H} \tag{1}$$

where all the heating power from the driving point J (in case of LEDs: it's the junction) flows through an isothermal surface in the measurement arrangement X. $\mathrm{T_J}$ refers to the isothermal temperature of the hottest point, the junction through which all of the internally generated heat is dissipated. T_X is the temperature of the reference environment – it can be seen as the "cold" isothermal surface [1]. There is a requirement that all of the heat stays constant in each surface (isothermal surfaces). These isothermal surfaces experience heat flow in a perpendicular direction. The unit of R_{thJX} is °C/W. The thermal resistance provides a simple and convenient means of the junction temperature. It is used to thermally characterize the whole device behavior. The thermal resistance should be as low as possible since the junction temperature is proportional to it.

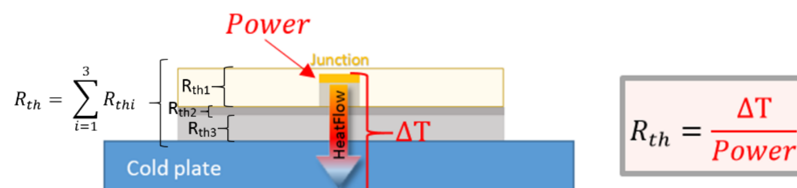

Figure 2: Schematic drawing of thermal resistance

However, this value doesn't include any information about the thermal dynamics of the component and about the contribution of the different components of the device. Neither will

it also predict the performance in an application-specific environment. The importance of the knowledge of the dynamic behavior – the internal heat flow - arises which consequently offers an insight in the internal construction of the LED [5].

2.3.2 Thermal transfer

There are different kinds of heat transfer mechanisms: conduction, convection and radiation. The *conduction* is the thermal energy transfer through a solid mass as a result of collision of molecules from one molecule to its neighbors. The *convection* is the heat transfer through the movement of fluids and gases. Radiation is the heat which is transferred through an electromagnetic field. The most important heat transfer mechanism is the conduction, if the evolution of the temperature of a given solid is considered as the point of interest. The *radiation* does not have a large effect on the thermal management within an LED package as the surface areas are relatively small. The convection is also incidental as it refers to the transfer of heat from the heat sink to the surrounding air [6].

Considering the evolution of the temperature of a given solid, the important heat transfer mechanism is the conduction. The idealized heat flow in an LED is a single path heat flow conducting from the junction area through the chip, through the package and at the end into the ambient of the device. There are many ways to improve the thermal management of LED. In order to ensure that the aspired results for heat dissipation are achieved, the correct type of thermally conductive material has to be chosen. A fast heat loss as well as a reduction of the thermal resistance are desired. The basis of the conduction can be described by the Fourier's law of heat conduction:

$$\frac{dQ}{dt} = -\lambda A \frac{dT}{dx} \tag{2}$$

The equation (2) states that the rate of heat flow ($\frac{dQ}{dt}$) through a homogeneous solid in direction normal to the surface is directly proportional to the area A of the surface and to the temperature difference along the path of heat flow ($\frac{dT}{dx}$). The proportionality ration λ is the thermal conductivity. λ is a physical property which is a measure of the material's ability to conduct heat [7].

$$\frac{dQ}{dt} = \quad = -\lambda A \frac{dT}{dx}$$

Figure 3: Graphical representation of Fourier's law

Figure 3 represents a steady state conduction where the temperature differences within the material are constant. After an equilibrium time the spatial temperature distribution in the material will not change anymore. That means that the temperature is only dependent on the position and not on the time. An important property of the steady state conduction is that the heat transfer of a system can be described by a thermal network using thermal equivalent circuits. It is based on the thermal-electrical analogy. All the laws of the current electrical conduction can be applied to "heat currents". *Table 2: Thermal- electrical analogy* summarizes part of the analogy that will be helpful in understanding the thermal component model.

Table 2: Thermal- electrical analogy

Thermal			**Electrical**		
Parameter	Symbol	Units	**Parameter**	Symbol	Units
Temperature	T	K	Voltage	V	V
Heat Flow	$\dot{Q}$	W	Current	I	A
Thermal resistance	R_{th}	K/W	Electrical resistance	R_{el}	Ω = V/A
Stored Heat	Q	J = Ws	Stored Charge	Q	C = As
Thermal capacitance	C_{th}	J/K	Electrical capacitance	C_{el}	F = C/V

The thermal-electrical analogy contains the analogy between voltage and temperature, current and heat conduction. In such a case it is possible to take the thermal resistance as an equivalent to the electrical resistance (see Figure 4). Since electrical resistance is the voltage drop between two points divided by the electrical flowing current, the thermal resistance can be regarded as the temperature drop divided by the heat dissipation (see eq. (1)). The heat conduction can be compared with Ohm's Law (see Table 2) for current flow $I = \frac{1}{R}(V_1 - V_2)$. Due to this thermal-electrical analogy the thermal resistance can be defined as $R_{th} = \frac{dx}{\lambda A}$.

Regarding the figure below, a steady state thermal system can be modelled by networks of such thermal resistance.

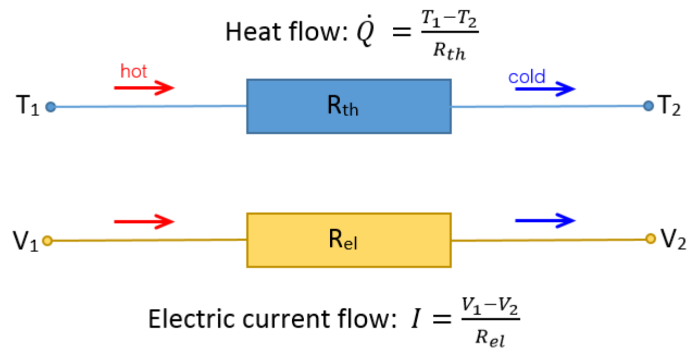

Figure 4: Analogy between thermal and electrical resistance

However, the temperature of a body varies not only with position, but also with time. In the case before, heat conduction under steady conditions was considered. The temperature at any point of the material does not change with time. Now a new dependency will be introduced – the time-temperature dependency. That means that there is a temperature change in time at any point of a body. This kind of thermal energy flow is termed transient conduction.

This transient conduction can be seen when a component makes a thermal transition from one equilibrium to another equilibrium, for example when a new perturbation of temperature happens. This perturbation starts at the time t = 0 and it is also the start of the heat transfer between the material and the new equilibrium. The total amount of heat transfer between the body and the environment can be described. It is simply the change in the energy content of the material: $\Delta T \cdot C_{th} = P \cdot t = Q$. So you can see the presence of thermal capacitances. The thermal capacitance formulates the ratio of change in heat energy of unit mass to the change in temperature. The body of the component has to be thermally "charged" for a temperature change. The thermal capacitance can be compared with the electrical capacitance. This can be expressed as the quantity of the charge equation $V \cdot C = I \cdot t$. This "charging" via conduction needs time. The total heat flow across the two isothermal surfaces stays constant, when calculating the thermal resistance (see eq. (1)). This requirement can only be true, if the thermal capacitance between the two surfaces has reached an equilibrium. Equilibrium means that there is no "charging" anymore. The greater the thermal capacitance of the component, the longer the duration of the period to get equilibrium will be [1].

Supposing that a power step is being applied at the top surface of a homogenous ideal rod. The power is uniformly distributed along the surface. The rod consists of one material with adiabatic surfaces and is surrounded by an ambient temperature (see Figure 5). The thermal power source will deliver a certain amount of heat. The heat will be distributed through the entire body up to a thermal equilibrium. Regarding the lower part of Figure 5, the homogenous rod can be simplified as a one-stage RC network. This is a simple approximation of a thermal

model. It begins with the driving point meaning that both heating and measuring of the temperature changes take place in this point. The capacitance has to be grounded to one side because the temperature difference in the energy storage is the temperature difference measured from the ambient.

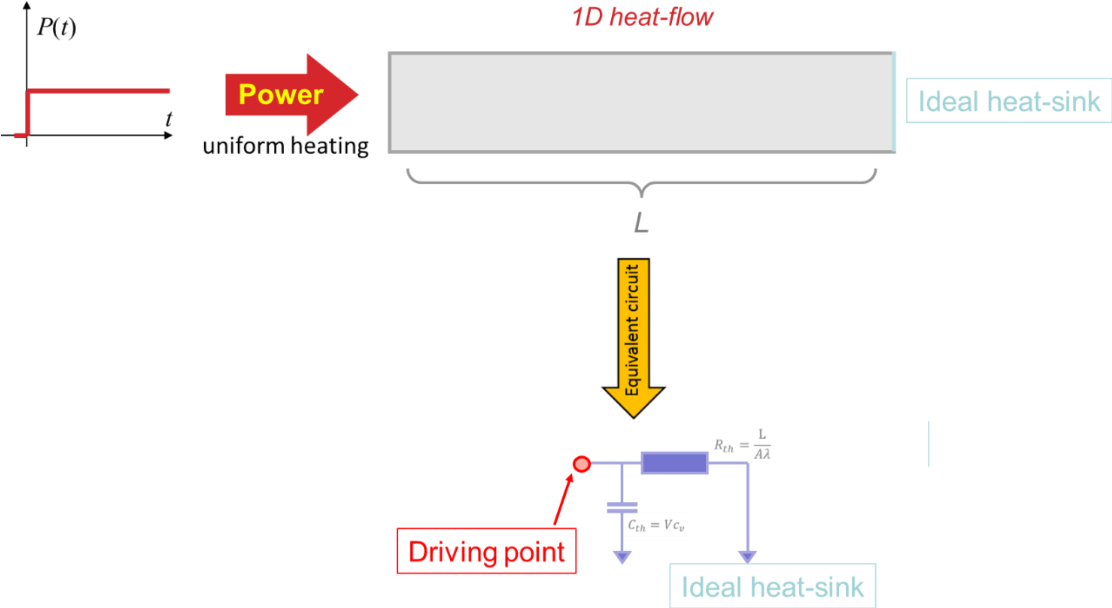

Figure 5: Thermal model of a homogenous rod a length of L, a thermal conductivity of λ and a specific heat of c_v and its one-dimensional thermal equivalent

However, in reality no material can be considered an ideal rod. A requirement of the lumped analysis is to assume a uniform temperature distribution throughout the material. Another demand of thermal systems is that they are assumed to be linear. Linearity means that the thermal resistance and capacitance are independent of the temperature. Therefore, the thermal conductivity and heat capacity are both constant values and equally independent of the temperature. If the homogenous rod from Figure 6 will be separated into segments with the length of ΔL. The segments themselves can be regarded as an ideal rod and they have a uniform temperature distribution and are linear. These ideal segments can be simplified again by an equivalent circuit. Hence, one segment corresponds to one RC pair. Due to the serial connection of ideal segments the thermal resistance can also be connected as series. Consequently, the slicing along the heat flow path results in a ladder of lateral thermal resistances between two thermal nodes and of thermal capacitances between node and ambient. This type of network is called Cauer-typed network model. The applied method is helpful for simplifying the distributed description of the $R_{th}C_{th}$ system into a compact form. Summarizing, a one-dimensional heat path can be simplified by a lumped $R_{th}C_{th}$ network (see Figure 6) [8].

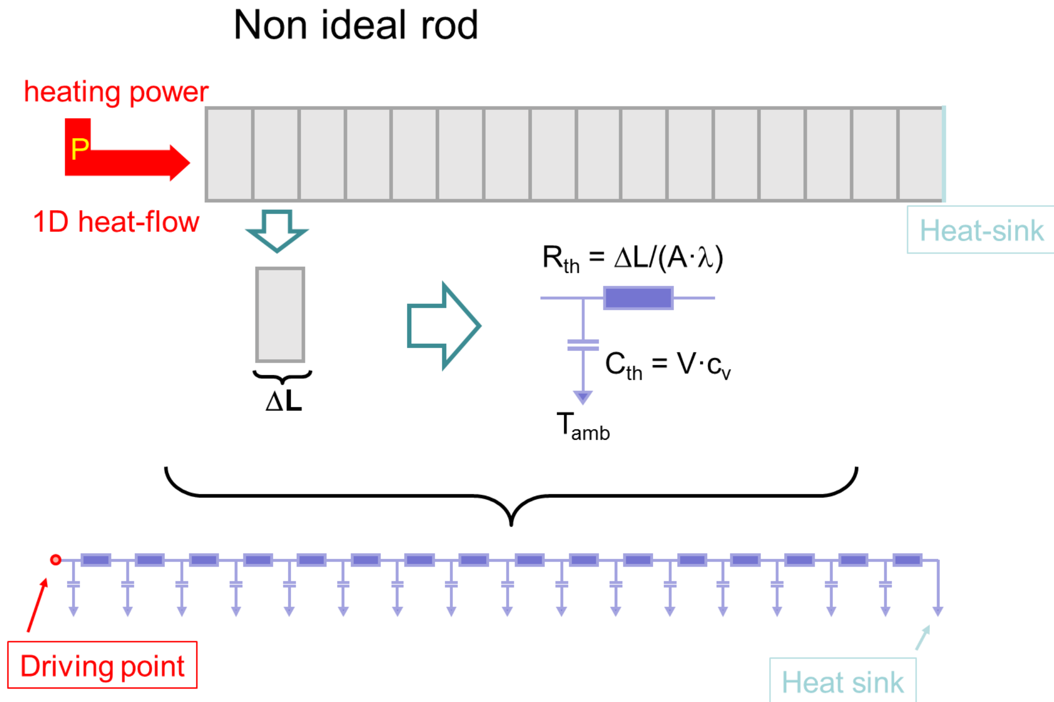

Figure 6: The RC model of the heat flow path of a sliced ideal rod

An important difference between electrical networks and thermal networks has to be mentioned. It is the fact that an electrical network can be perfectly represented by the lumped elements. In the case of a thermal network, it is just an approximation because of the distributed nature of thermal systems where the circuits are characterized by an infinite number of time-constants [9]. Based on the Fourier's law a one-dimensional heat flow with lumped $R_{th}C_{th}$-pairs is assumed. This assumption is sufficient, if the thermal networks are familiar such as the one-dimensional current flow in wires between discrete components. In other words, there has to be a serial connection of the different thermal regions. If the requirement of a one predominant heat flow path is fulfilled, the analogy can be adopted leading to a one-dimensional interpretation of a three-dimensional phenomenon.

2.3.3 Thermal transient

The thermal transient describes the temperature change during any period in time at one defined point within an object. Therefore, it can be used to characterize the dynamic thermal properties of electronic devices. The thermal transient can be obtained from both measurement and simulation (this will be described in a more detailed way in chapter 3 and 5). The standards of the thermal transient measurements for semiconductor device packages are created by the Joint Electron Device Engineering Council (JEDEC 51-series).

The thermal transient can be heating or cooling curves depending on the measurement. A heating curve shows an evolution of the increasing temperature at a constant heating current

until reaching the thermal steady state. The LED is forced from hot steady state to cool state by switching the power off at the cooling curves.

A thermal steady state means that both parameters, power dissipation and thermal environment, which are able to control the temperature, are constant for a sufficient duration – then a thermal equilibrium can be reached.

Prior to the thermal steady state there is the thermal transition [10]. It is the temperature change of the junction. At time t=0 the power step is applied to the device and at that time the temperature change ΔT is recorded. After the excitation the temperature change starts within a few microseconds and reaches an equilibrium after some hundreds or thousands of seconds (see Figure 7) [11]. The thermal transient can then be used for getting information about the heat-flow path of the LED. This function serves as a base of subsequent evaluation. On the basis of that, a good-quality transient record is needed. The noise of the measurement should be as well as possible suppressed. Moving average over the measured data points and a low-pass-filter are used to smooth the data.

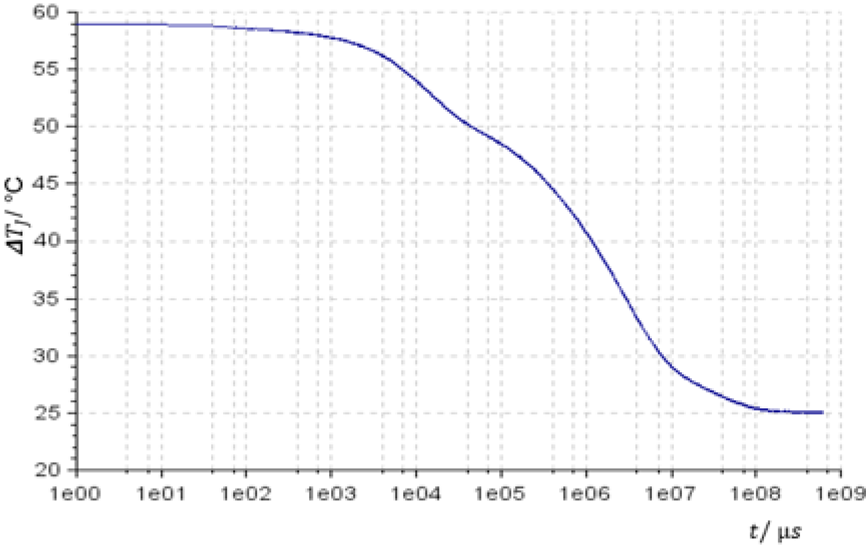

Figure 7: The cooling transient of an LED

The thermal transient can be used for getting information about the heat flow path. It is a complete thermal characterization of the investigated device.

2.3.4 Structure function

The problem regarding the thermal transient is that it is hard to interpret. It is rather difficult to see differences in the transient. Accordingly, it is better to use an alternative representation of the heat flow path: the **structure function**. From the thermal transient the structure function can be obtained by mathematical transformations. The basic idea of the structure function is to use the thermal-electrical analogy, as mentioned before, where a one-

dimensional heat flow has to be ensured. The structure function is a function of cumulative thermal resistance over the cumulative thermal capacitance. It is the cumulative sum from the first to the ith stage. The resulting $R_{th}C_{th}$ network represents the same thermal transient response for a given excitation as the real measured system [12]. The structure function provides a thermal capacitance – thermal resistance map of such heat flow paths.

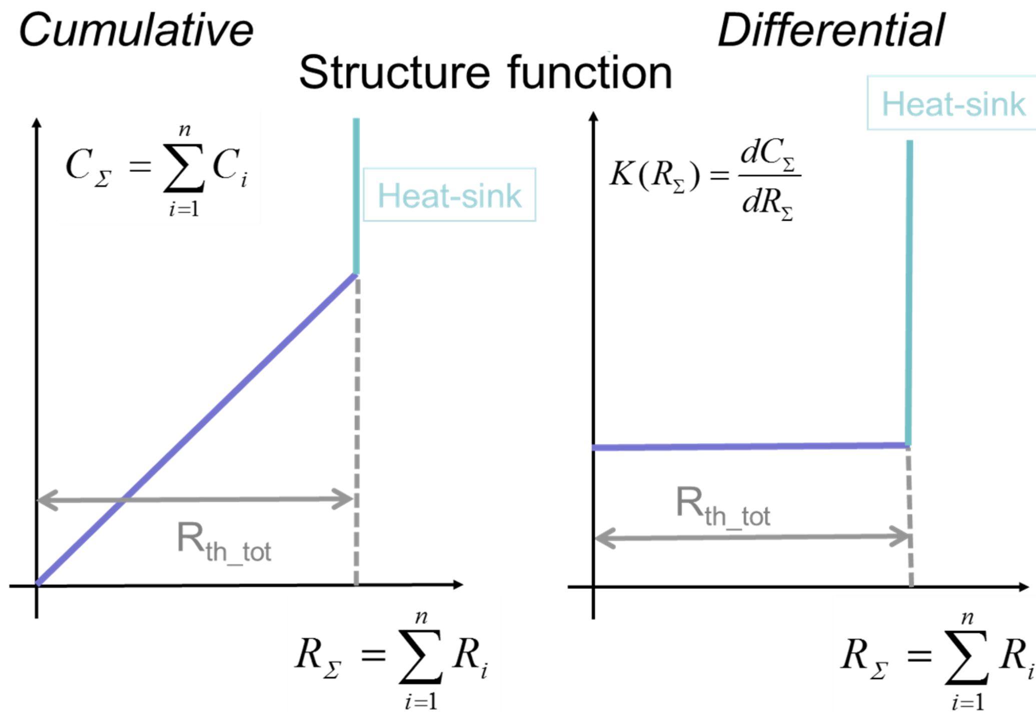

Figure 8: Cumulative and differential structure function of a homogenous rod

Considering the homogenous rod of chapter 2.3.1., where the thermal resistances and thermal capacitances do not change over the whole heat flow path, the ratio of the elementary thermal capacitances and thermal resistances in the network model will be constant. This means that the cumulative structure function of the rod will be a straight line with a constant slope. The structure function represents a function of the cumulative R_{th} over C_{th} (see Figure 8). Another representation of the structure function is the differential structure function. The differential structure function is the derivative of the cumulative structure function. As the slope of the cumulative structure function is constant, the differential structure function has the same value over the cumulative thermal resistance. The heat conduction path and so both kinds of the structure functions end in the ambient, which is characterized by infinite heat sinking capacity. Therefore, the cumulative thermal capacitance must tend to infinity. This means that the cumulative structure function should end with a singularity. This singularity corresponds to the location of the ambient. It also marks the value of the total thermal resistance of the rod.

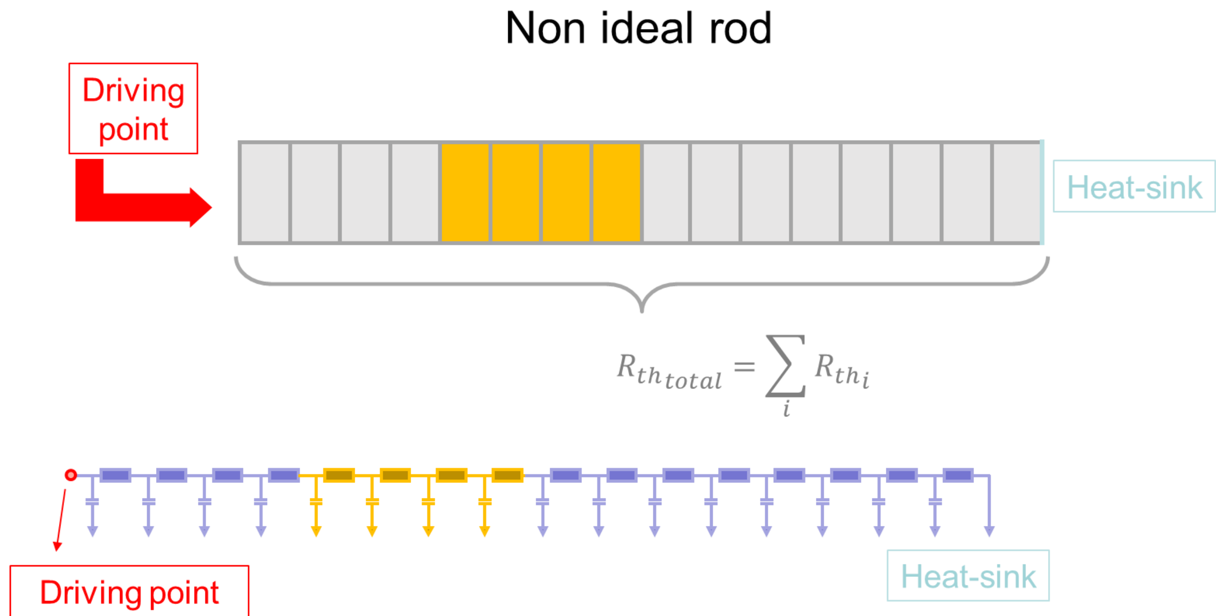

Figure 9: RC model of a non-ideal rod which consists of two types of RC pairs

However, a structure or a device that has to be investigated doesn´t consist of a single material. A rod where the R_{th} and C_{th} values vary in a given section in the middle of the road is assumed (see Figure 9: orange sections). For example the central part has a RC ratio which is twice as high as the rest of the material. The structure function of this material results in a steeper middle section in the cumulative structure function. The slope of this part has doubled. In the differential structure function this change results in a peak. The peak is twice as high as the value of the other sections (see Figure 10) [1].

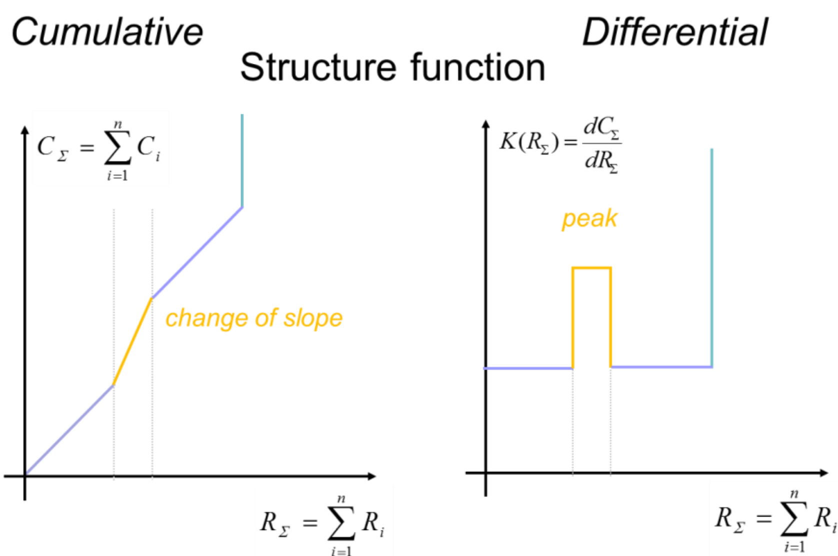

Figure 10: Cumulative and differential structure function of a two materials rod

As shown in Figure 9 and Figure 10, there is a one-to-one correspondence between the structure function and the actual structural elements of the heat flow path. So if an LED is investigated, the heat flow path of the LED can be represented with the help of its structure function. The structure function is used for getting information about the major elements of the one-dimensional heat flow path. It starts from the hottest point, the junction of LED, passes the other layers and ends up with the heat sink [10]. In such functions partial thermal resistances and capacitances in the heat flow path can be easily detected since the structure function is a graphical representation of $R_{th}C_{th}$ network of a thermal system (Figure 11) [13].

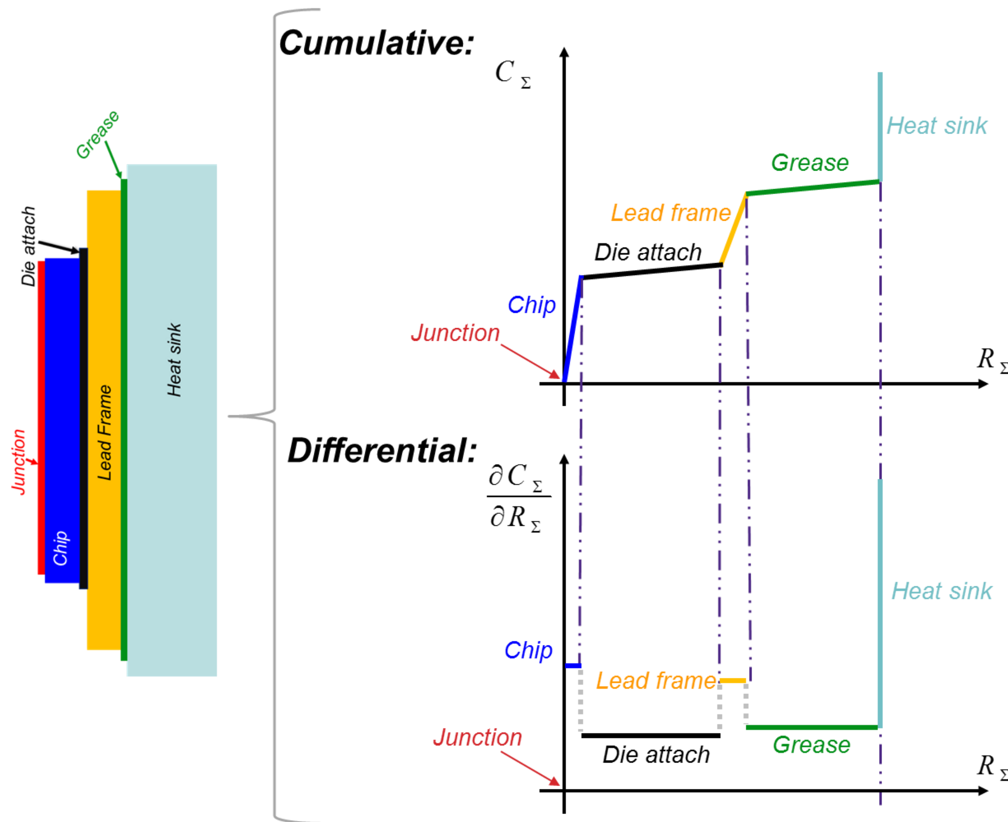

Figure 11: Schematic presentation of the structure function

As the thermal resistance of a slice/layer of the ΔL length is $R_i = dR_\Sigma = \frac{\Delta L}{\lambda A}$ and the thermal capacitance is $C_i = dC_\Sigma = Vc_v = \Delta LAc_v$, the value of the differential structure function is:

$$\frac{dC_\Sigma}{dR_\Sigma} = \frac{c_v A \, \Delta L}{\frac{\Delta L}{\lambda A}} = c_v \lambda A^2 \tag{3}$$

The value of the differential structure function is proportional to the material parameters, the specific heat c_v and the thermal conductivity λ, and to the square of the cross-sectional area

A of the heat flow. Consequently, it is related to the structure of the system and the material parameters and a change of the cross section can be directly read from the differential structure function.

The structure function evaluation of the thermal transient is a very useful method. With the aid of the structure function it is possible to interpret the inner structure of a device because it corresponds directly to the physical structure.

3 Measurement

Since 1990 JEDEC (Joint Electron Device Engineering Council), which is an industry group that develops open standardizations for the microelectronics industry, has provided a set of thermal measuring standards for semiconductor device packages – the JESD-51-xx series. It includes LED thermal testing guidelines. The repeatability of the measurement on the same device is one of the key issues of such standards [14][15].

In this thesis, the system of mentor graphics, the T3ster –the thermal transient tester, is used in which the JEDEC standard is implemented.

3.1 Measurement setup

There are four main parts of measurements: the power switching unit, the measurement unit, the temperature controlled environment and the controlling unit (see Figure 12). The power switching unit provides the step function of power. The measurement unit records the thermal transient. The controlling unit organizes the run of the measurement process and is responsible for the data processing. There the captured thermal transient is converted into a structure function. The JEDEC standard recommends specific settings to each part of the measurement setup.

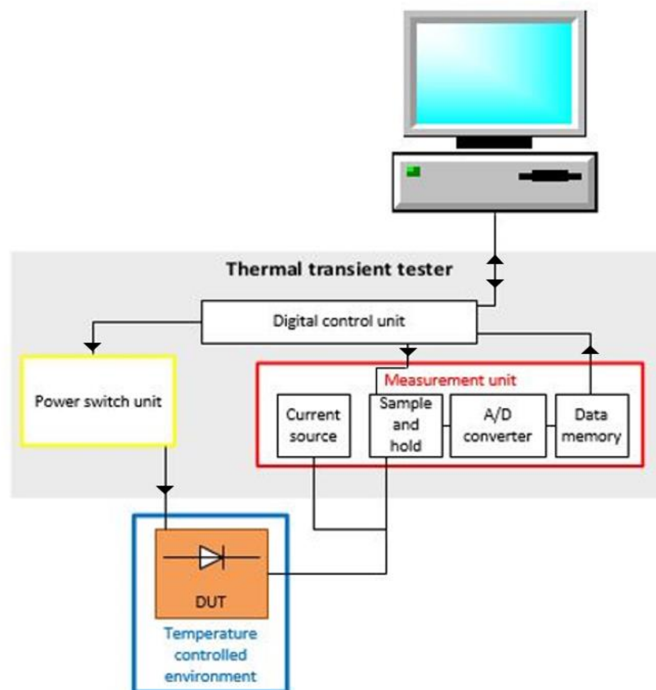

Figure 12: Diagram of the measurement setup of the DUT – device under test

3.1.1 Temperature controlled environment

A part of the JEDEC standard is the realization of repeatable boundary conditions. Therefore, the temperature controlled environment should be an active control element. It has to

maintain the thermal test environment to uniform conditions during the measurements. Another requirement is that it should provide uniform temperature in an area which is large enough to contain the tested device. The range of the provided temperature of the temperature controlled environment should be as wide as the working temperature range of LEDs [16].

For the measurement of thermal transients of LEDs a temperature controlled cold plate is recommended as thermal test environment. All the measurements are done by a liquid-cooled cold plate. The cold plate is attached under the device and for better thermal connection there a thermal paste between the device and the plate is used (see Figure 13).

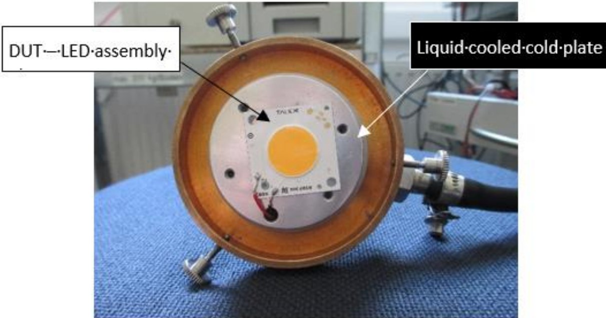

Figure 13: Actual test setup – LED on a liquid cooled cold plate

As mentioned in chapter 2.3.2, the main focus lies on the conduction. Therefore, the arrangement of the cold plate is used to guarantee a one-dimensional heat flow path from the LED's junction towards this cold plate (see Figure 14). The cold plate can be regarded as an isothermal surface. This setup provides a good approximation of the conditions of the formal definition of thermal resistance (see equation (1)) [1].

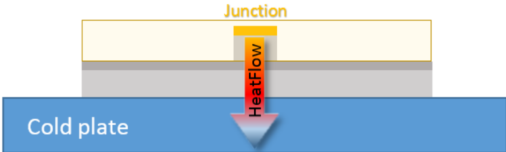

Figure 14: Illustration of the heat flow resulting from the junction of an LED

The cold plate can only remove a certain amount of heat. Problems can arise if the dissipative power of the LED is greater than that of the cooling capacity. Then, the full regulation is not achievable. Therefore, a cooling environment with a high capacity is required. In addition, the

temperature is controlled over the whole duration of the measurement and it can be stabilized above and below room temperature.

All the thermal characterization measurements of LEDs are done with the aid of a cold plate which is cooled by the refrigerated and heating circulator "Julabo –F25" (see Figure 15). The circulator has a working temperature range from -28°C to 200°C and a temperature stability of ±0.01°C. The cooling capacitance (Medium Ethanol) is 0.06 kW at -20°C and 0.26 kW at 20°C. [17]

Figure 15: Refrigerated and heating circulator – for the cold plate [17]

This temperature controlled environment is also important for the calibration of the temperature sensing in the device (see chapter 3.2.2).

3.1.2 Power switching unit

The power switching unit is suitable for switching the power on and off at the dissipative element (see Figure 16). This means that the power switching unit changes the forward current of the device. Since the thermal transient may already occur in the first 10 µs-100 µs after the power change, the transient has to be recorded by a sampling rate of microseconds at the beginning of the measurement. In addition, the switching time of the power unit has to be also less than 1 µs - 5 µs. This includes the electrical transient which will be discussed in chapter 3.3. The required power level depends on the package size.

Figure 16: T3ster Booster – power switching unit [18]

For an evaluation of the thermal impedance curve and additionally of the structure function the right value of the dissipation power has to be ensured by using a four wire sensing [1]. The electrical connection which forces the power and the wires used for sensing are separated (see Figure 17).[11]

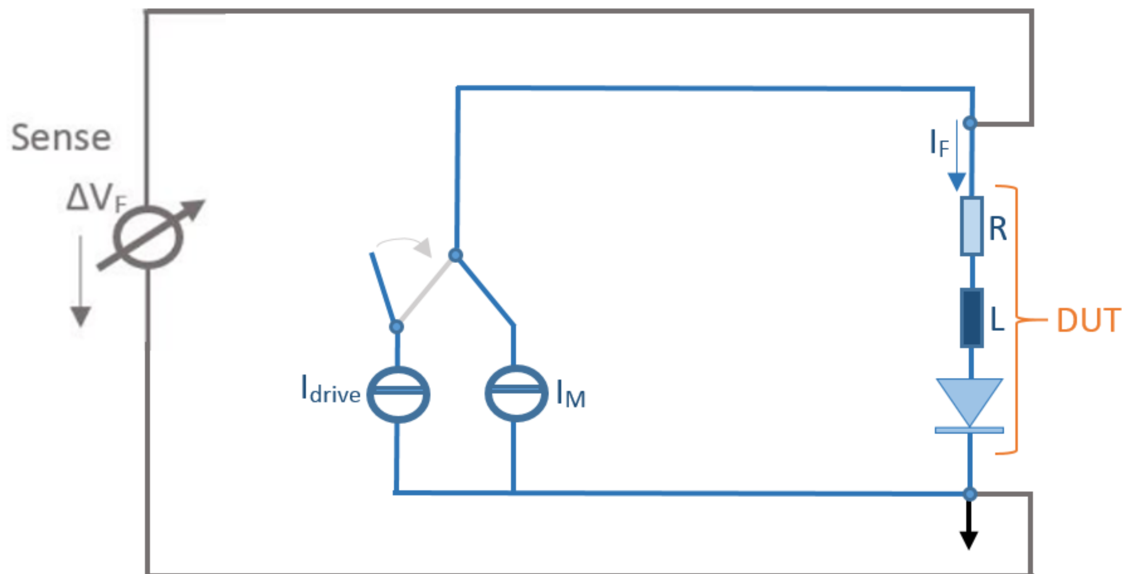

Figure 17: Measurement scheme of the thermal characterization of an LED, which is the device under test (DUT)

3.1.3 Measurement unit

The measurement unit (see Figure 18) is responsible for a constant operating point current for the sensor diode. It consists of a sample-and-hold amplifier and an analog-digital-converter. The measurement has to be as accurate as possible to get an interpretable result of the further computations.

In order to ensure an accurate measurement to get good results of the further computation, the accuracy of the temperature measurement has to be in the range between 0.1°C- 0.2°C. At the beginning of the measurement the recording has a fast sampling rate of 1 µs (sampling frequency: 1 MHz). In the time range of over 100 s there are no fast temperature changes, therefore a sampling rate of 1 s is sufficient.

In addition, the measurement unit also stores the measured data points in the local memory. After the measurement sequence the recorded data is transferred to the controlling unit where the data sets are evaluated [16].

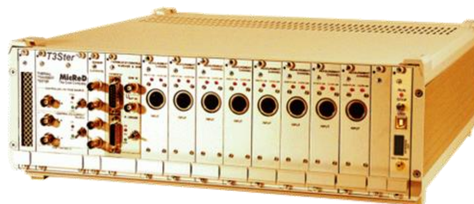

Figure 18: T3ster – measurement unit [19]

All the experiments of the thermal response use the thermal transient tester equipment (T3ster). T3ster captures the thermal transients in real time and records the cooling /heating curve. Before the LED is thermally investigated, the LED has to be thermally calibrated using temperature controlled environment and the T3ster (Details of calibration: see chapter 3.2) The analog-digital-converter in the T3ster has 12 bits resolution, that means a resolution of 25 µV in the 100 mV range. The noise does not exceed ± 1 bit.

3.2 Temperature sensing

For the thermal analysis of the LED the junction temperature has to be measured. There are also direct methods like infrared sensing. However, this method is only able to measure the junction temperature if the junction layer is on the top of the substrate [20]. If this is not the case, it is difficult to capture the junction temperature. Therefore, indirect measurements are provided like the above-mentioned electrical method, which uses only the electrical-temperature properties of the device. The junction itself is used as a temperature sensor. The measurement can be performed as a component characterization [11].

3.2.1 Temperature calibration

Before measuring anything a calibration is needed. This method is based on the intrinsic electro-thermal property – the temperature and voltage dependency featured by all semiconductor diode junctions (see Figure 19).

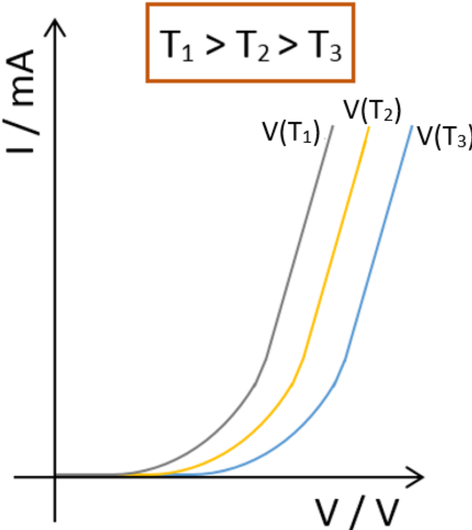

Figure 19: Diode characteristic (representation of the diode conduction equation) for different temperatures

This relationship comes from the diode conduction equation:

$$I_F = I_0\left(e^{\frac{V_F}{V_T}} - 1\right)$$

where $V_T = \frac{kT}{q}$ and $I_0 = CT^r e^{-\frac{qV_g}{kT}}$

(4)

I_F is the forward current of the diode; I_0 is the reverse bias saturation current; V_F is the forward voltage; q is the electron charge; k is the Boltzmann's constant; T is the absolute temperature; C is a constant including the density of states, the effective mass of electrons and holes, the carrier mobility, the doping concentrations, the recombination lifetime, the pn-junction sectional area and other physical effects; r is a material dependent factor and V_g is the bandgap voltage at absolute zero temperature. C, r and V_g are independent on temperature. [21]

A simplification of the diode equation can be made if $I_F \gg I_0$ is assumed, then the equation and the diode voltage can be rewritten as:

$$I_F = I_0\left(e^{\frac{V_F}{V_T}}\right)$$

$$V = \frac{kT}{q}\ln\left(\frac{I}{I_0}\right)(5)$$

(5)

The combination of the equation of the saturation current with equation (5) results in the following relation, which is also represented in Figure 20:

$$V_F = V_g + \frac{kT}{q}\left(\ln(I_F) - \ln(C) - rln(T)\right)(6)$$

(6)

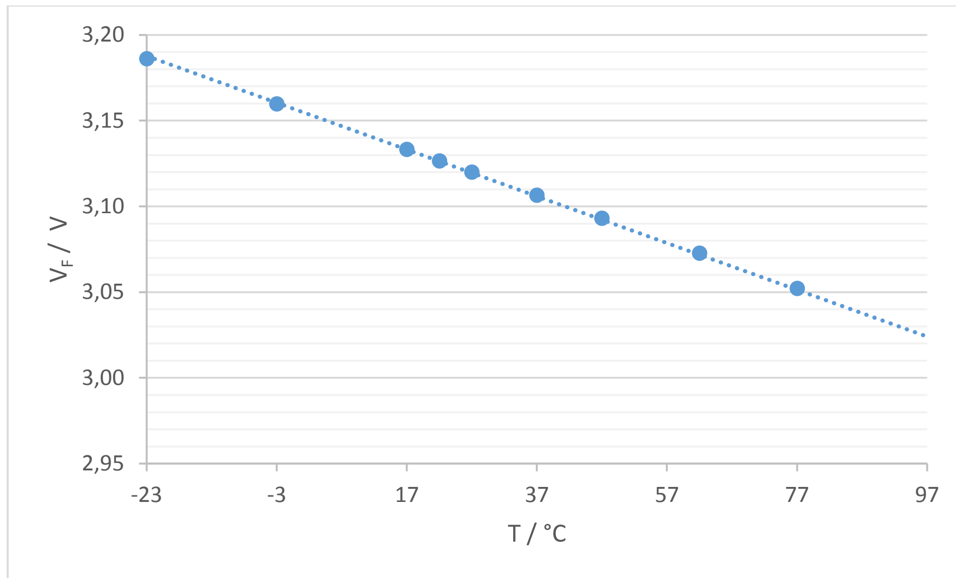

Figure 20: The nearly linear dependency between voltage and temperature, where V_g = 3.47 V, I_F = 0.01 A, r = 2 and C = 0,084 A/K^{-2} like in GaN

The relation shows only small non-linearity over a broad temperature range. The forward voltage drop can be seen as an almost linear function of temperature. Hence, the dependency between forward voltage and temperature can be expressed mathematically:

$$\mathrm{T_J} = m \cdot \mathrm{V_F} + \mathrm{T_0} \tag{7}$$

$$\mathrm{V_F} = \mathrm{K} \cdot \mathrm{T_J} + \mathrm{V_0} \tag{8}$$

m is the slope with the unit °C/V and its reciprocal K is known as the "K-Factor" with the unit mV/°C. The straight line intercepts the ordinate at $\mathrm{V_0}$ (see Figure 21) [22].

The equation (8) describes the correlation between voltage and temperature at constant current. Therefore, this relation offers a method for sensing temperature with diodes. The forward voltage drop of the junction serves as the temperature sensitive parameter of the junction. The linear relationship of voltage and temperature can be determined experimentally by driving the LED at different temperatures and at a constant forward-biased current. This constant current is called "measurement current" (see Figure 23). The "K-Factor" is always negative for semiconductor junctions and thus means that a decreasing forward voltage leads to an increasing junction temperature. The slope and the intercept are device-specific parameters. So each device has its own calibration parameter. These parameters are used to calculate the junction temperature in response to a power dissipation in the junction.

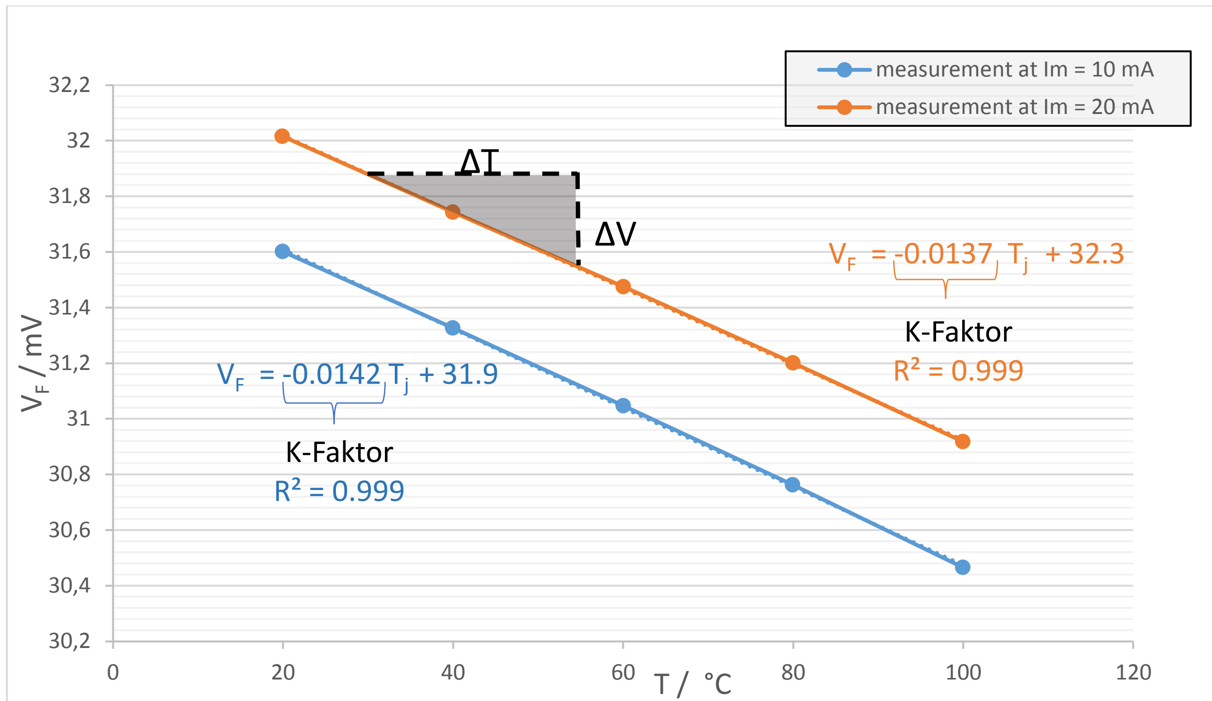

Figure 21: Calibration curve of one LED with two different I_m (10 mA and 20 mA) – almost no deviations of the linear fit delivering the K-Factors

The dependency between forward voltage and temperature at a specific measurement current results in a calibrated system for this specific junction. The voltage generated in response to the applied measurement current can be used to calculate the junction temperature by using the calibrated relationship – the "K-Factor". Device calibration has to be carried out for each new die type and also for each different measurement current [20].

3.2.2 Measurement of temperature calibration and thermal transient

The measurement of the device calibration can be done by measuring data pairs of temperature versus junction voltage at the measurement current. This measurement should be done with high precision. The junction temperature and the ambient temperature should be nearly the same. If the LED is electrically connected with a four wire sensing, the device calibration can start.

First of all, the measurement current has to be selected. The measurement current should be as low as possible. Its typical range is nearly around 10 mA which corresponds to the break in the diode's characteristic (see Figure 19). It has to be sufficiently large to get the conduction to the junction and a heat flow from the junction to the ambient. The measurement current should not be too large because it should generate the smallest amount of self-heating.

Furthermore, a thermal equilibrium between the device and the environment has to be provided. That means that the LED is situated in a constant temperature environment. There should be neither fluctuations of the diode voltage nor fluctuations of environmental

temperature (liquid cooled cold plate). It has to be mentioned that the equilibrium can only be reached after a waiting period which can take 30 minutes or more. The heat capacity of the device and the thermal resistance between device and ambient define the duration of this period. Then the temperature and the voltage can be measured.

The calibrating line becomes more significant if 5-20 data-pairs are measured. The data pairs lie in the range between 20°C to 100°C (see Figure 21). After performing the measurement a data fit (least squares linear regression) is applied to determine the best calibration parameter [1]. The usability of the calibration line can also be checked by the linear regression. If there is a non-linearity, the calibration is unsuitable. The more calibrating measurements are performed, the more accurate the calibration line becomes.

After calibration of the junction the thermal measurement can be started. During the measurements it has to be ensured that the LED is attached to the cooling unit. The electrical method of the thermal measurement is based on the measurement of the voltage drop of the device after a single step change in input power is applied to the device (see Figure 25). If you force the LED from a hot to cool steady state or vice versa by switching off or on, the transient recording of the cooling/heating curve can begin. Since the self-heating of the LED is not wanted, the cooling curve which has a low measurement current offers a better solution [23]. All further mentioned thermal transients are cooling curves (see Figure 22).

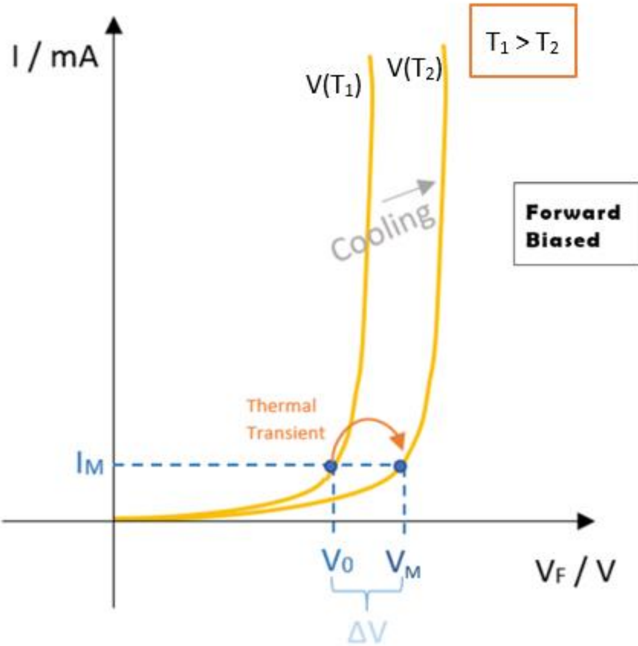

:

Figure 22: Thermal transient shown in the diode characteristic

Measuring the cooling curve starts with a device which is in the "hot" steady state – the junction has a higher temperature with respect to the ambient temperature. It can be expressed by $T_J = T_{amb} + \Delta T_J$, where T_J is the temperature of the junction and T_{amb} is the temperature of the environment. This hot equilibrium can be reached by applying a heating current on the device. The heating current (~100 mA-300 mA) is provided as a sum of currents – the driving current and the measurement current (I_M). Reaching the hot steady state level will take time (see Figure 23).

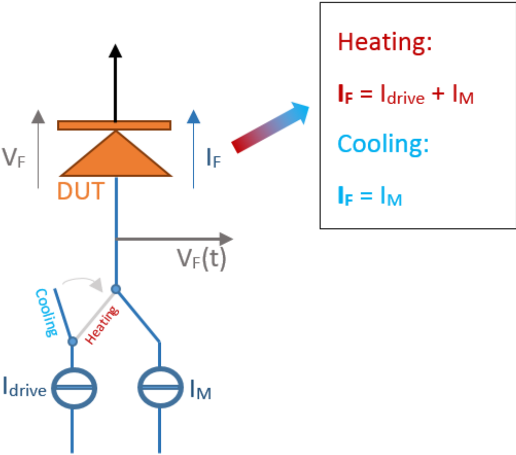

Figure 23: Applying driving (I_{drive}) and measurement current on a diode – reaching a hot steady state level & applying only measurement current – reaching a cool steady state level

When the device reaches the equilibrium by applied heating current, the drive current will be switched off and the temperature of the junction starts decreasing immediately. This decrease of the temperature from the hot steady state level up to the cool steady state level will be monitored. The monitored curve is a voltage change. Since the K-Factor is negative, the temperature decrease leads to an increasing of the voltage [1]. The device junction voltage is determined by $V_F = V_0 + \Delta V = V_0 + K\, T_J$ where V_0 is the initial voltage at hot steady state and ΔV is the change in junction voltage. Based on the temperature calibration (see chapter 3.2.1) the monitored values can be converted to junction temperatures. This time-dependent change of temperature ΔT(t) is called thermal transient.

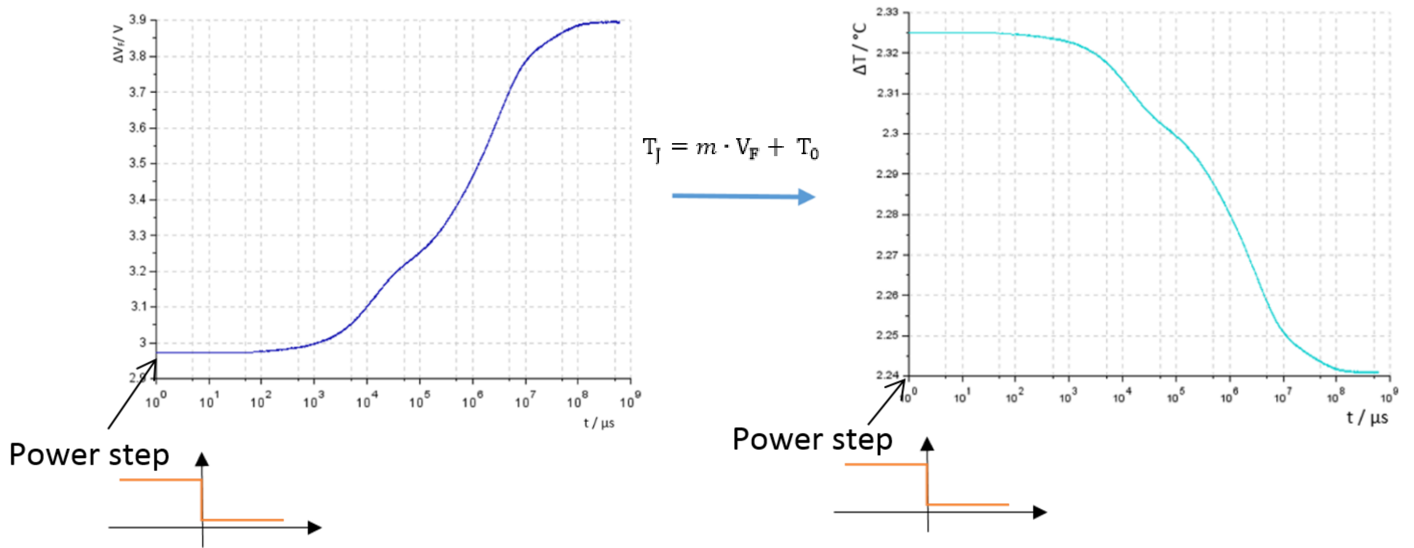

Figure 24: Recorded transient – starting from the measured increasing voltage (left) to the calculated temperature drop (right)

In Figure 24, a recorded transient is shown where at the time t=0 µs the power step is applied. The power step ΔP = $P_H - P_M$ (see Figure 25) describes the power difference between the heating power $P_H = I_H \cdot V_0$ and the measurement power $P_M = I_M \cdot V_M$. However, a bottleneck of the measurement is the capture of data points at the exact cessation of the power [23]. The fastest changes of the temperature take place in the first microseconds and the equilibrium is reached after hundreds of seconds. The cooling time is reduced by the attached cold plate [11]. The changes are measured in a linear time scale, while for a better identification of different thermal behaviors they are of course presented in a logarithmic time scale.

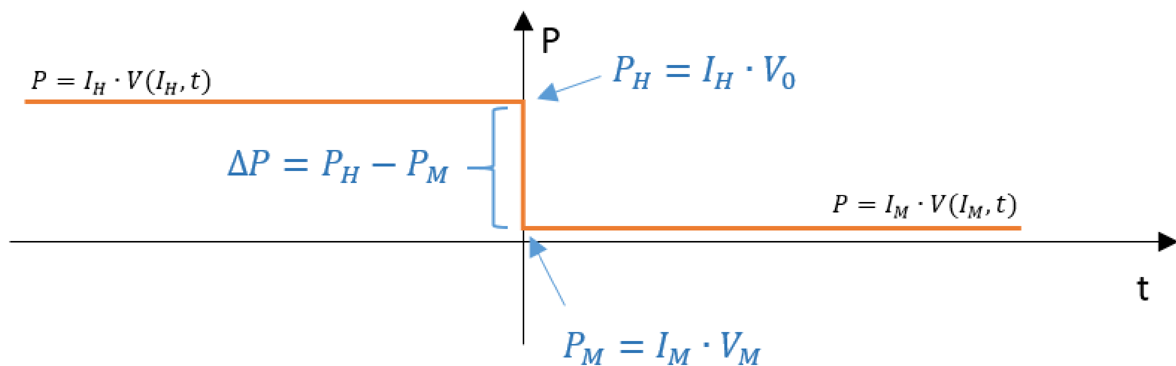

Figure 25: Power change at the cooling measurement on an LED

3.3 Electrical transient

In the range of microseconds, the thermal transient shows a steep voltage change immediately after the power step. The change indicates a non-thermal switching transient – electrical transient. The forward voltage goes from the “hot” voltage value belonging to the heating current in the diode characteristics to the lower “cold” voltage value belonging to the measurement current (see Figure 26: Electrical transient shown in the diode characteristic) [15].

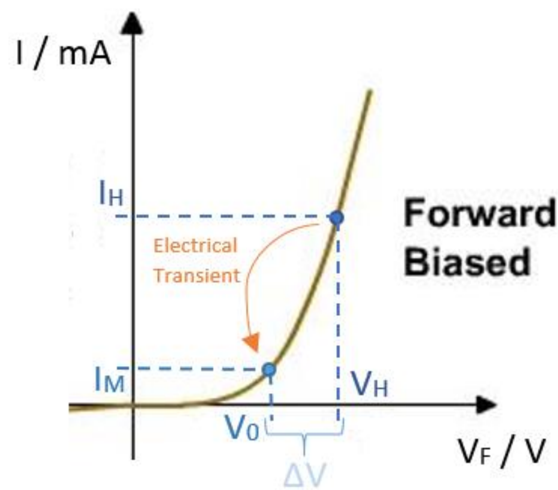

Figure 26: Electrical transient shown in the diode characteristic

The electrical transient can reach values of many hundred millivolts for diodes. The electrical transient occurs in the thermal transient if the test system cannot switch fast enough. That means, exceeding capacitance arises in the forward biased pn-junction where a large amount of stored diffusion charge has to be removed. The removal of the disturbing charge is found in the first microseconds of the recorded voltage change. It has to be mentioned that at the time of the electrical transient the junction temperature already changes. This temperature change cannot be recorded because it is covered by the electrical transient (see Figure 27 – left picture) [1].

This electrical transient should be corrected because it has no information about the thermal-induced voltage change. So the interesting part of the cooling curve starts just after the break in the curve. This can be taken as the new initial point [15]. From this initial point the data points of the thermal transient are used to extrapolate the time function back to the time t = 0s (the time of switching). For the extrapolation a linear relationship between temperature change and the square-root of time is used (see Figure 27 – right picture). This relationship can be derived from one-dimensional heat flow

$$\frac{\delta u(x,t)}{\delta t} = \alpha \frac{\delta^2 u(x,t)}{\delta x^2}$$

(9)

with the boundary conditions: u(x,0) = 0 and $\lambda \frac{\delta u(0,t)}{\delta t} = p_0(t) = \frac{P_{diss}(t)}{A_{Chip}}$, where u is the temperaturem rise at position x and time t; α is the thermal diffusity $\left(\alpha = \frac{\lambda}{c\rho}\right)$ and $p_0(t)$ is the power loss per area.

Then the solution of heat flow equation can be easily obtained introducing the Laplace transform of equation (9):

$$s\, U(x,s) = \alpha\, \frac{\delta^2 U(x,s)}{\delta x^2}$$

(10)

By using the equation (10) the general solution is:

$$U(x,s) = C_1 e^{-x\sqrt{\frac{s}{\alpha}}} + C_2 e^{x\sqrt{\frac{s}{\alpha}}}$$

(11)

In consequence of the boundary conditions C_2 becomes zero and C_1 is $\frac{P_0(s)}{\lambda\sqrt{\frac{s}{\alpha}}}$. The general solution appears now as:

$$U(x,s) = \frac{P_0(s)}{\lambda\sqrt{\frac{s}{\alpha}}}\, e^{-x\sqrt{\frac{s}{\alpha}}}$$

(12)

Due to that the temperature of the plate surface, which is the junction, (x = 0) is the point of interest, then the equation (12) can be written as:

$$U(0,s) = \frac{P_0(s)}{\lambda\sqrt{\frac{s}{\alpha}}}$$

(13)

Simplifying the tranformation back into the time doman $P_0(s)$ is assumed to be a step function $P_0(s) = \frac{1}{s}\frac{P_{diss}}{A_{Chip}}$. Then time domain representation of the step response of the equation (13) can be calculated [24]:

$$\mathrm{u}\,(0,\mathrm{t}) = \Delta T(t) = \frac{P_{diss}}{A_{Chip}} \frac{2\sqrt{\alpha}}{\lambda\sqrt{\pi}} \sqrt{t} = \frac{P_{diss}}{A_{Chip}} \frac{2}{\sqrt{\pi c \rho \lambda}} \sqrt{t}$$

(14)

This extrapolation can only be implemented at the beginning for very short times where the heat flow is in the region of the chip [14]. The thickness of the chip is the limitating factor of the duration of the extrapolation. Beyond this time the approximation is not valid anymore [25]:

$$t_{valid} = d_{Chip}^2 \frac{c\rho}{2\lambda}$$

(15)

In addition, this computation finds the start temperature of the junction V_0. An estimation of the chip area can also be made by using the slope *n* of the extrapolation and the equation (14):

$$A_{Chip} = \frac{P}{n} \frac{2}{\sqrt{\pi c \rho \lambda}}$$

(16)

A realistic value of the chip area A_{Chip} can be used as a check for an acceptable correction of the offset [14].

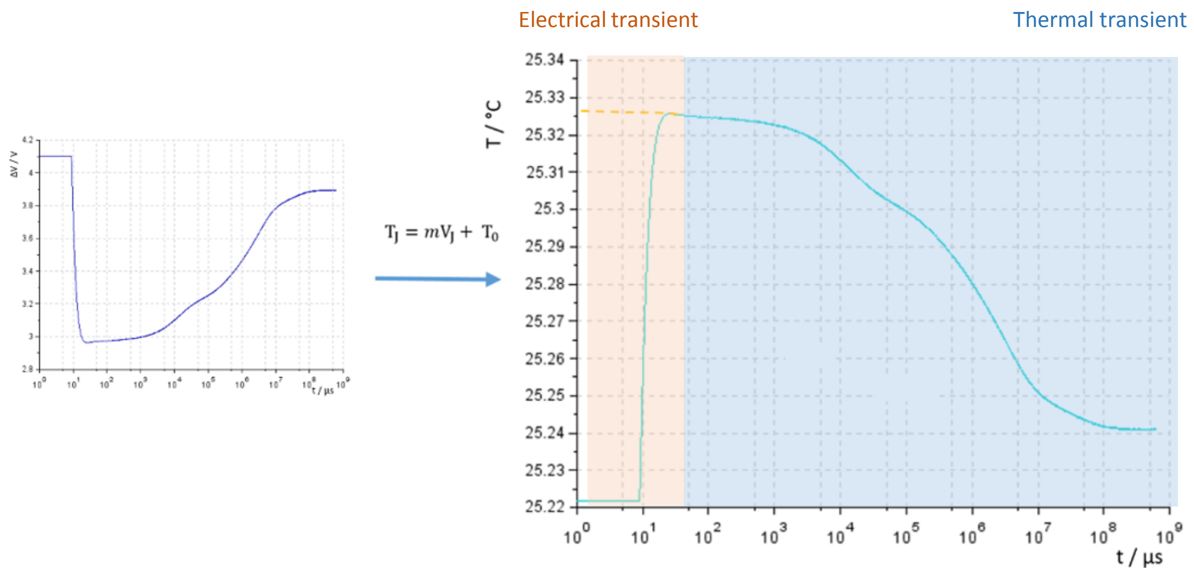

Figure 27: Recorded transient of an LED module (voltage change) and calculated temperature change with extrapolation

If the resolution of the temperature measurement is acceptable and the power change can be approximated to a step function, a short offset correction can be done. Hence, the investigation of the thermal transient provides a good insight into the inner structure of device. It also offers a base of further calculation and, hence, it allows the evaluation of the contribution of each layer (material) in the heat flow path.

4 Evaluation of the structure function

4.1 Introduction

In this work the mathematical transformation from thermal transient to the structure function (“structure function algorithm”). is performed using SCILAB SCILAB is one of the major open-source alternatives to MATLAB. However, the main motivation to do the evaluation of the structure function is that the implemented SCILAB- algorithm can be run on a measurement instrument – called “Red Pitaya” (http://redpitaya.com/). This instrument includes Radio Frequency signal acquisition and generation technologies, FPGA, Digital Signal Processing and CPU processing. The “Red Pitaya” is a network attached device based on Linux operating system [26]. Running “structure function algorithm” on “Red Pitaya” can replace the measurement setup (explained in chapter 3.1). The “Red Pitaya” has the size of a credit card. Therefore, it offers a compact form of the measurement setup. With this measuring system, an inline reliability test of LEDs is possible.

All the presented results performed for each calculation step are computed with SCILAB. The initial value of the computation is thermal transient. The thermal transient originates from a real measurement of the T3ster measuring system (see Figure 28). Here the measured LED experiences a power step of 58.123 W and the K-Factor of the LED is -1.09 mV/°C. Its thermal transient has a time range of 1 µs up to 120 s.

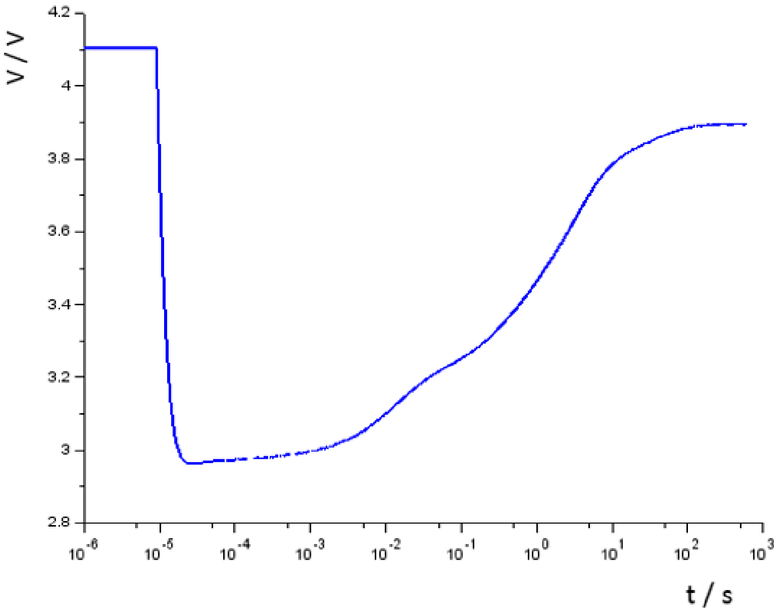

Figure 28: Measured thermal transient

4.2 Short overview of the calculation steps

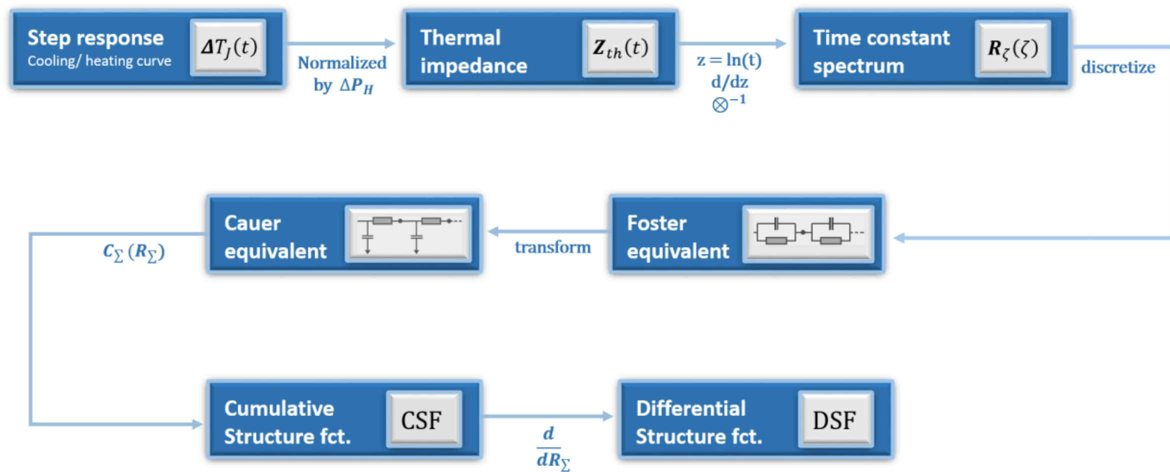

Figure 29: Summary of the calculation steps of the structure function

The thermal transient (or also called "step response") describes the thermal behavior of the device. As you can see in Figure 28, the graph of the thermal transient is hard to interpret. No destictive changes are apparent. That's the reason why another descriptive function is introduced – the structure function. The evaluation of the structure function starting from the thermal transient is not easy going. A schematics is shown in Figure 29.

First of all, you have to calculate the thermal impedance curve ($Z_{th}(t)$). The thermal impedance is the result of the normalization of the thermal transient. The real heating power step represents the scaling factor. The $Z_{th}(t)$ function directly provides the junction temperature response if 1 Watt of heating is applied. It can also be called the unit-step-response.

From the unit step response another descriptive function can be derived – the time constant spectrum. A convolution integral connects the time constant spectrum and the thermal impedance. The time constant spectrum can be processed, the discretization of this function leads to a Foster equivalent model. The Foster model is a thermal network of a series of parallel connected thermal RC pairs. The problem of the Foster network is that it represents no physical reality because there is no node-to-node thermal capacitance in thermal systems (see Figure 32). Thermal capacitances must be connected to the ambient. Therefore the Foster network has to be transformed into a Cauer network so that it can be interpreted.

These RC values of Cauer network can be easily transformed into the cumulative structure function. For a further enhancement of the heat flow path details, the derivative of the cumulative structure function – the differential structure function – can be determined.

4.3 Thermal impedance Curves - $Z_{th}(t)$

The first step of the subsequent proceeding of thermal transient is to get the thermal impedance curve. It can be seen as the generalization of the temperature measurement. The thermal transient is normalized by the applied power step ΔP. It provides the junction temperature response if 1 Watt of heating is applied:

$$Z_{th} = \frac{\Delta T}{\Delta P} \tag{17}$$

The thermal impedance Z_{th} is defined as the temperature change ΔT between two isothermal surfaces divided by the power step. The thermal impedance is broadly speaking thermal resistance without the requirement of the maintenance of the total heat flux at both isothermal surfaces. Thermal impedance at thermal equilibrium can be seen as thermal resistance. There is also an analogy to the electrical impedance where reactance only manifests itself during periods of transition.

The applied power step ΔP has a negative sign if the thermal transient is a cooling curve – where the change of the temperature is also negative. Recording the heating curve these signs become positive. Therefore, the thermal impedance curve is an increasing function and the direction of the heating is also positive.

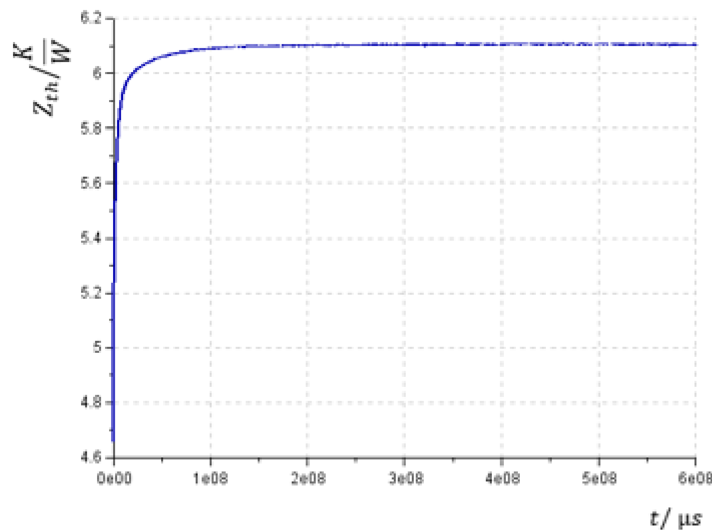

Figure 30: Thermal impedance curve – linear time scale

The Figure 30 illustrates the thermal impedance of an LED as a function of the cooling duration in response to a power step. It contains the complete characteristic of the thermal behavior of the device ranging from transient to steady state. Theoretically an equilibrium state requires an infinite time but – as seen in the graphic above – for practical purposes equilibrium

begins after 100 seconds (10^8 µs). The time axis is linear where zero is the instant of step-initiation. Due to the long-time range a large portion of this plot represents the steady state data. The changes of the thermal impedance within the first microseconds cannot be seen. Therefore, the unit step response is transformed into a logarithmic time scale.

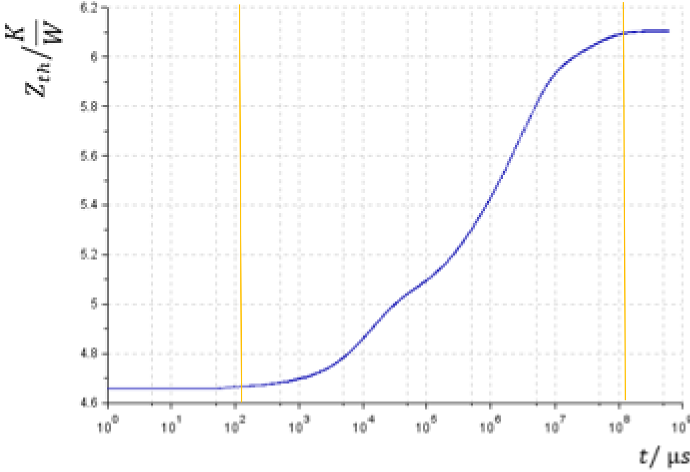

Figure 31: Thermal impedance curve – logarithmic time scale

Figure 31 represents the thermal impedance curve with a logarithmic time scale which exhibits its bumpy nature. The main part of the logarithmic time plot shows the non-equilibrium data (Figure 31 – region between the lines- 10^3 s-10^8 s). Since the thermal characterization of a device focuses on the transient data, this kind of representation is mainly used for analyzing the device structure. The scale change additionally produces noise reduction in the last part of curve. The shape of Z_{th} is resulted by the superposition of the heating of the structural elements of the device. It can be observed that in the beginning the chip heats up, following the internal package elements and then the package, the board and so on. This fact can be used to get information about the structure of the device, e.g. the height and the position of the bump can be investigated to check the reliability of the LED.

However, the structure identification of the thermal impedance curve has the same problems as the investigation with thermal transient, that is, small details may remain hidden. Starting from the Z_{th} curve a much clearer and more refined representation of the structure of the device and its environment can be determined [1].

4.4 Time constant spectrum

An essential step for the thermal characterization is the determination of the time-constant spectrum. The time-constant spectrum can be calculated by the thermal impedance with the NID-method (**N**etwork **I**dentification by **D**econvolution) [27].It's a descriptive function which uniquely represents the linear and passive thermal structure of a system. This function along the time constant (τ) axis shows the related magnitudes (R) of the time constants of the distributed system, either in form of discrete values or in form of a continuous spectrum [9].

The continuous representation is caused by the fact that real thermal systems are infinite, distributed thermal systems [1]. If the time constants and their magnitudes are known, a compact thermal model can be determined. As mentioned in the chapter 2.3.1, a compact thermal model consists of a RC network where the resistances are a lumped version of the 3d distributed thermal resistance between the junction and the ambient and the capacitances represent the 3d thermal mass distribution [5].

Starting the model with the simplest case of a RC ladder network, a network with a single RC pair. The thermal resistance expresses the heat conduction and the parallel thermal capacitance expresses energy storage (see Figure 32).

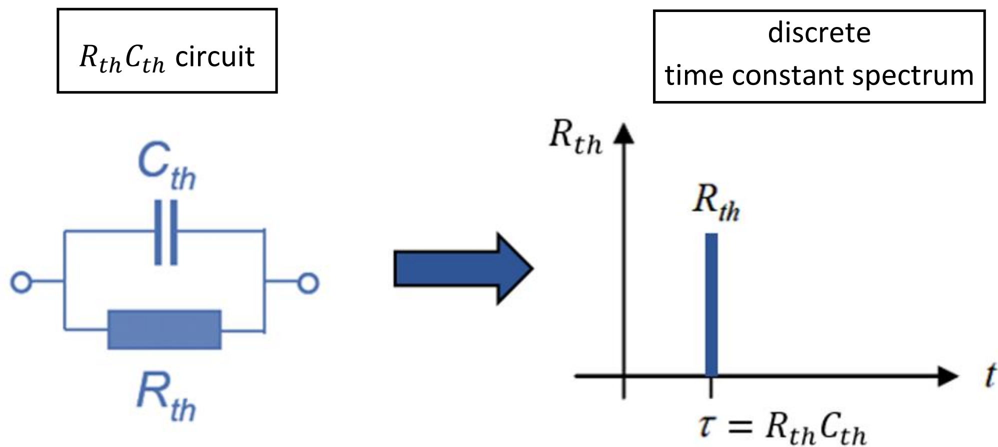

Figure 32: The simplest thermal model: a parallel resistance and capacitance and its discrete time constant representation

If a stepwise power change is applied, the response function grows quickly until t = $R_{th} \cdot C_{th}$ and it stabilizes at the temperature $T = R_{th} \cdot P$.

Due to the solution of 1d heat conduction equation thermal resistance can be expressed like in equation (1) where $R_{th} = \frac{T_1 - T_0}{P} = \frac{T_1 - T_0}{dQ/dt}$. There is a temperature drop when power flows through surfaces which have the temperatures T_1 and T_0. The thermal energy is also stored in this material. This means: if there is a heat flow into the material, in a short time interval dt the energy changes. This energy change can be expressed by the thermal capacitance $dQ = Pdt = CdT$.

Summarizing the equations above, the heat flow follows this equation when there is only one RC pair (one material):

$$P = \frac{dQ}{dt} = (T_1 - T_0)R_{th} = C_{th}\frac{dT}{dt}$$

$$\frac{dT}{dt} R_{th}C_{th} = (T_1 - T_0)$$

(18)

The integration of this equation leads to:

$$T(t) = (T_0 - T_1)\, e^{-\frac{t}{RC}} + T_1$$
$$T(t) = R_{th} \cdot P \left(1 - e^{-\frac{t}{RC}}\right)$$
(19)

Based on this result, it can be seen that the step response function for a single RC stage follows the exponential function $Z_{th} = R_{th}\left(1 - e^{\frac{-t}{\tau}}\right)$.

Remembering the chapter "Thermal impedance Curves - Zth", the heat, and also the thermal impedance, of the structural elements are superposed. Hence, the Z_{th} curve of a lumped circuit can be easily constructed by the sum of such exponential decays [1].

$$Z_{th}(t) = \sum_{i=1}^{n} R_{th_i} \cdot (1 - e^{-\frac{t}{\tau_i}})$$
(20)

The summation is in accordance with a model network as a chain of these parallel RC stages. The same power– 1 Watt - flows along the chain of parallel RC stages and the total thermal impedance can be calculated by adding up all components. This model network is called the Foster model. This circuit can be completely described by the knowledge of the values of R_{th_i} and C_{th_i}. The time-constant spectrum is the visual representation of this Foster model where the R_{th_i} is the magnitude of the spectrum and the τ_i ($\tau_i = R_{th_i} \cdot C_{th_i}$) is in the place of a "bump" along the time axis. In general, the Foster model can be considered as a black box model of the thermal impedance as this model describes the time response of the thermal impedance (Figure 33). In our case the black box can be seen like in Figure 33.

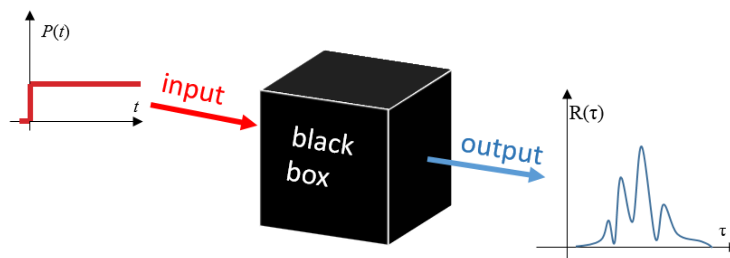

Figure 33: Schematic drawing of a black box model

As mentioned before, real thermal networks are infinite and they have a continuous time constant spectrum, the summation of the exponential terms should be replaced by an integral over the entire range of the possible thermal constants:

$$Z_{th}(t) = \int_0^\infty R_\tau(\tau) \cdot \left(1 - e^{-\frac{t}{\tau_i}}\right) d\tau$$

(21)

The discrete R_{th_i} magnitude values are replaced by the $R_\tau(\tau)$ thermal constant spectrum (see Figure 34).

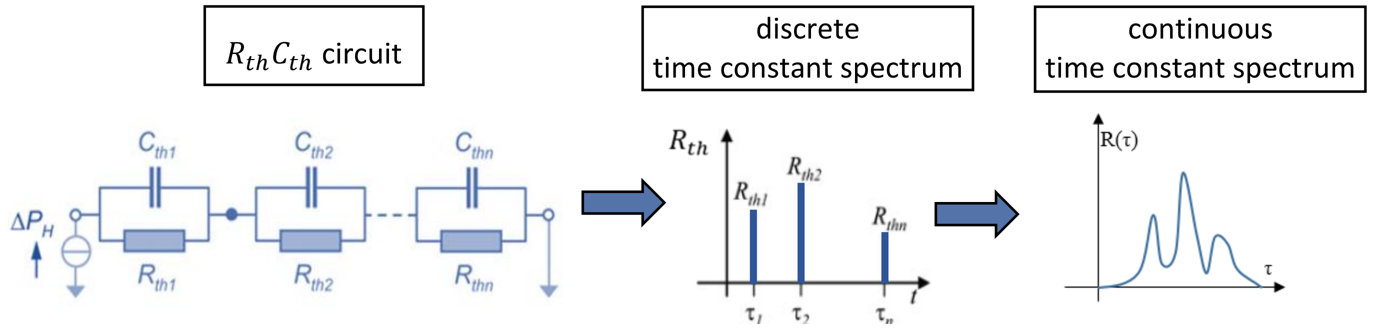

Figure 34: Distributed infinite RC systems represented as the time constant spectrum

4.5 Network Identification by Deconvolution – method (NID-method)

Displaying the junction temperature transients in the logarithmic time scale has advantages for the long-time range (see chapter 2.3.2)

The internal time constants of a chip are in the range of (1-100) microseconds, while the package-ambient system lies in the range of hundreds of seconds. For all the subsequent evaluation steps, the logarithmic time scale is used which shows more clearly the fast temperature changes which may remain hidden in a linear representation.

$$z = \ln(t)$$

(22)

$$\zeta = \ln(\tau)$$

(23)

Including this, the measured thermal response has to be transformed into this new variable [11]:

$$Z_{th}(t) = \int_{-\infty}^{\infty} R_\zeta(\zeta) \cdot \left[1 - e^{-\frac{t}{e^\zeta}}\right] d\zeta$$

(24)

with $R_\zeta(\zeta) = R_\tau(e^\zeta) \cdot e^\zeta$ as the logarithmic time constant. Subsequently, the time constant spectrum refers to $R_\zeta(\zeta)$. Another simplification is $Z_{th}(t = e^z) = Z_{th}(z) = a(z)$ and so it can be written:

$$\frac{d}{dz}a(z) = \int_{-\infty}^{\infty} R_\zeta(\zeta)[e^{z-\zeta-e^{z-\zeta}}]\ d\zeta$$

(25)

Another definition – the weighting function – is introduced $w_z(z) = e^{z-e^z}$ (its graphical representation: see Figure 36) and it can be written in this form:

$$\frac{d}{dz}a(z) = \int_{-\infty}^{\infty} R_\zeta(\zeta)\, w_z(z-\zeta)\ d\zeta$$

(26)

This allows to express this equation as a convolution between the spectrum and the weighting function [1]:

$$\frac{d}{dz}a(z) = R_\zeta(z) \otimes w_z(z)$$

(27)

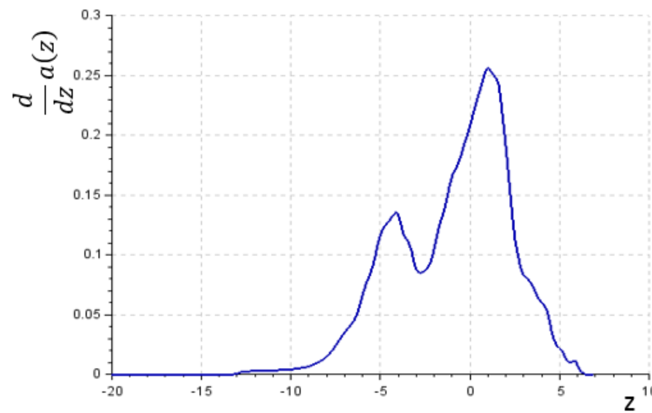

Figure 35: The derivative of a(z)

This equation (27) shows that the derivative of a(z) (see Figure 35) can be regarded as the blurred replica of the time constant spectrum. The convolution averages the values of the function R(z) over a range intended by the width of the weighting function $w_z(z)$.

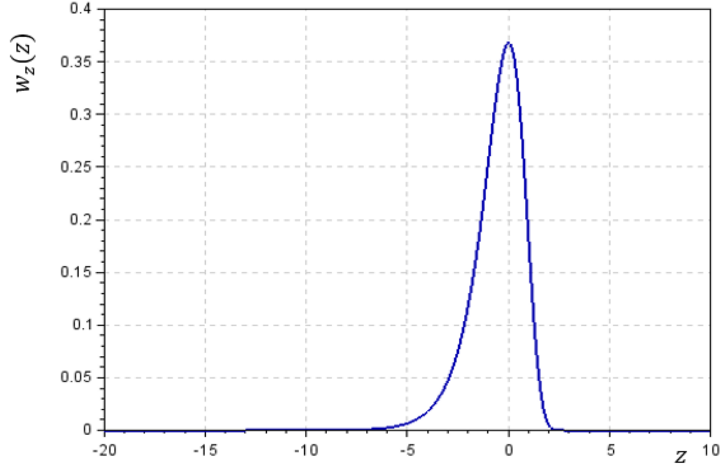

Figure 36: Shape of the weighting function $w_z(z)$

The degree of blurring is most effective in the region of the maximum. This region can be calculated by the half width of $w_z(z)$: Δz = 2.446 = 3.53 octave = 1.06 decade. This means that details which are closer than one decade cannot be distinguished in $\frac{d}{dz}a(z)$ [11]. R(z) is more precise and the time constant spectrum can be obtained using the inverse operation of the convolution: the deconvolution.

$$R_\zeta(z) = \left[\frac{d}{dz}a(z)\right] \otimes^{-1} w_z(z)$$

(28)

The implementation of the deconvolution is not straightforward. Deconvolution can be performed in the time domain by Bayesian iteration or in the frequency domain by Fourier. domain inverse filtering [1]. Unfortunately, the deconvolution is only an estimation, because the measured response are influenced by inaccuracies and by noise [11]. Both the derivation and the deconvolution operation enhance the noise. If the time constant spectrum is created by a measured thermal transient curve, a noisy signal can include false values in the time constant spectra causing misleading artifacts in the results of further post processing steps. The $Z_{th}(t)$ curve should be extremely noise less under these circumstances [1]. The increase can be avoided during the deconvolution only if limitations are applied for the enhancement in the resolution.

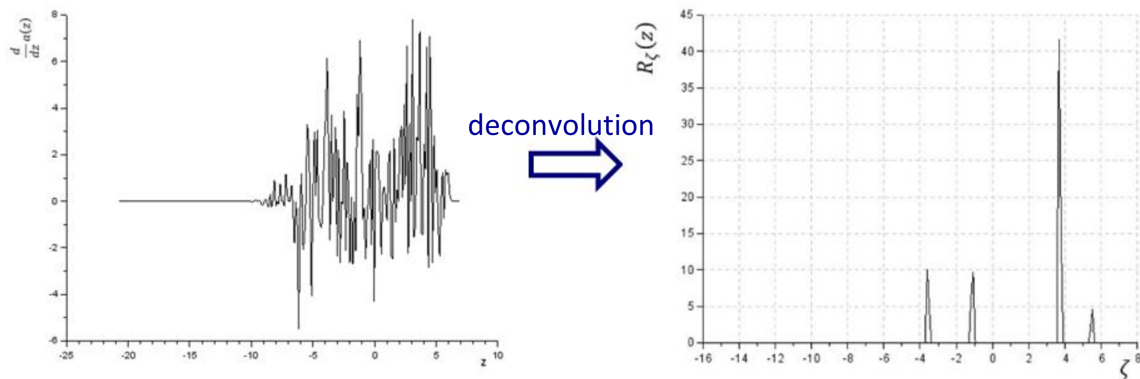

Figure 37: The derivative of the unprocessed signal and its time constant spectrum

As seen in Figure 37, even the derivative of the data (left picture), which is unprocessed, enhances the noise extremely. If the deconvolution is applied, the noise amplitude becomes additionally larger and the obtained result becomes unusable (right picture).

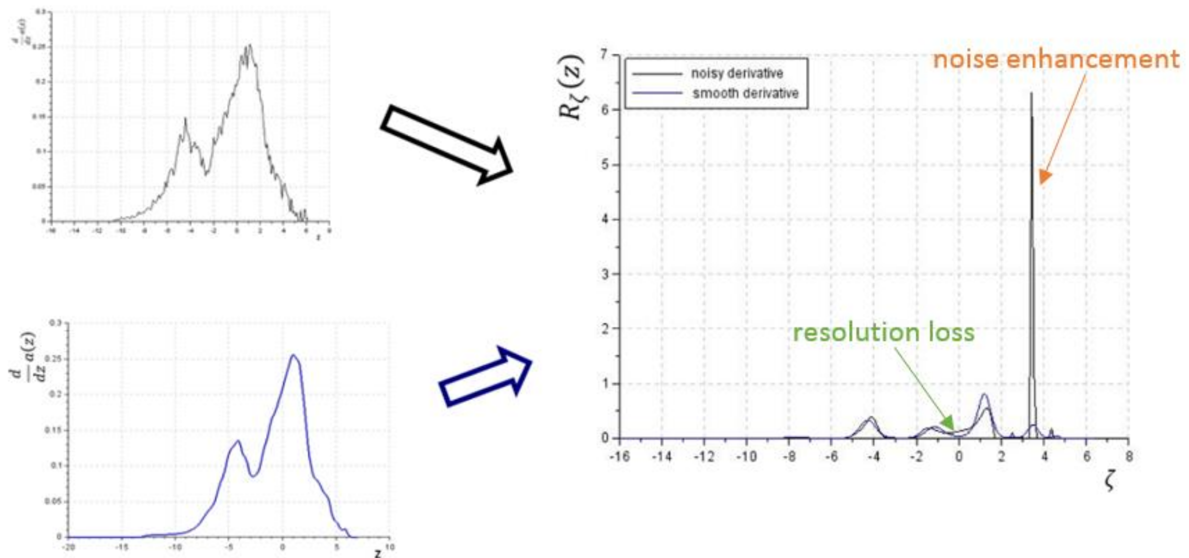

Figure 38: Comparing the time constant spectrum of a noisy and smooth derivative of thermal impedance

Generally speaking: if the response is affected by noise or measuring inaccuracies, the result of the time constant spectrum becomes less accurate. This effect can also be seen in Figure 38, where the black one (upper) has noise and the blue one (lower) has a lower signal-to-noise ratio. The enhancement of the noise can be clearly seen at $\zeta = \sim 3.5$ in the time constant spectrum (Figure 38- right picture – orange arrow). Additionally the diminishment of the

resolution can be seen at the lower ζ (-2 - 2) as the peaks are not so well separated anymore (Figure 38- right picture – green arrow). Subsequently, the inaccurate values of the smaller time constants induce higher numerical oscillations in the structure function.

4.5.1 Deconvolution

One kind of deconvolution is the **Fourier-domain inverse filtering.** There the convolution integral has to be turned into the Fourier domain. The equivalent formula in the Fourier domain has a multiplication instead of a convolution:

$$\frac{d}{dz}a(z) = R_{\zeta}(z) \otimes w_z(z) \rightarrow A'(\Phi) = R(\Phi) \cdot W_t(\Phi)$$

(29)

It has to be mentioned that the transformation from $a'(z)$ to $A'(\Phi)$ is not a common transformation into the frequency-domain because z is the logarithm of the time. The frequency Φ can be seen as the number of waves per time decade. The deconvolution can be done by a simple division:

$$R(\Phi) = \frac{A'(\Phi)}{W_t(\Phi)}$$

(30)

It should not be forgotten that noise n(z) is present in each measurement. It superimposes the signal $a'(z)$. So the measured data and its Fourier transforms can be interpreted like this:

$$m(z) = \frac{d}{dz}a(z) + n(z) \rightarrow M^*(\Phi) = A'(\Phi) + N(\Phi) = R^*(\Phi) \cdot W_t(\Phi) (31)$$

(31)

In this case the noise will also be present in the deconvolution.

$$R^*(\Phi) = \frac{M^*(\Phi)}{W_t(\Phi)} = \frac{A'(\Phi)}{W_t(\Phi)} + \frac{N(\Phi)}{W_t(\Phi)} \quad (32)$$

(32)

Parallel to the fact that $W_t(\Phi)$ is small at higher Φ there is an unwanted enhancement of the noise which can result in such a large noise completely hiding the useful signal. Therefore, the noise builds the ultimate limit of the resolution enhancement.

Filtering $F(\Phi)$ in the Φ domain is a way to suppress the noise at the higher frequency part. Additionally, the filter should not change the low frequency components of $M^*(\Phi)$ [11]. The response function of the filter should not contain oscillations. [4]. The application of the Gaussian Filter can be used to get rid of the noise [11]:

$$R_f(\Phi) = \quad R^*(\Phi) \cdot F(\Phi) = \frac{M^*(\Phi)}{W_t(\Phi)} \cdot F(\Phi)$$

(33)

$F(\Phi) = e^{\left(-\frac{\Phi}{\Phi_0}\right)^2}$ with its response function $f(x) = \sqrt{(\pi)}\,\Phi_0 e^{-(\pi\Phi_0 x)^2}$. The half –value width of the response function is dependent on the cut-off frequency Φ_0:

$$\Delta x = \frac{2\sqrt{ln2}}{\pi\phi_0} = \frac{0.53}{\Phi_0}$$

(34)

After applying the inverse Fourier transformation of $R_f(\Phi)$, the R(z) time constant spectrum is calculated (see Figure 39).

Deconvolution with the Fourier-domain inverse filtering does not always give a result if the noise becomes larger than the essential part of the signal at low Φ. It can be suppressed by the Gaussian Filter with a soft cut-off but at the price of the resolution. Another solution can be offered by using a less accurate weighting function. If there is a noise or an inaccuracy, the denominator must not be small in the high Φ range; the result is that the unpleasant emphasis of the noise does not occur in the resulting function. This process must be repeated several times by using different added noises (pseudorandom numbers) and then the results must be averaged, to get rid of the added noise in the resulting function [4].

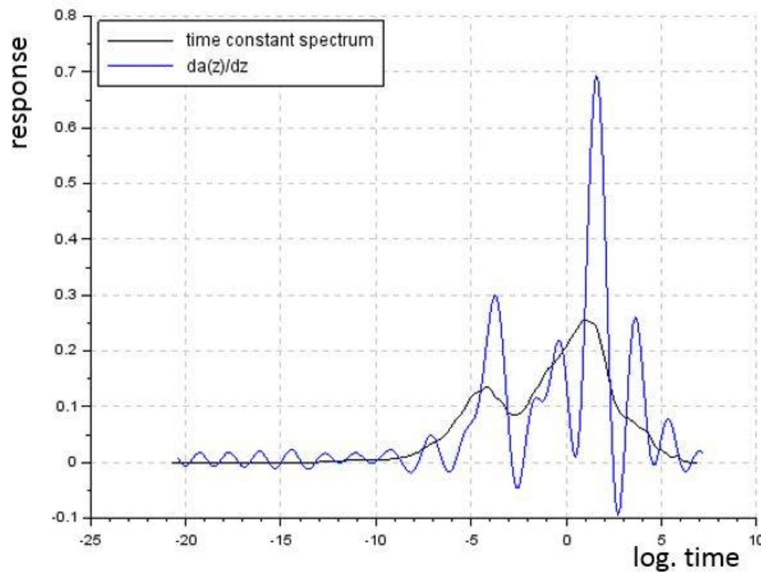

Figure 39: Time constant spectrum – calculated with the Fourier-domain inverse filtering

There is another way to execute the deconvolution: the **Bayes iteration** based on the Bayes theorem of probability theory [11].

$$P(H|D) = \frac{P(D|H)P(H)}{P(D)}$$

(35)

,where $P(D|H)$ is the posterior probability - degree of belief having accounted for H and where P(H) is the priori probability - the initial degree of belief in H. The quotient $\frac{P(H|D)}{P(D)}$ represents the support D provides for H. There is an algorithm which offers a solution of the equation (29) in terms of the Bayes' theorem:

$$P(R_i|A'_k) = \frac{P(A'_k|R_i)P(R_i)}{P(A'_k)} = \frac{P(A'_k|R_i)P(R_i)}{\sum_j P(A'_k|R_j)\,P(R_j)}$$

(36)

On the basis of the equation (35) where A'_k depends on R_i through W the following relation can be established;

$$P(R_i) = \sum_k P(R_i|A'_k)\,P(A'_k)$$

(37)

which leads to

$$P(R_i) = \sum_k \frac{P(A'_k|R_i)\,P(R_i)\,P(A'_k)}{\sum_j P(A'_k|R_j)\,P(R_j)}$$

(38)

The desired solution $P(R_i)$ appears on both sides of the equation. The Bayes' postulate (all probabilities are equal) must be applied for calculating the Bayes' theorem. An iterative relationship can be introduced where after n cycles the current estimate of $P(T_i)$, exactly $P^{(n+1)}(T_i)$, can be calculated:

$$P^{(n+1)}(R_i) = P^{(n)}(R_i) \sum_k \frac{P(A'_k|R_i)\;P(A'_k)}{\sum_j P(A'_k|R_j)\,P(R_j)}$$

(39)

For $P^{(0)}(T_i)$ an equiprobable distribution is proposed. The latter equation can be reduced to a more easily workable form by $P(R_i) = \frac{R_i}{R}$ and $P(A'_k) = \frac{A'_k}{A'} = \frac{A'_k}{R}$ since the probability is conserved and R = A', and $P(A'_k|R_i) = \frac{W_{ki}}{W} = W_{ki}$, because $\sum_k W_{ki} = W = 1$. Then the equation becomes $\frac{R_i^{n+1}}{R} = \frac{R_i^n}{R} \sum_k \frac{W_{ki}\,\frac{A'_k}{R}}{\sum_j W_{kj}\frac{R_j}{R}}$ or $R_i^{n+1} = R_i^n \sum_k \frac{W_{ki}\;A'_k}{\sum_j W_{kj}\,R_j}$. The summation over k appears as the corrective factor on R_i. [28]. The finite size of the arrays allows that the equation can be rewritten as the following iterative formula:

$$R^{(n+1)}(z) = R^n(z)\left(w_z(z) \oplus \frac{a'(z)}{w_z(z) \otimes R^n(z)}\right)$$

(40)

$R^n(z)$… n-th approximation for the R(z) time constant spectrum / the estimation of the a priori distribution after n iterations

In each iteration step at equation (40) there is one convolution $\otimes$ and one correlation integral $\oplus$. This process is time-consuming [11]. The initial estimate $R^0(z) = \left(w_z(z) \oplus \frac{a'(z)}{w_z(z)}\right)$ is used on the basis of the Bayes' postulate [29]. The Bayes iteration can only be used for functions of positive values – so it is not suitable for a transfer function which can have negative magnitudes [11]. The non-negativity has the property, if the first estimate $R^0(z)$ is positive, all of the further estimates will be positive. The algorithm usually converges slowly to the suitable solution and then diverges again. The true signal can be calculated via the Bayes iteration before it amplifies the noise. Therefore, a stop criterion has to be introduced. It can either have an absolute number of iterations or the difference between two estimators $R^n(z)$ and $R^{n+1}(z)$ such as $\Delta R = \frac{\sum_z R^{n+1}(z) - R^n(z)}{\sum_z R^n(z)}$ [30]. A sufficient number of the iteration steps is in the order of 1000 [11]. It is important to use a pre-denoised signal before planning to use the Bayes iteration to deconvolve the signal [30].

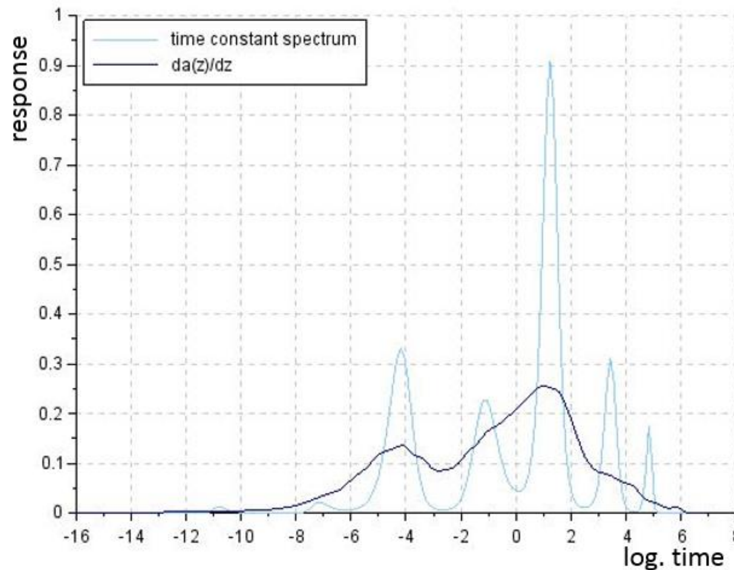

Figure 40: Time constant spectrum – calculated with the Bayes iteration

Comparing now the two methods (Fourier-domain inverse filtering and Bayes iteration) of the calculation of the time constant spectrum, it can be clearly seen that the Bayes iteration offers a more accurate spectrum than the Fourier-domain inverse filtering. In the Bayes iteration the peaks are well distinguishable. One big difference can also be noticed between

Figure 39 and Figure 40. The first one has negative values compared to the second one. That comes from the restriction of the theory of probability, where the function only allows positive values. However, time constant spectra can be interpreted both for driving point and transfer impedance. In this setup, the Bayes iteration offers the better solution for the evaluation of the time constant spectrum [1].

4.5.2 Discretization

The time constant spectrum can be represented either in form of discrete values or in form of a continuous spectrum. As mentioned before, it can be seen as a dynamic compact model of a series of parallel connected $R_{th}C_{th}$-pairs, which is also called a Foster network. The values of R and C can be obtained directly from the time constant spectrum. Through the deconvolution the values of the R(z) are known, because the magnitudes of time constant spectrum are the thermal resistance of the Foster network. The thermal capacitances can be calculated by the time constant ($\tau_i = R_{thi} \cdot C_{thi}$).

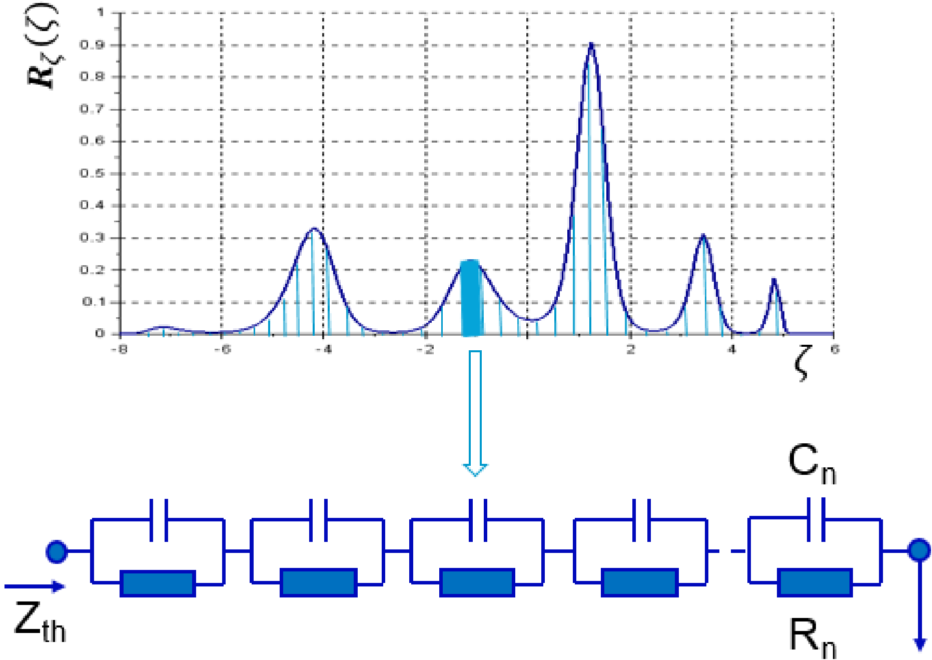

Figure 41: Drawing of the time constant spectrum and its relationship with a thermal RC circuit

The construction of this lumped element (Figure 41) model is based on the approximation of the continuous function by a set of discrete spectrum lines. It is a trade-off to approximate this function. The number of the lines should be as low as possible to minimize the size of the model network but you should also keep an eye on the error of the approximation. The first approach is the direct discretization of the spectrum. The most straightforward possibility is to use an equidistant division along the z axis which has its relevant part from z_a to z_b. The placement of the poles, which represent the time constant set of the approximate lumped

model, is given by $z_i = z_a + \left(i - \frac{1}{2}\right)\Delta z$ with i=1,2,...N. N is the number of lines of the approximation and $\Delta z = \frac{(z_b - z_a)}{N}$. A magnitude has to be ordered to each z_i. It can be calculated by the following expression [12]:

$$K_i = \int_{z_i - \frac{\Delta z}{2}}^{z_i + \frac{\Delta z}{2}} R(\zeta)\, d\zeta \tag{41}$$

Another method gives better results, for example simple linear weighted summations [4]:

$$K_i = \int_{z_i - \Delta z}^{z_i + \Delta z} (1 - \frac{|\zeta - z_i|}{\Delta z}) R(\zeta)\, d\zeta \tag{42}$$

The total steady state thermal resistance of the measured transient curve can be calculated as $R_{th}(t) == \int_{-\infty}^{\infty} R(\zeta)\, d\zeta$ [1].

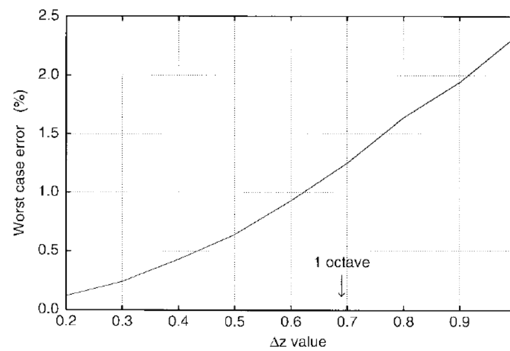

Figure 42: Worst-case error of the direct discretization dependent on the distances of the lines (in the case where R(z) is constant)[4]

In Figure 42, the magnitude of the worst case error can be seen as a function of the distance between the nodes Δz. The R(z) was taken as constant. As you can see, the upper bond of the error is [16]:

Table 3: Values of the worst case error as a function of the distance between the poles

Δz / ln(s)	Δz / octave	Relative error / %
0.346	0.5	0.47
0.693	1	1.8
1	1.44	3.58

The error is calculated by the deviation from the true transient response related to its asymptotic value. This error is much less perceptible for the practical spectra than these worst case errors [4].

4.6 Foster network

The Foster normal form of the thermal one- port can be calculated by this discretized spectrum Figure 34 [16]. The chain model of parallel RC stages can be quantitatively described by table of R_i and C_i [1]. There is an accordance between the ith line of the discretized spectrum and the ith stage of the circuit: $R_i = K_i$ and $C_i = \frac{\tau_i}{R_i} = \frac{e^{z_i}}{R_i}$ [16]. Each segment with the width of Δz corresponds to a parallel RC circuit (see Figure 43).

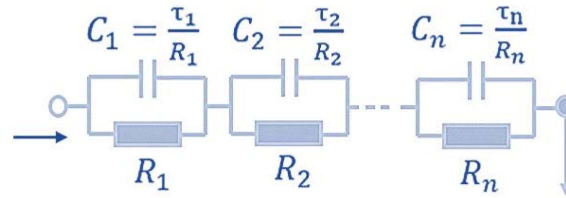

Figure 43: Drawing of a Foster network and their RC values

In summary, the time constant spectrum function is the extension of the Foster model for the continuous distributed systems and the discretization of the time constant spectrum results in a Foster network [14]. Considering one basic element of the Foster network (see Figure 32), the transfer function and also the complex impedance of the network can be calculated by the Laplace-Transformation [31].

$$\frac{V}{I} = Z_F(s) = \frac{R * \frac{1}{sC}}{R + \frac{1}{sC}} = \frac{R}{(1 + C \cdot s)} \tag{43}$$

s is the complex frequency because s can be written as $s = j\omega$ and ω is the angular frequency of a small sinusoidal signal. If s has the value of $= -\frac{1}{\tau}$, the impedance function has a local singularity – a so-called pole there [14].

If there is a chain of the parallel RC ports and if the number of time constants is finite, the thermal impedance has the form of a sum of the elements based on equation (43):

$$Z_F(s) = \sum_{i=1}^{n} \frac{R_i}{(1 + C_i \cdot s)} \tag{44}$$

The equation (44) belongs exactly to the transfer function coming from a multiexponential function – see equation (20).

It would be deceptive to assign these thermal resistance and thermal capacitance to physical regions of the heat conduction path structure. The entire model represents the thermal impedance, but the individual elements values (RC stages) are “fictitious” [1]. The Foster network is only a behavioral description of the system [32]. Real thermal capacitances are always connected to the datum node (ground) of the system. The node-to-node thermal capacitances belong to no physical reality as the thermal energy depends on the temperature of one node and not on the temperature difference of two nodes as suggested by the Foster model [14].

4.7 Cauer network

However, there is an equivalent network model providing a RC model which is suitable to characterize thermal structures. It is called Cauer model and it can be calculated from the Foster model. This model offers a great solution for associating the circuit elements with physical regions. That is the base of the heat flow path identification via structure functions. The Foster to Cauer transformation is a standard technique in the region of linear electrical circuits [1]. The Cauer network is a ladder network which has the following basic element (see Figure 44).

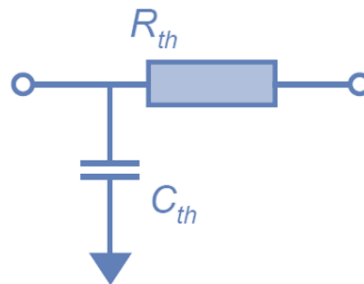

Figure 44: Basic element in the Cauer network

In accordance with the transfer function of this basic element:

$$\frac{V}{I} = Z_C(s) = \frac{R}{(1 + C \cdot s)} \tag{45}$$

the correspondence between the Foster network and the Cauer network can be seen. For one RC port the values for R and C are the same for both types of networks. However, if there are more than one element, the R and C values become more and more different. If there are more RC ports (see Figure 45), the impedance of the Cauer network can be written as a continued fraction expansion,

$$Z_C(s) = \cfrac{1}{C_1 \cdot s + \cfrac{1}{R_1 + \cfrac{1}{C_2 \cdot s + \cfrac{1}{R_2 + [\dots]}}}}$$

(46)

where the impedance of each of the branches in the network occurs explicitly [31].

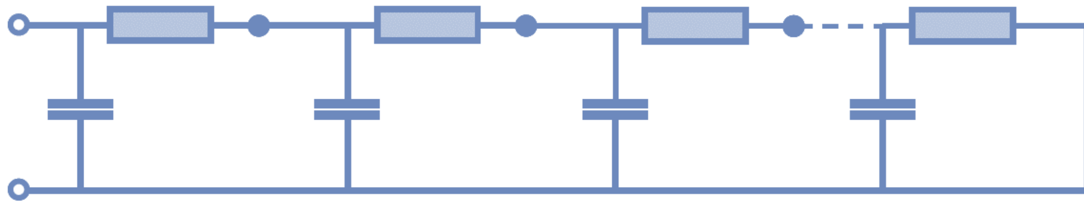

Figure 45: Chain of RC ports in the Foster Network

4.8 Foster to Cauer transformation

There is a basic algorithm of the calculation of the Foster to Cauer transformation which is described below [31].

Based on the impedance of the Foster network – see equation (43) – the summation results in the quotient of two polynomials:

$$Z_F(s) = \frac{n_o + n_1 s + n_2 s^2 + \cdots + n_{N-1} s^{N-1}}{d_o + d_1 s + d_2 s^2 + \cdots + d_N s^N}$$

(47)

n_i, d_i... coefficients of real values

The transformation from the transfer function (44) to the equation (47) is the most time consuming operation in calculating the structure function. As you can see in Figure 46, the approximation of the transfer function as their polynomial functions is the most expensive calculation in the whole operation. This computation time can be reduced by using fewer time constants, which on the other hand decreases accuracy.

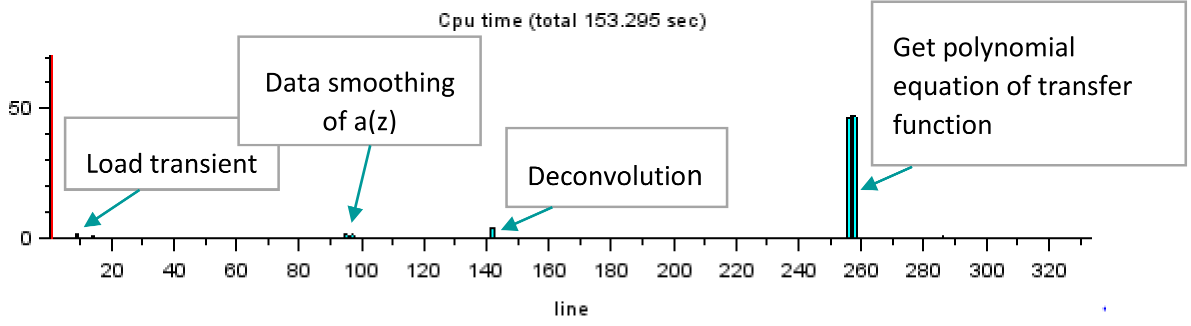

Figure 46: Profile of the structure function calculation

This operation must already be calculated with a large number of digits because the equation (47) has to be as accurate as possible. This requirement is needed for the next calculation step where this equation is the starting point to get the elements of the Cauer network.

4.8.1 Fraction decomposition

First of all, a parallel capacitance will be obtained from Z(s) through an approximation: $\mathrm{Y}(s) = \frac{1}{Z(s)} = \frac{d_N}{n_{N-1}}\ s = C_1 s$, where s→ ∞. Consequently, the extracted capacitance is:

$$C_1 = \frac{d_N}{n_{N-1}}$$

(48)

Subtracting the first capacitance from the inverted impedance, the s^N element vanishes [14].

$$\begin{aligned} Y^*(s) = Y(s) - C_1 \cdot s &= \frac{d_o + d_1 s + d_2 s^2 + \cdots + d_N s^N}{n_0 + n_1 s + n_2 s^2 + \cdots + n_{N-1} s^{N-1}} - C_1 \cdot s \\ &= \frac{d_o + [d_1 - C_1 \cdot n_0]s + [d_2 - C_1 \cdot n_1]s^2 + \cdots + [d_N - C_1 \cdot n_{N-1}]s^N}{n_0 + n_1 s + n_2 s^2 + \cdots + n_{N-1} s^{N-1}} \\ &= \frac{d_o^* + d_1^* s + d_2^* s^2 + \cdots + d_{N-1}^* s^{N-1}}{n_0 + n_1 s + n_2 s^2 + \cdots + n_{N-1} s^{N-1}} = \frac{1}{Z^*(s)} \end{aligned}$$

(49)

As you can see above (49) $d_o^* = d_o$ and $d_i^* = d_i - C_1 \cdot n_{j-1}$ [31].

In a second step, the first serial resistance value of the Cauer network will be calculated from $Z^*(s)$. It is assumed that s → ∞ and so the approximation is as follows [14]:

$$Z^*(s) \cong \frac{n_{N-1}}{d_{N-1}^*} = R_1$$

(50)

Next, R_1 has to be subtracted from $Z^*(s)$,

$$Z^{**}(s) = Z^{*}(s) - R_1 = \frac{n_o + n_1 s + n_2 s^2 + \cdots + n_{N-1} s^{N-1}}{d_o^* + d_1^* s + d_2^* s^2 + \cdots + d_{N-1}^* s^{N-1}} - \mathrm{R}_1$$
$$= \frac{[n_o - R_1 \cdot d_0^*] + [n_1 - R_1 \cdot d_1^*]s + [n_2 - R_1 \cdot d_2^*]s^2 + \cdots + [n_{N-1} - R_1 \cdot d_{N-1}^*]s^{N-1}}{d_o^* + d_1^* s + d_2^* s^2 + \cdots + d_{N-1}^* s^{N-1}}$$
$$= \frac{n_o^* + n_1^* s + n_2^* s^2 + \cdots + n_{N-2}^* s^{N-2}}{d_o^* + d_1^* s + d_2^* s^2 + \cdots + d_{N-1}^* s^{N-1}}$$

(51)

where $n_1^* = n_i - R_1 \cdot d_i^*$ [31]. Through the subtraction the s^{N-1} element vanishes. This results in an impedance formula like (47) again, but the order of the polynomials is reduced. The numerator has now the order of N-2 instead of N-1 and the denominator is now a polynomial with the order of N-1 instead of N. The same process has to be repeated in order to get the next capacitance and the next resistance of the Cauer network. This procedure finishes when Z=0 is reached [14].

The conversion works well for models with a little number (~15) of RC pairs. Nonetheless, there are concerns about a numerical issue – the floating point. A floating point is the representation of a number in computing. The number usually appears with a significant number with fixed digits times scaled by a power of 10. The standard floating point number of SCILAB has a number range from 10^{-308} to 10^{308} and the fixed number consists of 20 digits. Here the standard floating point number representation has not the suitable range of orders of magnitude and it has not enough numbers of decimal digits [1]. Generally speaking, the larger the number of stages in the Foster network, the more precision digits are demanded to get a reliable and trustworthy result [31]. Therefore, a derivation of the basic algorithm of the calculation of the Foster to Cauer transformation is demanded.

4.8.2 Fast algorithm

This alternative algorithm as shown is faster than the algorithm above mentioned (see chapter 4.8.1). However, it has still the same problem concerning the floating point number. The chapter 4.9.1 will expand on these concerns. As mentioned in chapter 4.8.1, the network can express iteratively based on a one port impedance Z_{th}^{n} with n thermal resistors and n capacitors. The initial impedance Z_{th}^{0} is zero. As shown above in equation (44), the Foster-type impedances can be written as

$$Z_F^n(s) = \frac{R_n}{(1 + C_n \cdot s)} + Z_F^{n-1}(s) \quad (52)$$

(52)

and also as a rational function in s

$$Z_F^n(s) = \frac{p_N(s)}{q_N(s)}.$$

(53)

The polynomial degree of $p_N(s)$ is smaller by one than that of the polynomial $q_N(s)$. According to the equation (46) the recursive definition of the Cauer impedance is

$$Z_C^n(s) = \frac{1}{C_n \cdot s + \frac{1}{R_n + Z_C^{n-1}(s)}}.(54)$$

(54)

It is a continued fraction representation. For the transformation the recurrence relation (54) is used in the form:

$$\frac{1}{Z_C^n(s)} = C_n \cdot s + \frac{1}{R_n + Z_C^{n-1}(s)}.(55)$$

(55)

Its rational function $\frac{1}{Z_C^n(s)} = \frac{q_n(s)}{p_n(s)}$ can be substituted by the standard Euclid's algorithm into a polynomial linear in s and a rational function $\frac{rem_n(s)}{p_n(s)}$ as remainder, where the polynomial degree of $rem_n(s)$ is smaller than the polynomial degree of $p_n(s)$:

$$\frac{1}{Z_C^n(s)} = \frac{q_n(s)}{p_n(s)} = C'_n \cdot s + \mathrm{k_n} + \frac{rem_n(s)}{p_n(s)}(56)$$

(56)

The equation (56) and the equation (55) have to be compared. C'_n can be identified by C_n and $\frac{rem_n(s)}{p_n(s)}$ with $\frac{1}{R_n+Z_C^{n-1}(s)}$. This leads to the following relation: $\frac{rem_n(s)}{p_n(s)} = \frac{p_n(s)}{k_n \cdot p_n(s) + rem_n(s)} = R_n + Z_C^{n-1}(s)$. According to the Euclid's decomposition $Z_C^{n-1}(s)$ can be written as rational function $Z_C^{n-1}(s) = \frac{p_{n-1}(s)}{q_{n-1}(s)}$. The following identities can be used now:

$$R_n = \frac{1}{k_n}$$

$$q_{n-1}(s) = p_n(s) + rem_n(s)$$

$$p_{n-1}(s) = \frac{rem_n(s)}{k_n}$$

(57)

Hence, the resistance R_n and the capacitance C_n of the Cauer network can be calculated. Determining the next Cauer RC-part $Z_C^{n-1}(s) = \frac{p_{n-1}(s)}{q_{n-1}(s)}$ is used in the same way as $Z_F^n(s) = \frac{p_N(s)}{q_N(s)}$ above. The abort criterion is reached if $p_0(s) = 0$. Every Cauer parameter is determined unambiguously by the Foster-Cauer transformation. This fact points out the physical meaning of the Cauer network as mentioned above. Not more than 15 RC pairs are needed for each different layer in the device to get their representation of the thermal impedance [32].

4.9 Structure function

After generating the resistances and the capacitances of the Cauer network from the time constant spectrum, two new further simple definitions are introduced. The new parameters are the cumulative thermal resistance

$$R_{th\Sigma} = \sum_i R_{thi} \quad (58)$$

(58)

and the cumulative thermal capacitance

$$C_{th\Sigma} = \sum_i C_{thi} \, .$$

(59)

The cumulative thermal capacitance can be interpreted as a function of the cumulative thermal resistance (see Figure 47). This introduced function is called the cumulative structure function (CSF) (see equation (60)). The beginning of the structure function is the driving point. Due to the cumulative summation of the $C_{th}R_{th}$ Cauer element values, the function shows the subsequent heat flow path sections:

$$CSF = C_{th\Sigma}(R_{th\Sigma}).$$

(60)

The cumulative structure function is the graphic representation of the thermal RC equivalent of the system and it helps to understand the heat flow path in the device. The origin can be interpreted as the junction. The function and also the heat flow path end in the ambient. The curve is increasing and it should end with a singularity because all thermal capacitances are positive and the heat sink capacitance should tend to infinity. Consequently, the junction-to-ambient thermal resistance is easy to read from the structure functions. It is the distance between origin (junction) and singularity (ambient). The cumulative capacitance extends in a wide range and that’s why the cumulative structure function has a logarithmic scale for the values of the capacitances [7].

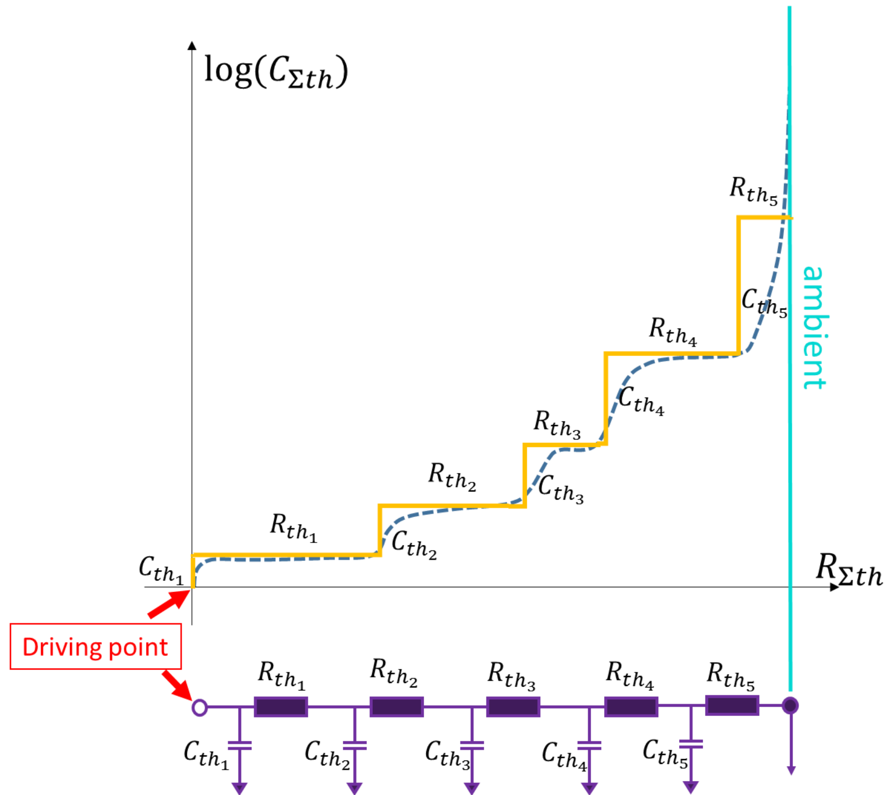

Figure 47: Cumulative structure function (CSF)

If there is a one-dimensional heat-flow, the structure function can be seen as a map of the heat flow path. E.g. an LED has an essentially one-dimensional heat flow path, where the junction layer is the heat source. The heat flow starts at the junction passes different layers and ends up at the ambient (compare with chapter 2.3.4). That allows us additionally to identify the partial thermal resistance related to the physical structure in the device. Furthermore, the cumulative structure function can be approximated by a stair function with just a few steps. Each step corresponds to a stage of a Cauer network and so the structure function can be summarized by a Cauer – type compact model. These stages can be found by the subsequent inflection points in the cumulative structure function [10]. This leads to an identification of different regions/materials in the heat-flow path. Knowing the thermal resistance, the thermal conductivity of the material can be calculated using the following equation: $\lambda = \frac{1}{R_{th}} \frac{L}{A}$, where L is the distance of the surfaces and A is the area of the heat flow path. This equation comes from the Fourier's law (eq. (2)) and eq. (1) [7].

The derivative of the structure function is used for an easier identification of the different sections of the heat path. It is called the differential structure function (DSF). The differential structure function simplifies the detection of the change of a slope in the cumulative structure function.

$$DSF = \frac{dC_{th\Sigma}}{dR_{th\Sigma}} \quad (61)$$

(61)

In this case a change of the slope of the cumulative structure function corresponds to a peak or a valley in the differential structure function. This slope has a constant value:

$$DSF = \frac{C_{th}}{R_{th}} = c\lambda A^2 \quad (62)$$

(62)

The value of this derivative is dependent on thermal properties and the cross sectional area of the heat flow through the material. This feature enables the identification of the different physical sections on the differential structure function. If there is a change of one of these parameters, the heat flow path and additionally the structure function will also change. For example, if the cross section area A is known, the thermal conductivity λ can be figured out. A peak in the DSF means a region of high thermal conductivity and a valley a region of low thermal conductivity [1].

4.9.1 Computational effects

4.9.1.1 Floating Point Number

Generally speaking, the Foster to Cauer transformation is an ill-disposed problem. The transformation needs a high precision computation. The higher the number of terms which have to be transformed, the higher the number of digits which are needed. There is no formula indicating the number of digits which are needed to calculate the transformation with enough accuracy. If the number of digits is too low, numerical oscillations can appear. As you can see in the figure below the number of used digits (double precision → 25 digits) is too low for 150 RC pairs. These oscillations can lead to negative values of the thermal resistance or the thermal capacitance of the Cauer network. The negative values are only results of the less precision and do not relate to any physical interpretation [31]. The calculated structure function cannot be used for interpreting the different layers of the device. In Figure 48 it can be seen that the evaluation of the structure function is done with the two Foster to Cauer transformation - algorithms (see chapter 4.8.1 (Fraction decomposition) and 4.8.2 (Fast algorithm)). Regarding Figure 48, the “fast algorithm” of the Foster to Cauer transformation offers a better solution than the simple fraction decomposition. The “fast algorithm” shows fewer numerical oscillations. In the “fraction decomposition” algorithm the thermal resistance has the value of -1.5 °C/W or 3 °C/W. These values cannot be valid because thermal resistances should not become negative. The cause of their appearance can only come from numerical failures. Therefore, all the following calculations are done with the “fast algorithm”.

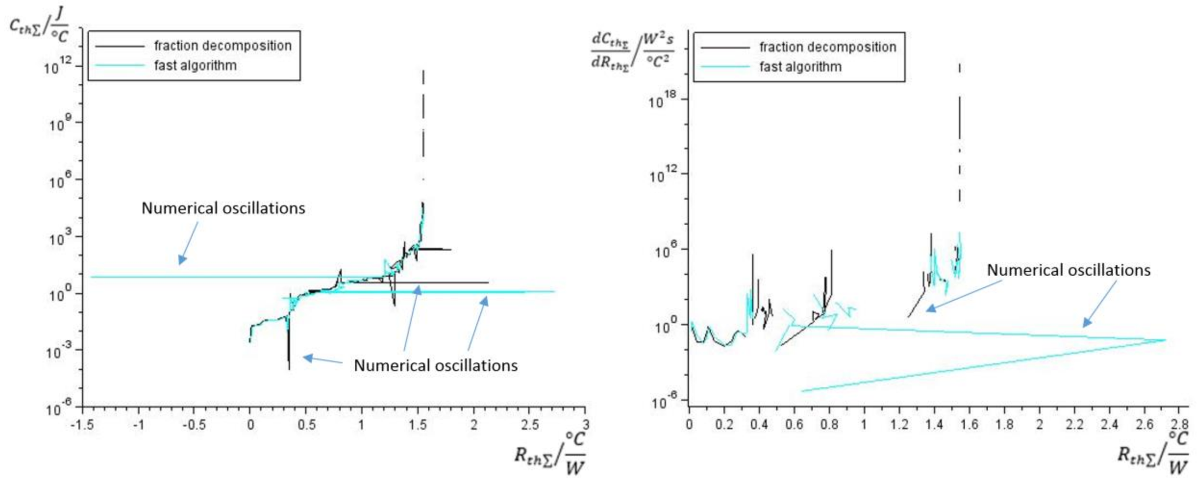

Figure 48: Cumulative and differential structure function calculated with double precision

Regarding the double precision calculation of the structure function as unusable the floating point number has to be expanded. Hence, all further computations are done with quad precision. A quad precision number has 63 significant digits in decimal. The higher number of digits reduces the numerical oscillations (see Figure 49).

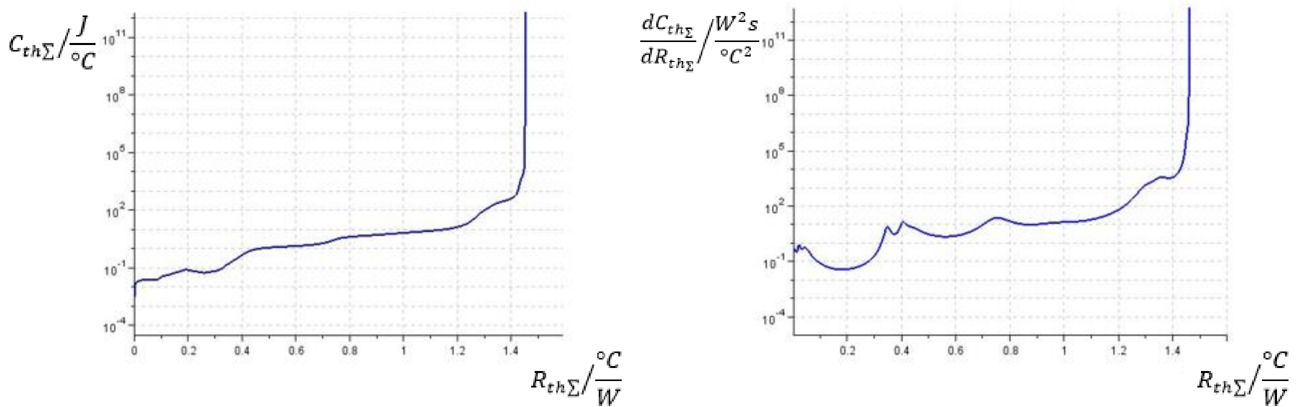

Figure 49: Cumulative and differential structure function calculated with quad-precision

4.9.1.2 Number of RC elements

As mentioned before, the number of RC pairs is significant for the accuracy, but on the other hand a high number causes numerical oscillations. The number of RC pairs (time constants) can be determined by calculating the discretization. In this case, the 101 RC pairs offer the best compromise between accuracy and numerical stability.

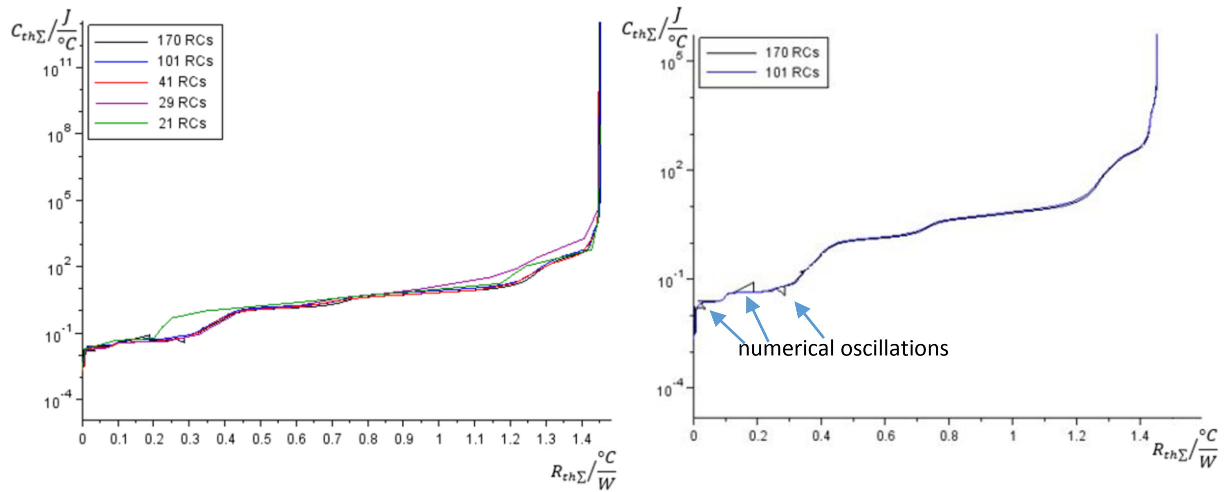

Figure 50: Cumulative structure function with different number of time constants – regarding 101 RCs as best solution

Regarding Figure 50, it can be clearly seen that the cumulative structure functions which are lower than 29 are completely unusable. They do not show the characteristic of the measured device, artifacts may appear. On the right picture the numerical oscillations of the Foster-to-Cauer transformation become visible. Doing the transformation with quad-precision, the computation cannot handle more than 100 RC pairs. The numerical oscillations just occur in low $R_{th\Sigma}$-$C_{th\Sigma}$-regions using more than 100 terms. Concluding, small time constants induce higher numerical oscillations. The differences of the structure curve can be recognized more easily by the differential structure function (see Figure 51).

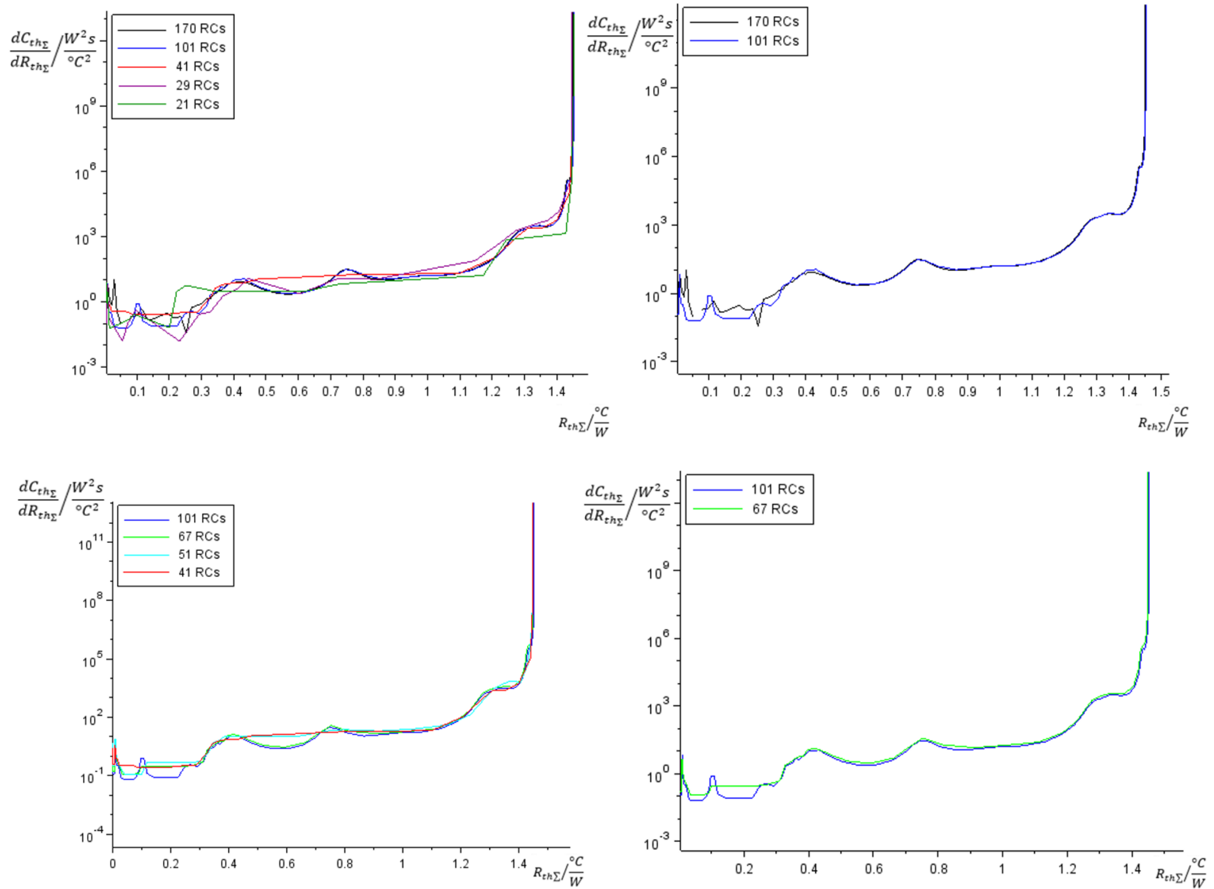

Figure 51: Differential structure function with different numbers of time constants- referring 101 RCs as best compromise

The numerical oscillations occurring at low $R_{th\Sigma}$-$C_{th\Sigma}$-regions can be better seen in the differential structure function representation for 170 RC pairs. The oscillatory behaviour of the curve comes from the Foster-to-Cauer transformation. This happens when a value of the time constant is overestimated. This overestimation is compensated by underestimating the neighbour's time constant. Regarding the cumulative structure function in Figure 50 the calculation with 41 terms can be accepted as a valid result (best resolution without oscillations). However, the differential structure function in Figure 51 shows different conclusions. The computation with 67 RC pairs is already too low since there is a peak vanishing at the low $R_{th\Sigma}$-$C_{th\Sigma}$-regions. Concluding, the discretization with 101 RC pairs offers the best compromise between resolution and numerical stability. The discretization is strongly related to the precision. The number of discretizations (RC pairs) should be selected according to the calculating accuracy.

4.9.1.2.1 Resolution of the measurement (measurement rate)

The resolution of the measurement is also an important parameter determining the accuracy of the structure function. The structure function is very sensitive to the measurement. The

higher the measurement rate the better the resolution of the structure function. The chosen thermal transient has a measurement rate of 1MHz which is the highest possible measurement frequency. This measurement offers the best resolution of the structure function and serves here as reference.

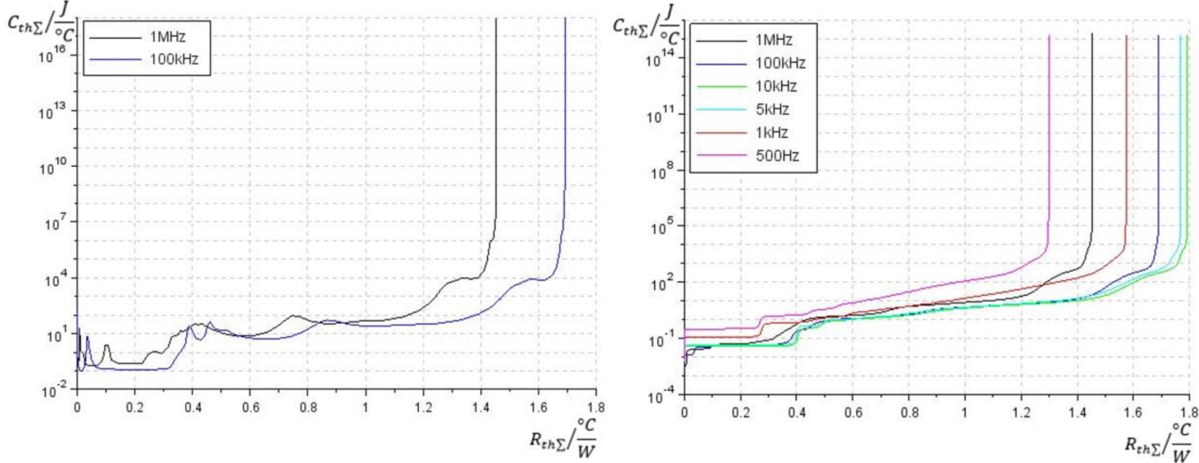

Figure 52: Cumulative structure function with different measurement rates

Even when changing the measurement rate from 1 MHz to 100 kHz, changes in the structure curve can be seen like in Figure 52. A non-negligible effect is that also the junction-to-ambient resistance changes with a changing measurement frequency.

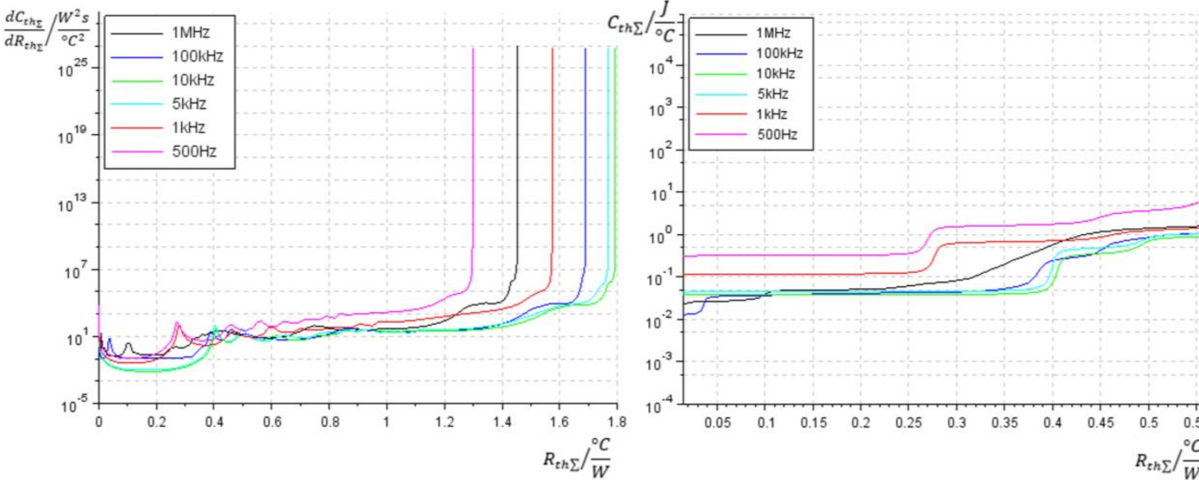

Figure 53: Differential structure function with different measurement rates

In the differential structure function (see Figure 53), big differences can be seen in the low $R_{th\Sigma}$-$C_{th\Sigma}$-region. In this region many features of the differential structure function are hidden when the measurement rate is too low. This comes from the fact that there are no measurement datas. A single RC pair is supposed there.

Generally speaking the evaluation of the structure function is very sensitive to the thermal transient. It depends on a lot of parameters. One important issue is that the measurement should be as accurate and noise-free as possible. Such inaccuracies can be removed by smoothing the input data and choosing a good deconvolution method. However even small errors can produce errors in the time constant spectrum, and as a consequence, in the structure function. Additionally, the Foster-to-Cauer transformation is an ill-posed process too, which requires a high precision calculation. This additionally limits the accuracy of the structure function. If the whole sensitive parameters are chosen correctly, a realistic model of the device's structure can be explored.

5 Simulation

As mentioned in the chapter 2.3.3 that the thermal transient can also be obtained by simulation. Hence, the goal of the simulation is to reconstruct an LED module that has also been measured. The simulation is done a simulation software, called FloTHERM.

5.1 Overview about FloTHERM

The simulation software we used is a 3D computational fluid dynamics software (CFD – Software) called FloTHERM (see Figure 54). FloTHERM specializes in constructing a thermal design of electronic components and systems. Virtual models of electronic equipment are created to perform a numerical thermal analysis. It allows a prediction about the air flow, temperature and heat transfer in and around electronic equipment. This also includes the coupled effects of conduction, convection and radiation [33].

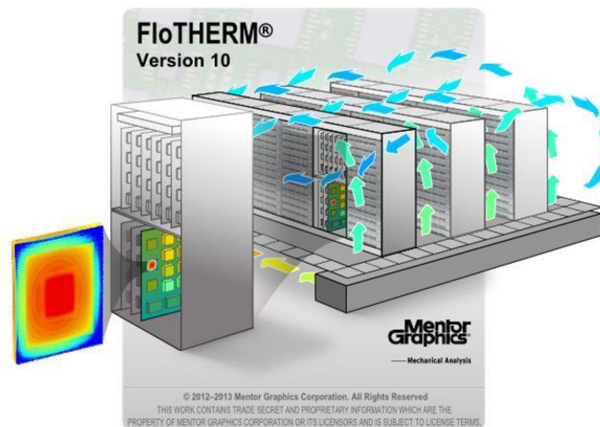

Figure 54: Splashscreen of FloTHERM® [34]

In FloTHERM, the conservation equations are applied and converted into a finite volume form. [35] The space which encloses the model is split up into a finite number of volumes (called grid cells) which are not overlapping. A finite volume form implies that the converted equations demand values of solution in each grid cell. The solution is the resolution of the differential conservation equation with a numerical integral. The number of grid cells determines the number of calculations. In general, the more calculations, the better the resolution, but the longer the computation time will be. Usually, more grid cells are set in regions of the model where the gradients of the variable are expected to be the greatest ones.

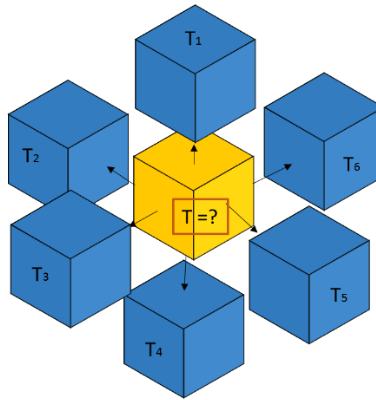

Figure 55: Schematic of finite volume method – Determination of the middle-cube's temperature (T) and the influence of its neighbors

The cell's conservation equation is dependent on the solution of its surrounded grid cells (see Figure 55). So the calculation takes place in an iterative way. The break condition of the iteration is determined by the error of the conservation equation. The solution error should converge. FloTHERM can solve the velocity, the pressure and the temperature in each grid cell. As the heat flow is the point of interest in this scientific work, the temperature is the wanted solution. The temperature should satisfy the conservation equation of thermal energy. The discretized values of the temperature field are situated at the centers of the grid cells. In the region between the two temperature points the solution is simply interpolated. In Figure 55, T stands for the temperature, and the differential equation of the inner volume connects all its 6 neighboring cells ($T_{1\text{-}6}$).

The algorithm of the finite volume method for heat transfer can be summarized as follows [35]:

- Initialize the fields of temperature
- Increase outer iteration count by 1
- Set up coefficients for temperature field T
- Solve algebraic equations for the value of T in each cell by performing a number of inner iterations
- Check for convergence and return to 2 if required

5.2 Geometries and Material parameters

The object for which heat transfer has to be analyzed requires modeling. In the FloTHERM-software the user constructs the geometry of the model and its material parameters (density, heat conductivity, specific heat). The overall dimension of the volume has to be defined which is superimposed by a computational grid. Also the boundary condition of the model has to be set like the temperature of the ambient, the setting of convection (air flow), radiation and heat sources. After these settings the solution can be calculated and the results can be displayed.

At the beginning of the simulation it is of great benefit to take one's time to assess the model. It is important to know the key features (topology, layer thicknesses and material parameters) of the structure of the model. In this thesis, a LED module with one chip is simulated (see Figure 56). This LED is investigated with the aid of a light microscope and a scanning electron microscope (SEM). This helps to see how the "buildup" of the LED is and how much features are included.

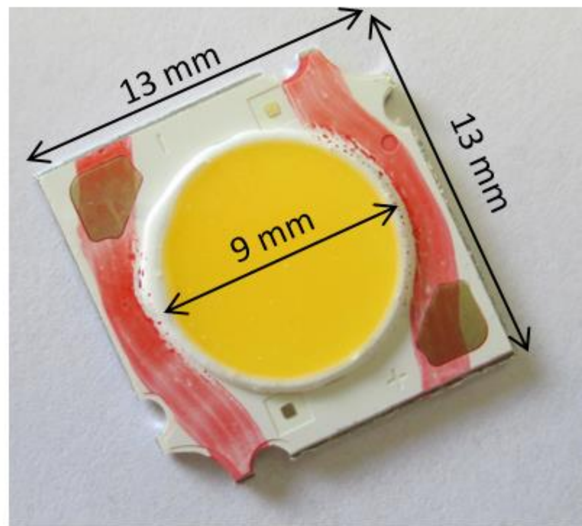

Figure 56: Picture of the investigated one chip - LED module, which has an outer measurement of 13 mm x 13mm and a filler´s diameter of 9 mm

As seen in Figure 56, the outer feature of the LED can be measured, but for the investigation of the inner structure a cross section is needed. As a preparation of the cross section the LED is mounted. The cross section itself is done with a diamond saw. Now the "buildup" of the LED, especially the LED Chip, can be investigated with the light microscope.

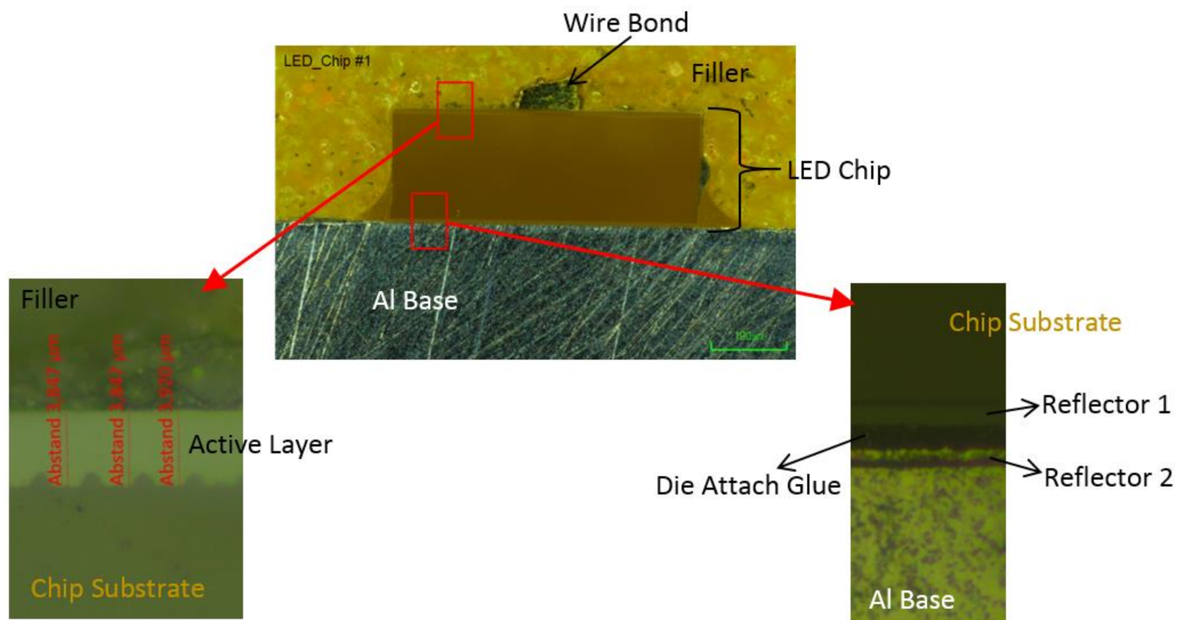

Figure 57: LED cross section investigation at the place of the LED chip via light microscope

With the help of the light microscope the active layer of the LED chip can be seen (see Figure 57) and its thickness can be measured. Furthermore, a multilayer design can be seen under chip substrate. The first layer under the substrate is a reflector layer for an improved light emission. This reflector layer is located next to the active layer and the substrate part of the LED Chip. The next layer is the die attach glue. By means of the die attach glue the LED Chip is mounted on the Aluminum base. As seen in the above picture in Figure 57, the glue has formed a meniscus around the chip which comes from the die attach process. Below the glue layer and above the Al Base another reflective layer can be noticed. For a more precise investigation of the structural buildup an additional investigation with the SEM has been done.

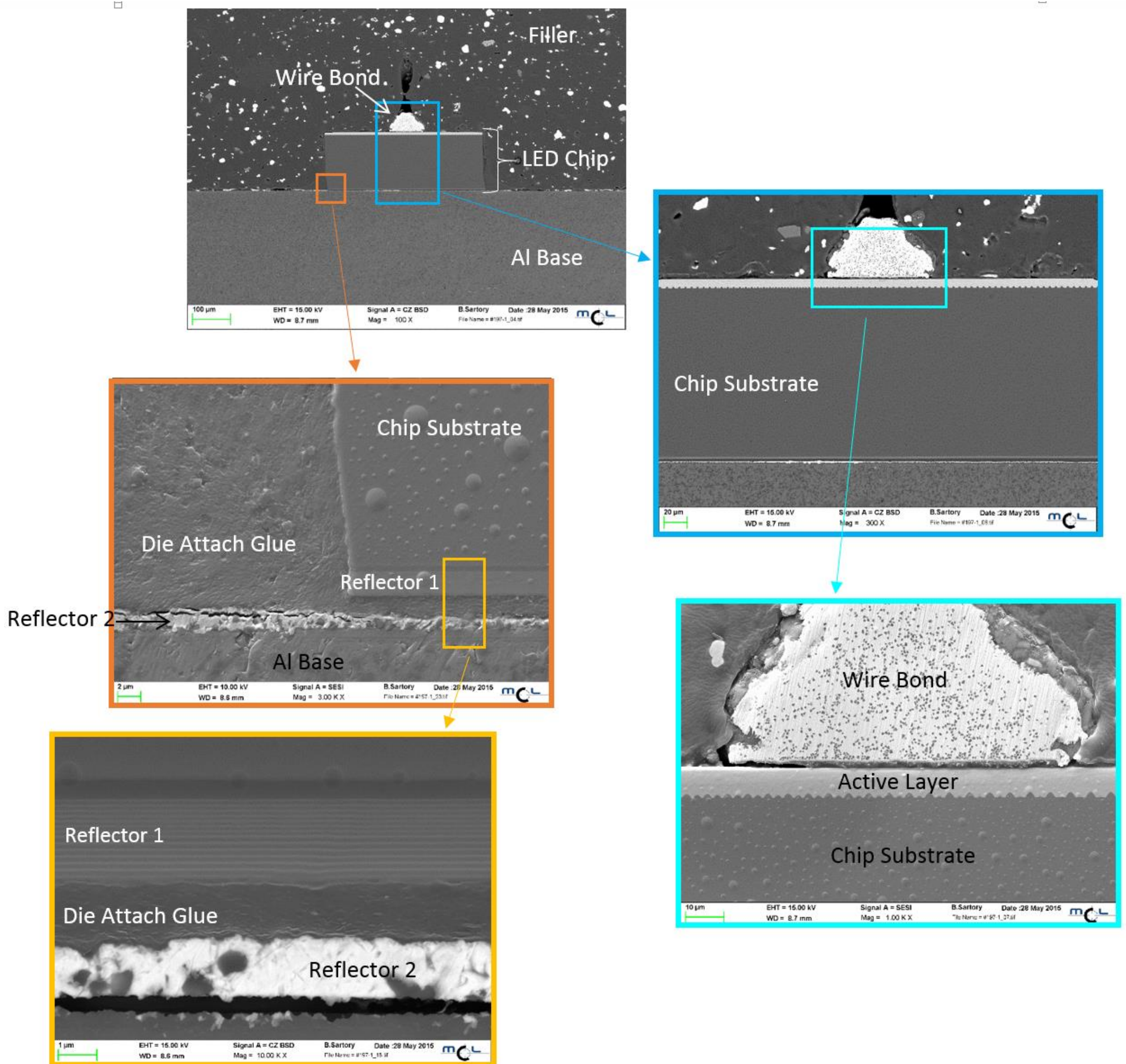

Figure 58: LED cross section investigation with SEM concentrating on the region of the LED chip

On the basis of the SEM pictures (see Figure 58) the multilayer structure can be seen more exactly and the thickness of each layer can be measured. But also the dam of the filler has been investigated; it has the shape of a ring where the LED chip is situated in its center (see Figure 59).

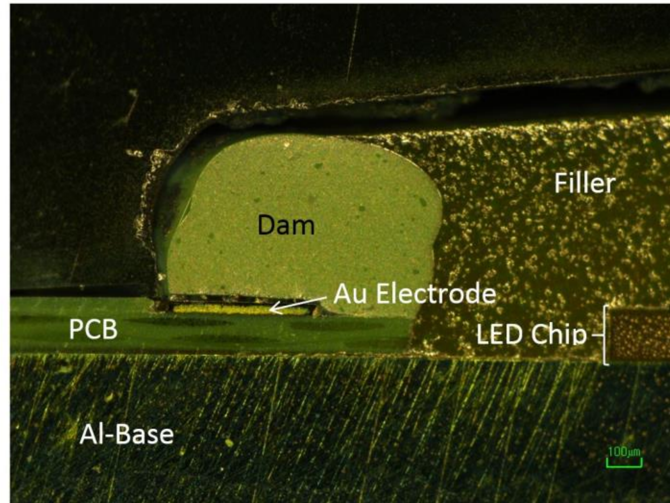

Figure 59: Investigation of the left part of the dam at the cross section

All the measured dimensions of the cross section are summarized in Table 4.

Table 4: Measured dimensions of the investigated cross section of the LED module (all the measurements have a relative error of 5% which comes from the inaccuracy of measuring)

Region	**Height / µm**	**Width / µm**
Active Layer	7.2	510
Chip Substrate	150	510
Reflector 1	2.7	510
Die Attach Glue	1.7	510
Die Attach Glue Meniscus	40	40
Reflector 2	1.3	13000
Al Base	1500	13000
Dam	480	760
PCB	100	4000
Au Electrode	32	400

Based on the knowledge of the investigation a schematic of the cross section can be made (Figure 60):

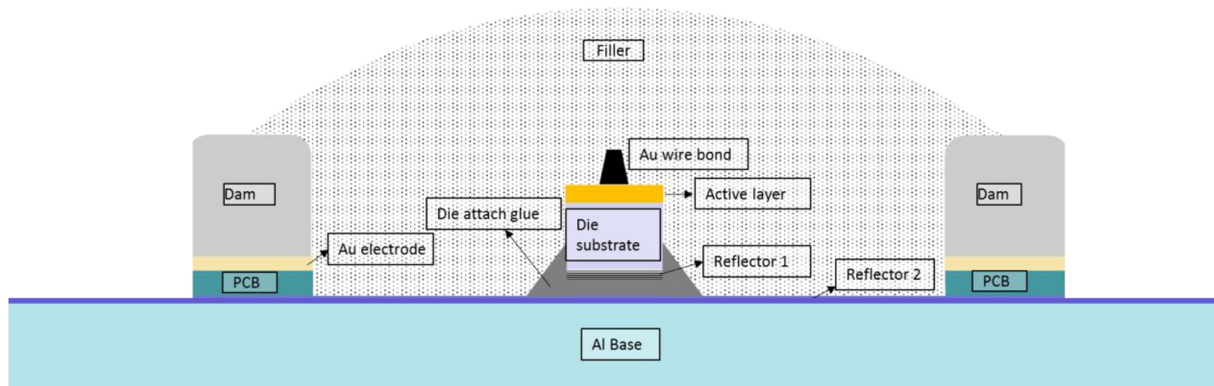

Figure 60: Schematic buildup of the investigated LED

Another important factor, beside the dimensions, which may affect the result of a simulation are material parameters. For the most common materials the material parameters are supposed to be known and so literature values are used. Other materials, whose properties are not known, need an investigation with the aid of EDX (**e**nergy **d**ispersive **X**-ray spectroscopy). This is an additional investigation feature on the SEM. Via EDX-investigation an element analysis of the material is possible. Additionally, a literature search should be performed in order to have an idea of the range of probable material parameters. The presented overview table (Table 5) shows all the initial material properties of the simulation.

Table 5: Material properties (density, specific heat and thermal conductivity) of each region in the chosen LED

Region	Assumed equivalent material	Density/ $\frac{g}{cm^3}$	Specific heat/ $\frac{J}{kgK}$	Thermal conductivity/ $\frac{W}{mK}$	Source
Active Layer	GaN	6.1	490	130	[36]
Chip Substrate	Sapphire (Al_2O_3)	4.0	761	17	[37]
Reflector 1	TiO & SiO_2	4.0	680	17	Datasheet
Die Attach Glue	-	1.2	1423	0.2	Datasheet
Reflector 2	Ag	10.5	235	385	FloTHERM
Al Base	Bulk -Al	2.7	963	180	FloTHERM
Dam	Silicone	1.2	1400	0.2	FloTHERM
PCB	FR4	1.2	800	0.3	FloTHERM
Au Electrode	Au	19.3	132	296	FloTHERM
Filler	-	1.2	1600	0.3	Datasheet

These values are only literature values and do not always correspond to the real materials in the LED. After the initial setting the model can be built in the CFD-software (Figure 61).

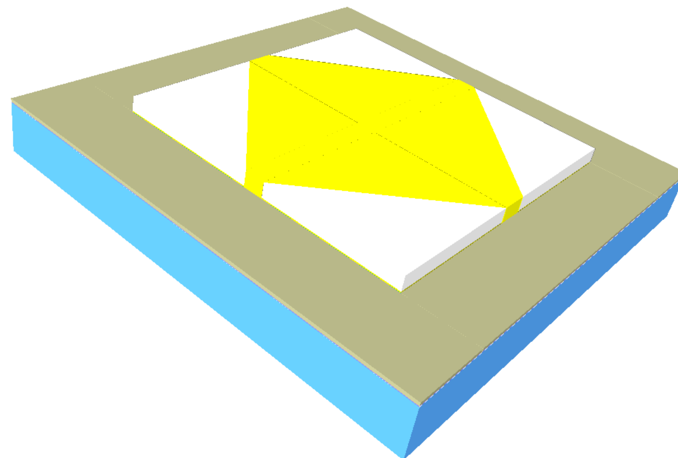

Figure 61: Appearance of the simulated LED

5.3 Process of simulation

The modeling takes into account not only the 3D-structure, but also the topology of the cell generation. FloTHERM is a finite volume-based software. The volumes (cells) have to be defined for the model. They are based on a Cartesian grid system. The number of the cells can be defined separately for each object. Near the heat source, there are key features of the model. It is substantial to concentrate more cells at these objects, because the greatest temperature gradients can be found there. In the LED's case the essential part is the active layer which is also the heat source of the device. Furthermore, it is recommended that there are at least three cells in each object.

Before running the simulation the boundary condition of the model has to be set. The boundary conditions should be as close as possible to the ones in the real LED during the experiment:
The simulation has an ambient temperature of 25°C.
The computational domain has the same size as the LED model itself.
The heat only dissipates through conduction due to the fact that the structure function is basically a conduction issue. The convection and the radiation are neglected because they have little influences.
The liquid-cooled cold plate has been realized as a volume with a fixed temperature (25°C).
The junction has a power of 307 mW, which is the same power step used in the experiment.
Applying the junction's power the model reaches an equilibrium after some time. This equilibrium is the initial steady state of the model. It's the so-called "hot" steady state of the simulation (see Figure 62).

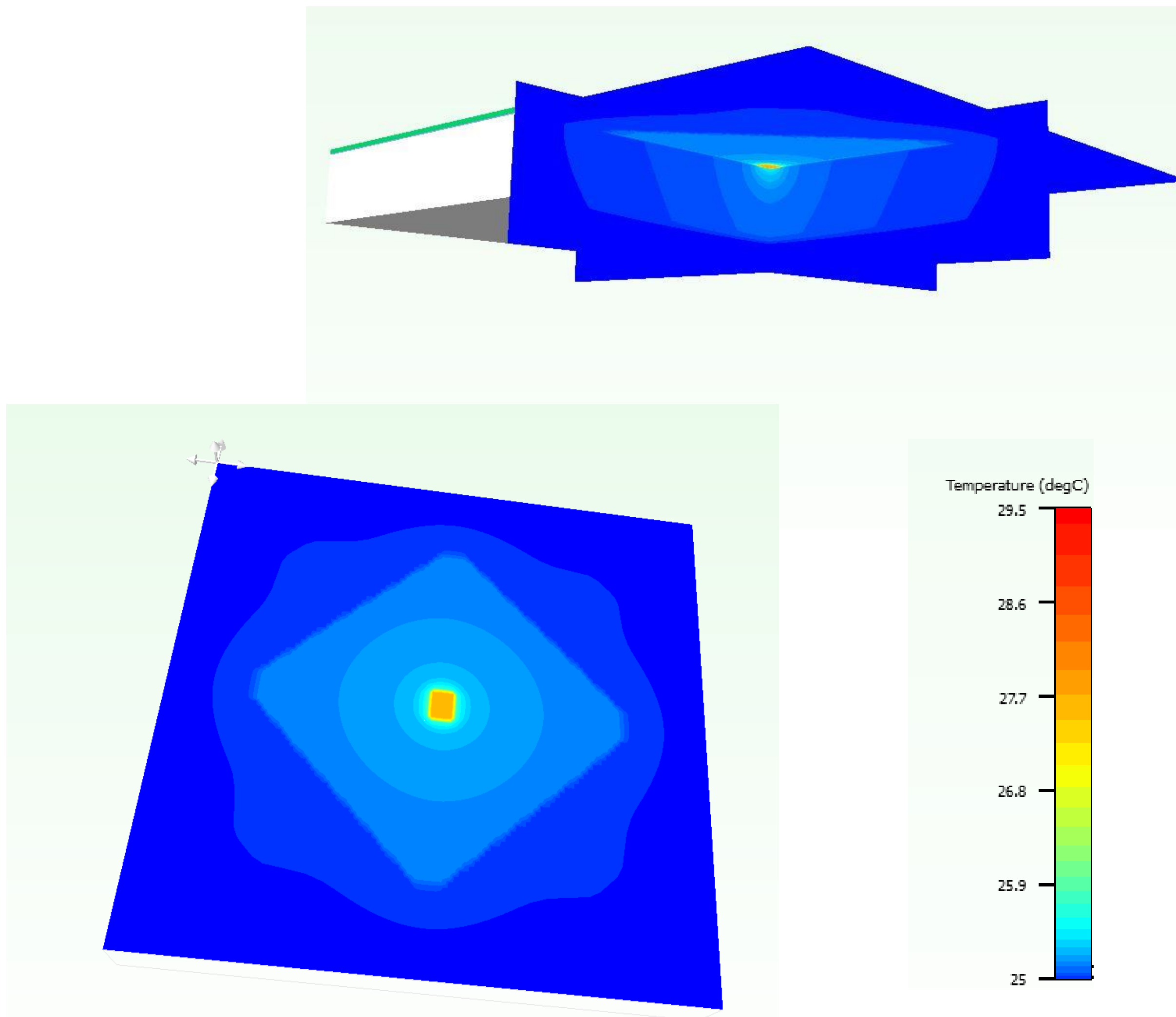

Figure 62: Hot steady state of LED model -the active layer has a power of 307mW (lower picture: top view; upperpicture: side view)

After reaching the “hot” steady state in the simulation, the power of the active layer can be turned off (P = 0W) at t = 0 s. This results in a time-dependent temperature change from the “hot” to “cold” steady state. The temperature of the cold steady state should be the same as the ambient temperature. This temperature drop as a function of time can be recorded if a monitor point is placed into the key area (LED: center of the active layer). The time range of the temperature change can be configured. This results in a simulated thermal transient. The simulated transient is the time dependent temperature change of the center of the active layer of the LED after the power step. Before trusting the simulation results an estimation of the results should be made by doing a “sanity check” of the simulation outputs. Here the estimation comes from a measurement of the real LED with the same power step. Monitoring this temperature drop, makes it possible to investigate the thermal behavior of a 3D-modell as a one dimensional function.

6 Calibrated system

The implementation of a geometrical model of the LED device in CFD simulation software (see chapter 5.2 and 5.3) allows to compare simulation results and experimental measurements. Now it is possible to verify the thermal model against the real model. This permits the establishment of a validation flow to gain a calibrated model.

6.1 Validation Flow

In order to get a calibrated CFD-model a validation flow, as depicted in Figure 63, is applied.

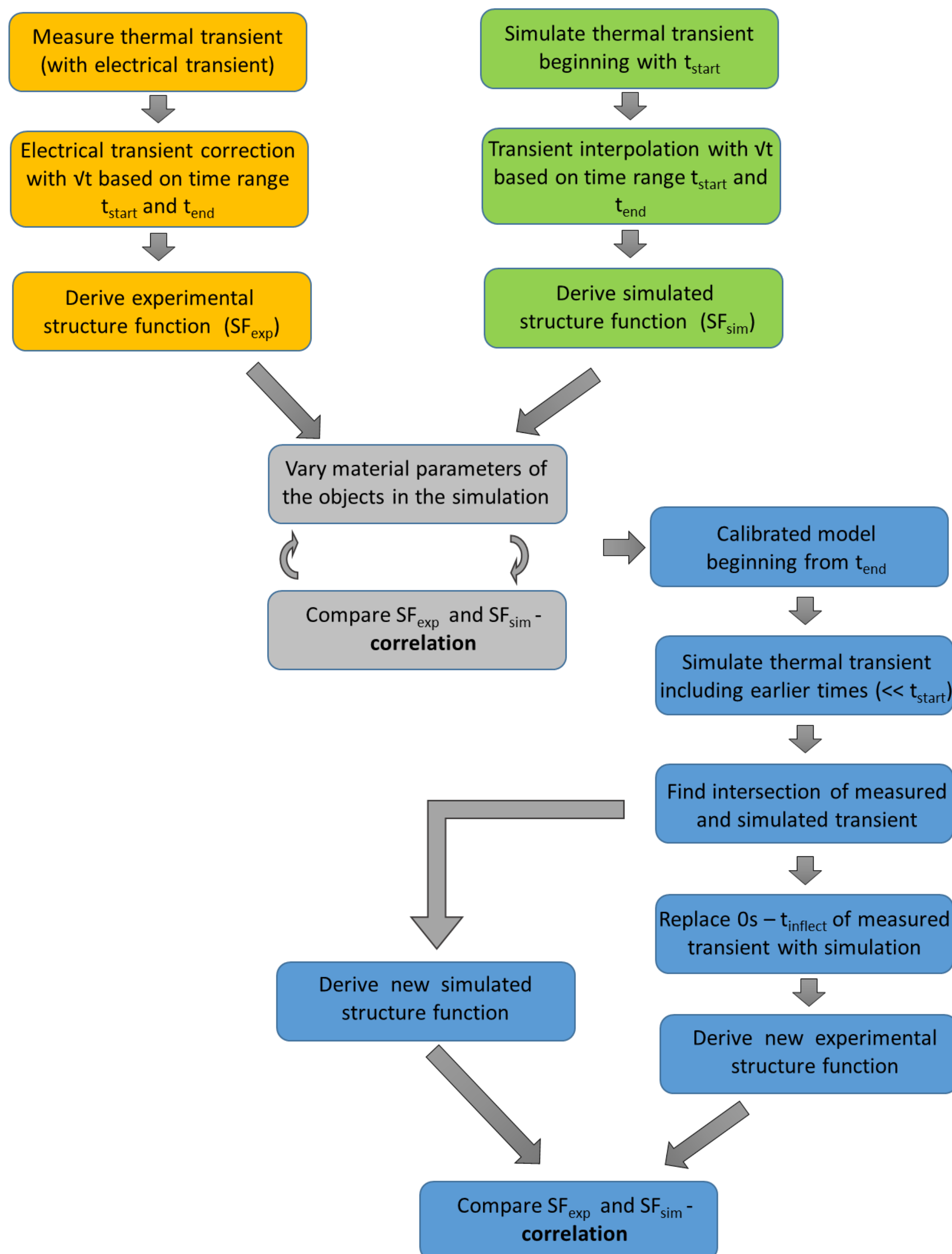

Figure 63: Schematic representation of the validation flow

6.1.1 Experimental structure function

The validation flow starts with obtaining the thermal transient from the measurement. In this experiment the LED module, which is described in chapter 5.2, is mounted with a thermal paste on a liquid-cooled cold plate. The ambient temperature is held to 25°C. The measurement is done using the T3ster system (as described in chapter 3.1). The voltage of the LED's junction is calibrated resulting in a K-Factor of -1.023 mV/°C. The applied power step has a value of 300 mW causing a junction temperature change. The duration of thermal transient record is 120 s, allowing to get from one steady state to the other. This thermal transient still includes the electrical transient (see chapter 3.3) which has to be corrected. The correction of the thermal transient is done by a square root interpolation over the time. The extrapolation of the line should fit the curve in the chosen time range t_{start} - t_{end} as well as possible. After the electrical transient correction the structure curve can be evaluated (SF_{exp}) (see Figure 64).

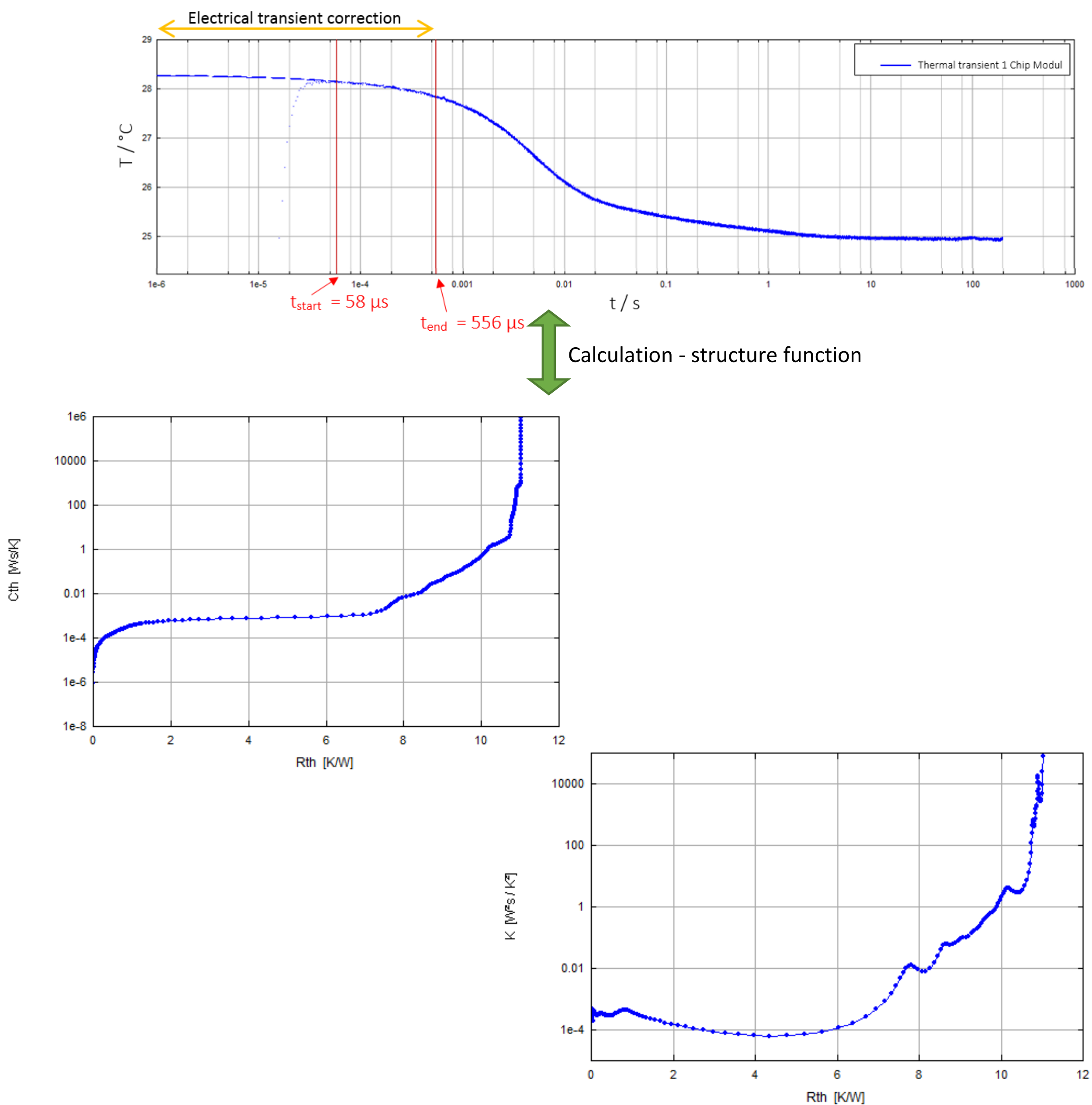

Figure 64: Thermal transient (upper picture), CSF (left lower picture) and DSF (right lower picture) of measured one Chip-LED-module

Additionally, the experiment is again performed with the same LED and the same settings except there is no thermal paste between device and cold plate. Comparing the two measurements of the chosen LED, gives a hint which part of the structure function belongs to the device and which part belongs to the heat sink and the thermal paste. The knowledge of this is helpful for the interpretation of the structure function and serves also as an orientation in the simulation. Figure 65 shows that the divergent point and the beginning of the thermal paste are at a thermal resistance of ~9 K/W.

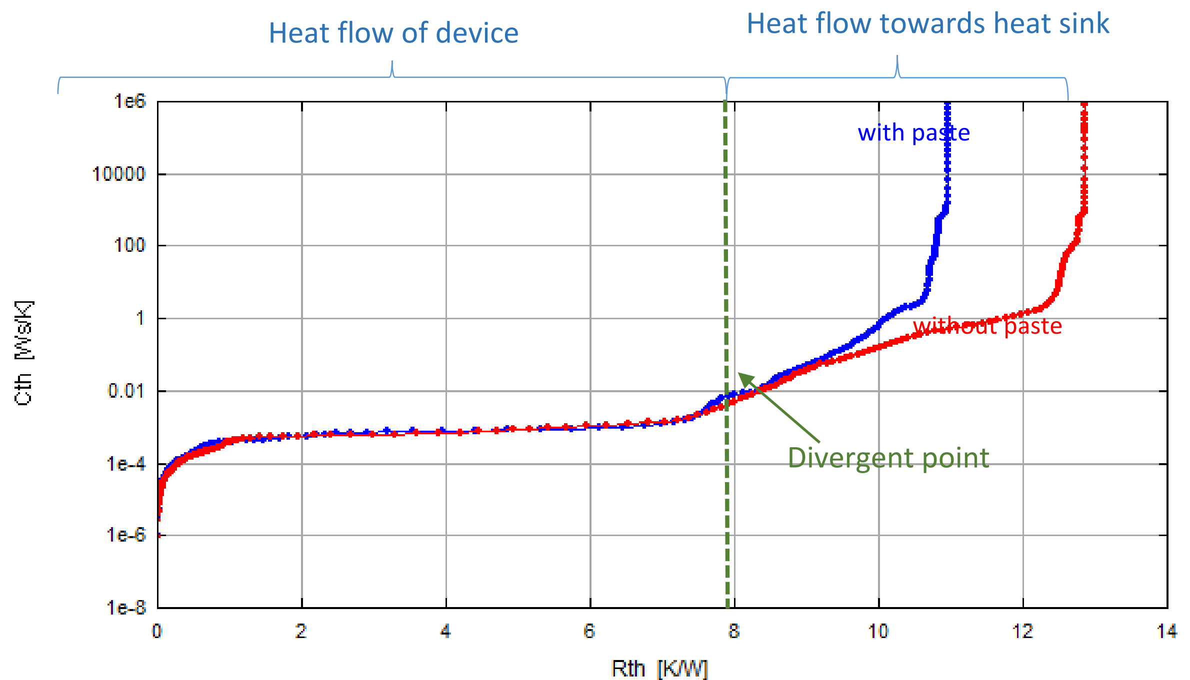

Figure 65: Structure functions of measurement – one with thermal paste, other without thermal paste

6.1.2 Simulated structure function

As described in chapter 5, a CFD simulation model of the above mentioned experiment is established by using FloTHERM. As initial value the active layer has a power of 307 mW and at time t = 0 s it is turned off. This power switch results in a temperature change which can be calculated in the software. The simulated thermal transient is the temperature change of the central point of the active layer. The simulated thermal transient has the same duration as the experiment. 15 time steps are defined per decade starting from t_{start}. The time steps increase in size and subsequently allow to achieve a smooth transition from one time step to the other between different decades. Since the starting time is not 0 s, the same transient extrapolation, as in the experiment, has to be made. Then the transient can be converted into the corresponding structure function (SF_{sim}) (see Figure 66).

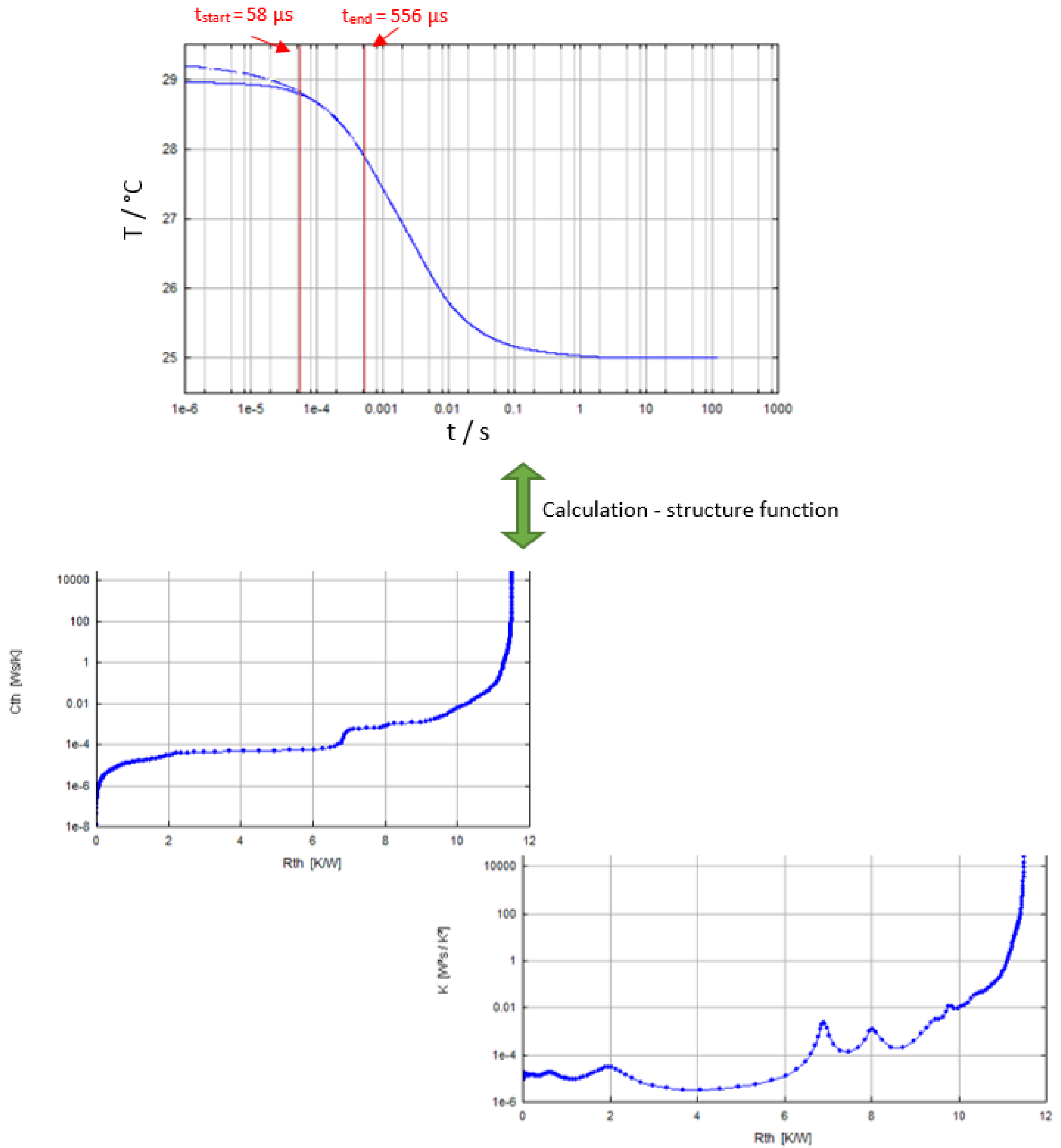

Figure 66: Cumulative (left) and differential (right) structure function of the simulated thermal transient (upper picture)

6.1.3 Correlation between measured and simulated structure function

The simulated structure function is iteratively adjusted to the experimental structure function in the following way. In a first step it is assured that the simulated structure function shows the same topology as the experimental structure function, thereby evidencing that all relevant layers and interfaces have been considered (see Figure 67). In Figure 67, the arrows try to match the peaks in the differential structure function between measured and simulated. The peaks correspond to objects where the thermal capacitance is much higher than the thermal resistance. E.g. this can be related to metallic objects. Vice versa, valleys have a lower relation

between R_{th} and C_{th}. The next step is to do perturbations to the numerical model at known locations starting at the die and going through each layer in the model. By subsequent iteration steps, one finally arrives at a ‘good enough’-model. If the two structure functions match sufficiently, the numerical model can be regarded as “calibrated”.

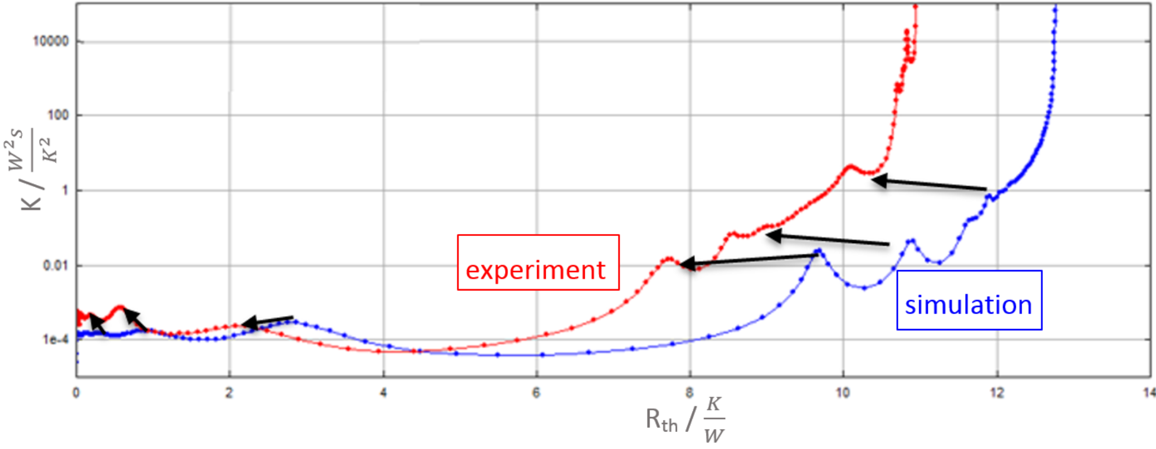

Figure 67: Comparison of the differential structure function of experiment and simulation – assure the correct number of objects in the model

6.1.3.1 Calibration of die

It is helpful to start the calibration from the heat source outwards. Therefore, the iterative correlation process of the LED starts with the adjustment of the active layer (see Figure 68). In Figure 68, the blue line is the measured structure function. First, it can be seen that the thermal capacitance of the initial simulated structure function (green line - named a) is too low. Therefore, the capacitance of the active layer has to be increased. The capacitance can be modified by enhancing the area of the active layer, changing the density and the specific heat of the GaN. All these modifications (the area is 0.2 mm^2 bigger, the density and specific heat are doubled) result in the red line. The red line shows an exceptionally high thermal capacitance; therefore the density is reduced again. After making these changes the enhancement of the area and the doubling of the specific heat helps to move the thermal capacitance to correct level. The yellow line represents the new initial position of further variations.

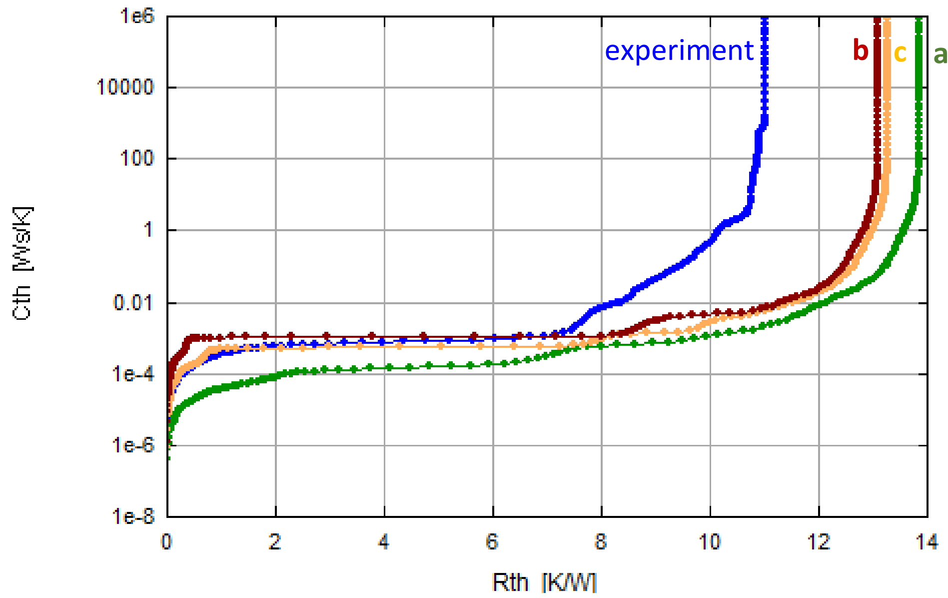

Figure 68: Correlation of the active layer; starting the iteration from a to b to c

The next layer, where perturbations are made, is the substrate of the chip. In Figure 69, it can be seen that the first flat section of the curve corresponds to the die substrate. Alternating the thermal conductivity of the sapphire leads mainly to a change of the flat section's length (thermal resistance). In addition, the thermal resistance of the section behind the curve's flat region is also slightly influenced by the thermal properties of the chip substrate. Modifications of the die substrate's capacitance show no effects in the curve.

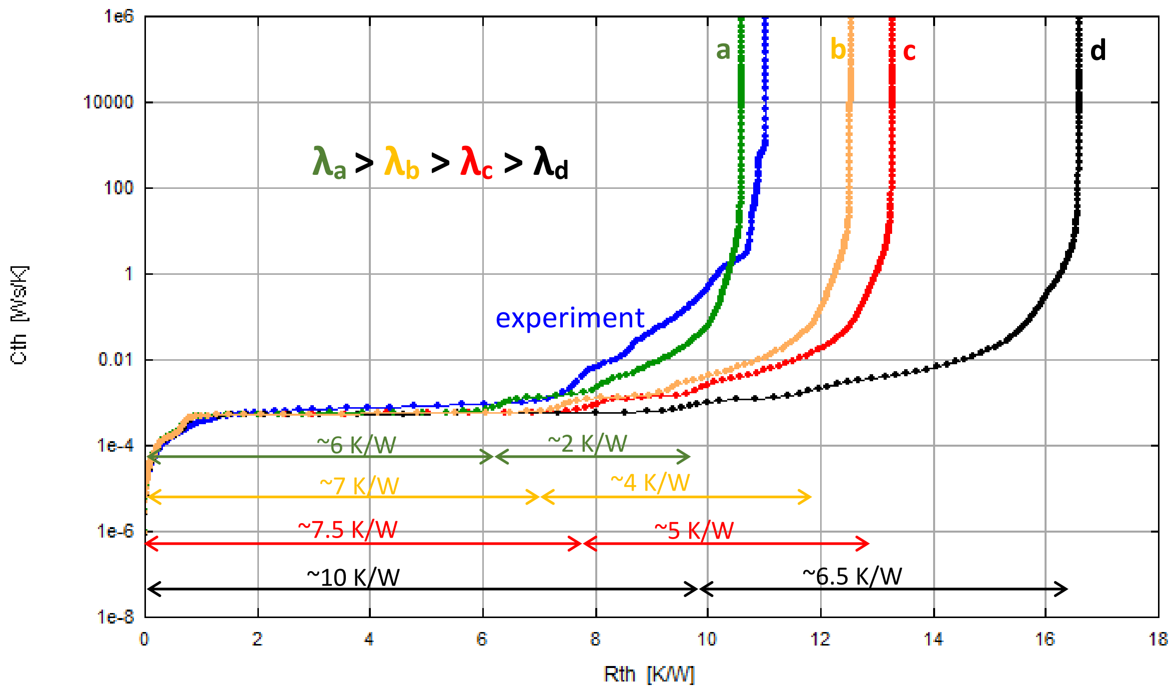

Figure 69: Modification of the die substrate – simulations have different thermal conductivities

Variations of the reflective layer under the die substrate do not show any changes in the structure function.

6.1.3.2 Calibration of the die attach

The next layer which is modified, is the die attach (see Figure 70). Variations of the die attach's thermal conductivity influence the thermal resistance of the flat section and also the length of the further part of the curve. Changing the specific heat of the die attach glue doesn't shape the simulated structure function. The thermal conductivity of the die affects more the thermal resistance of the flat section than the die attach glue. The curve b in Figure 70 is now the initial point of further modifications.

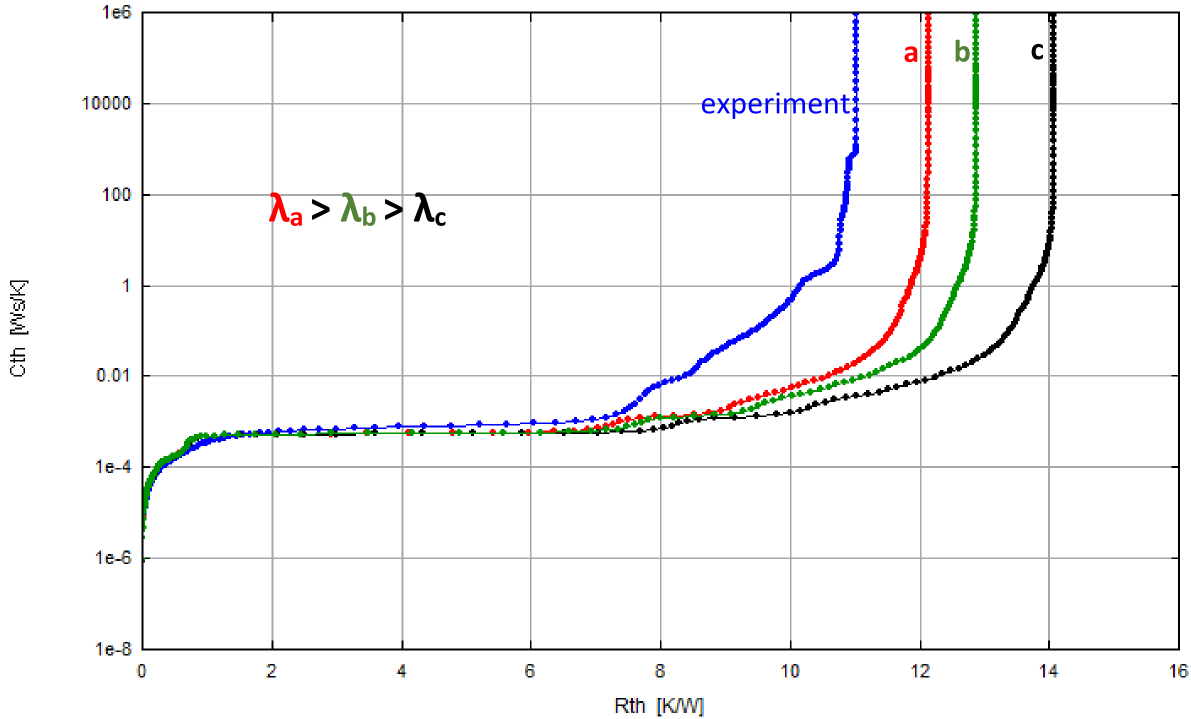

Figure 70: Modification of the die attach glue – different thermal conductivities

6.1.3.3 Calibration of filler

The next step is changing the filler capacitance in order to see its effects in the structure function. Starting the perturbations with the grey line (d) (see Figure 71:) from the previous iteration step (see chapter 74766.1.3.2) the filler corresponds to the steep section right after the flat region. Based on d, the ratio between capacitance and resistance of the filler is changed by varying the specific heat (higher) and the conductivity (lower) of the filler. This variations result in line c, which still shows a capacitance which is too low. Therefore the specific heat is enhanced again – line a and b. The yellow line b shows a pretty good fit to the experimental structure function.

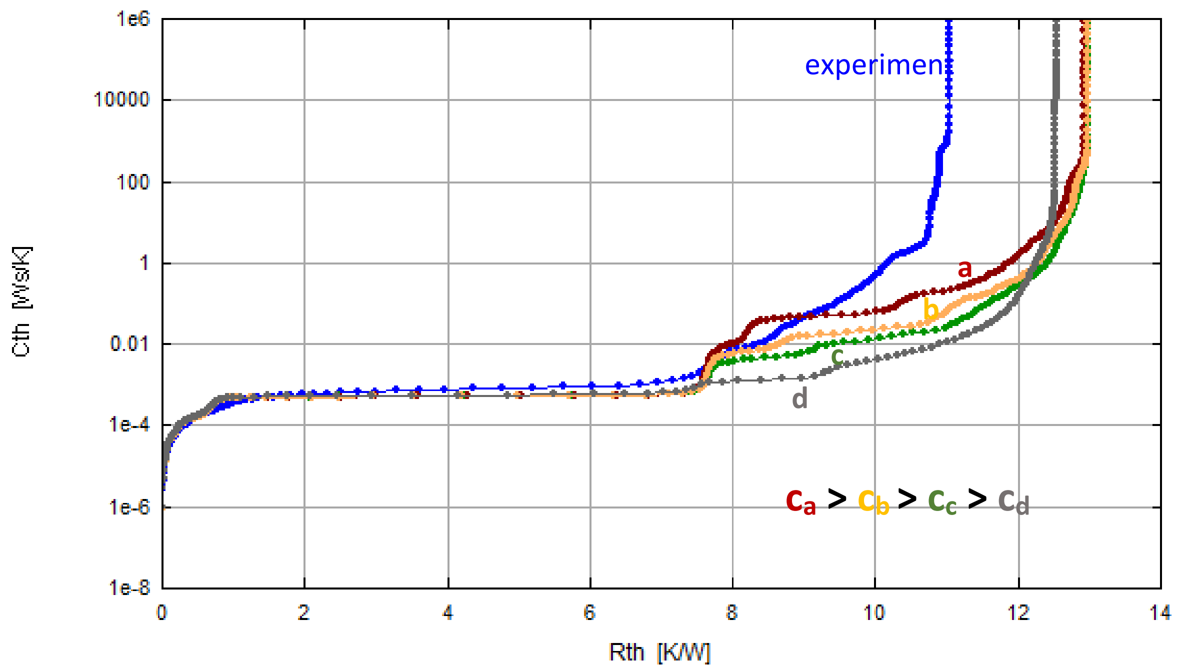

Figure 71: Filler calibration – the lines have different specific heat values, line b shows the best fit to the experiment

However, the total thermal resistance in Figure 71 does not show the right value compared to the measurement. The influence of the thermal conductivity of the filler has to be investigated (see). The thermal resistance of the filler has great influence on the ratio between flat section and the rest of the structure function. A higher thermal conductivity means a larger thermal resistance of the curve behind the flat section. The arrows in Figure 72 indicate the regions where the thermal resistance becomes higher.

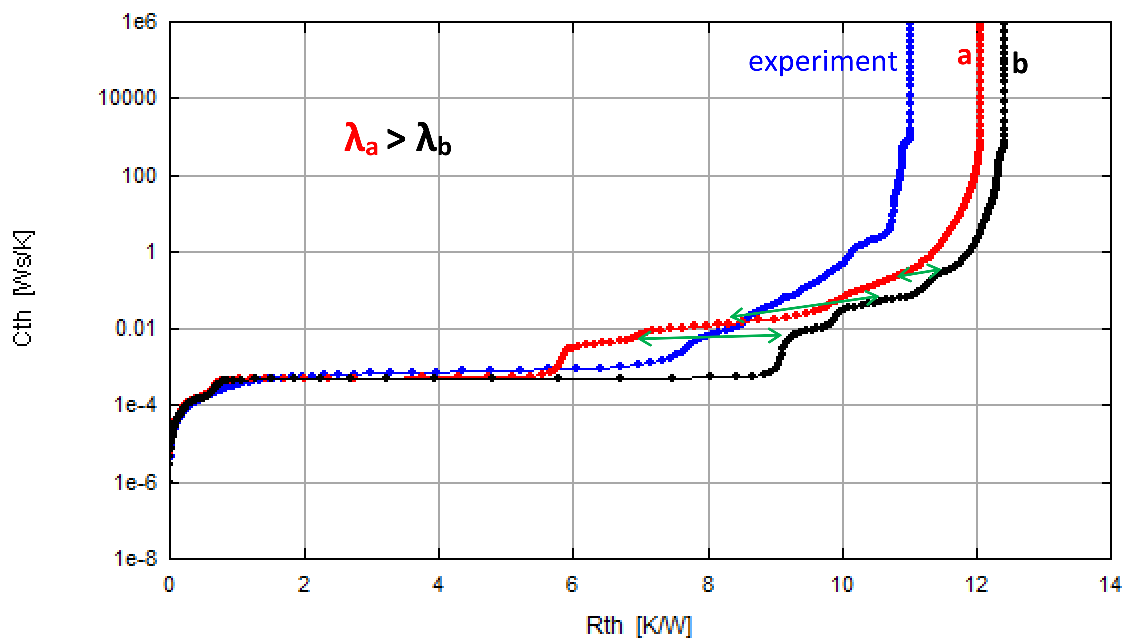

Figure 72: Influence of the filler's thermal conductivity

With the knowledge of the different influences of the layers (described in 6.1.3.1, 6.1.3.2 and 6.1.3.3) in the structure function, it is important to find the right relation between their thermal resistances. The first steep section is a good indicator of the correct thermal conductivity of the objects. This process is not easy as many iterations are required. To be precise, only three iterations (a, b, c) are shown in Figure 73. Starting with the line a it can be seen that the total thermal resistance is too high. Following the thermal conductivity of the filler and of the die substrate has been reduced and the one of the die substrate has been enhanced resulting in curve b. The line b has a total thermal resistance which is too low, therefore the thermal conductivity of the die attach glue has been reduced and the thermal conductivity of the die substrate has been enhanced. Its outcome is line c where the total thermal resistance of the simulation matches the experimental one. Further modifications of the structure function have been done with line c.

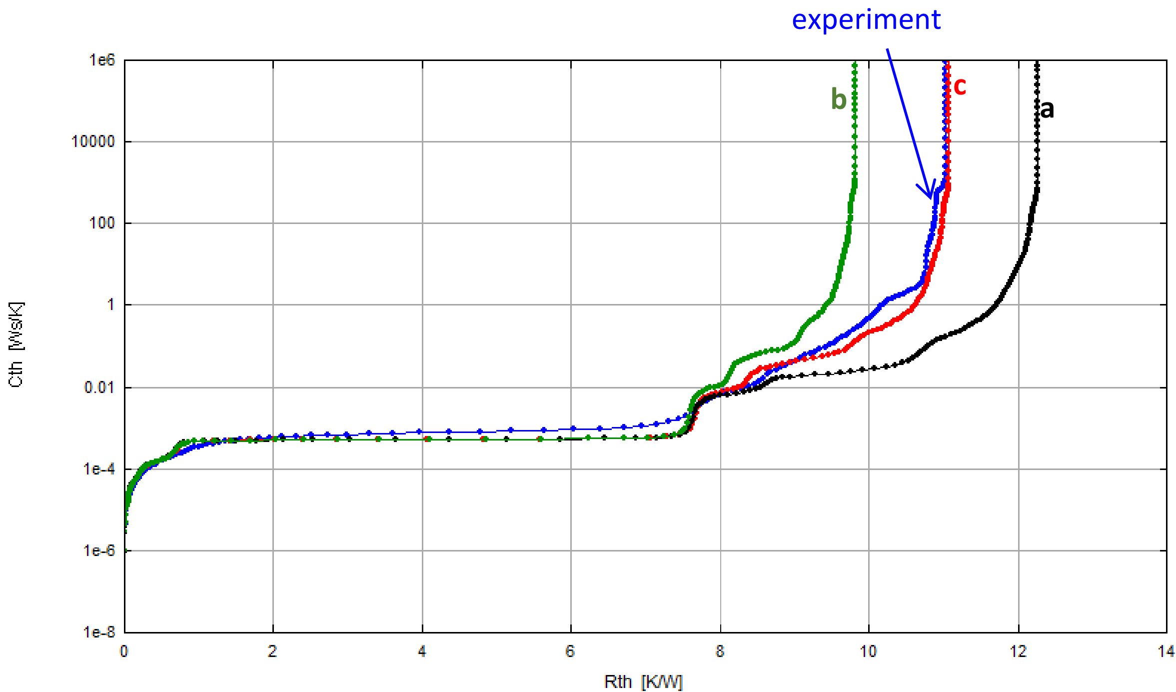

Figure 73: First iterative adjustment of the structure function

6.1.3.4 Calibration of Al base

After the adjustment of the flat section and the total thermal resistance further calibrations can be done. The Ag- Recflector, which is situated above the Al base, has been modified. It has no influence on the shape of the curve. Hence, the thermal properties of the Al base have been varied (see Figure 74). With the iterative modifications the model fits more and more the experiment. In the first step from 1 to 2 the specific heat of the Al's thermal capacitance has been enhanced. Then the specific heat of the filler followed by the thermal conductivity of the Al base has been reduced. Further the specific heat of the filler was reduced again. From 4 to 5 the value of the thermal conductivity of the Al base and the specific heat has been

lowered. As a last step the specific heat of the Al base has been enhanced. The resulting structure function in Figure 74 – picture 6 offers a quite good match between simulation and measurement.

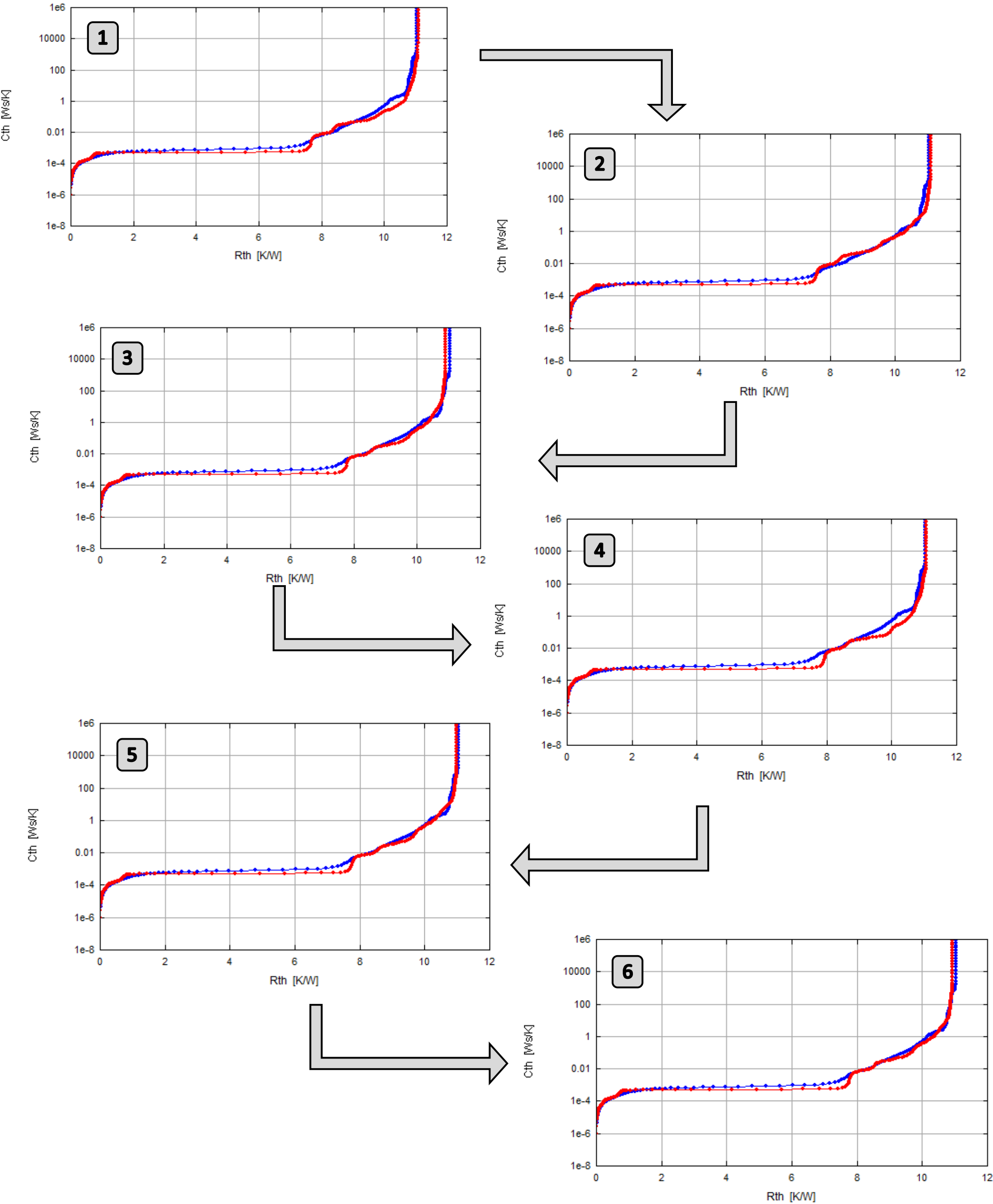

Figure 74: Correlation of the simulated (red) to the measured (blue) structure function with the help of modification of the properties of the Al base

6.1.4 Electrical transient correction based on the simulation

After the calibration process it can be assumed that the simulation offers an approximation of the measurement. Also the measured and simulated thermal transients are approximately the

same. The correction of the electrical transient which occurs in early sections of the thermal transient measurement is also a good approximation. However, the calculation of the valid time *(t_{valid} = 2 µs)* (see equation (15)), in which the correction is allowed, is exceeded. Substituting the electrical transient of the experiment with the simulated transient can offer a better initial transient correction. First of all the intersection point of the measurement and simulation has to be found to combine the two curves [38]. The appropriate point should lie in the time range between t_{start} and t_{end} (see chapter 710). After finding the time of the intersection (here: 4.5 µs) the early section of the electrical transient can be replaced by the simulated transient (see Figure 75).

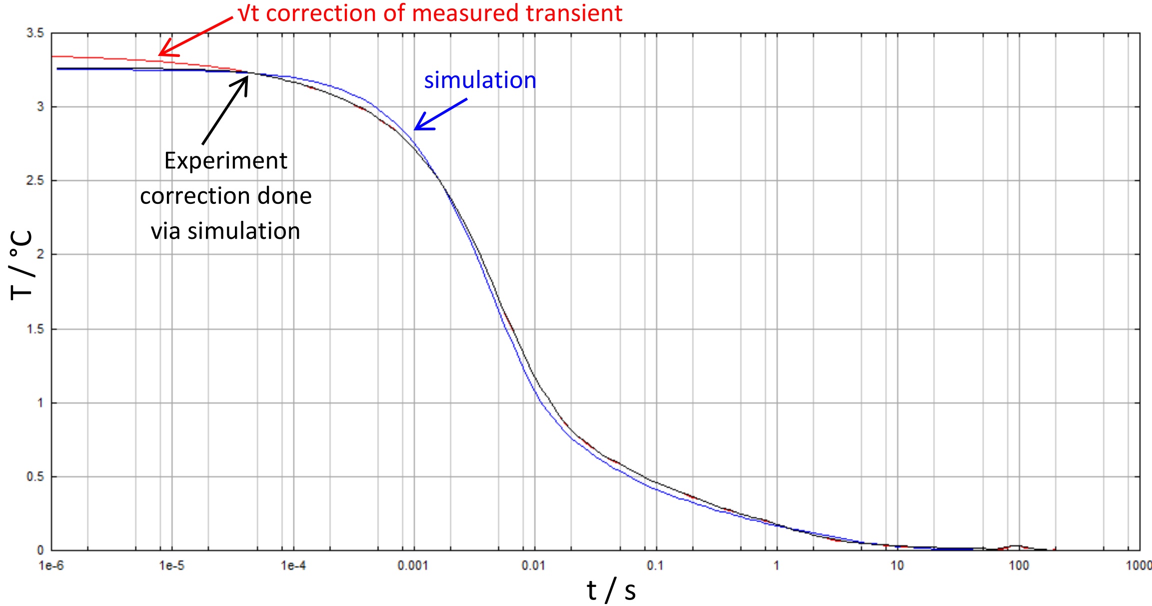

Figure 75: Replacement of the early sections of the measured thermal transient

After correcting the "newly" measured thermal transient the simulated and uncorrected thermal transient is transferred into their structure function again. In Figure 76 the two new calculated structure functions are compared to the √t-corrected structure function of the experiment. It can be seen that the initial slope (in the range of 0 K/W to 1 K/W) is caused by a numerical artefact of the square root correction. It does not correspond to a physical object in the LED. Due to lower initial temperature of the newly corrected thermal transient the total thermal resistance is also lower.

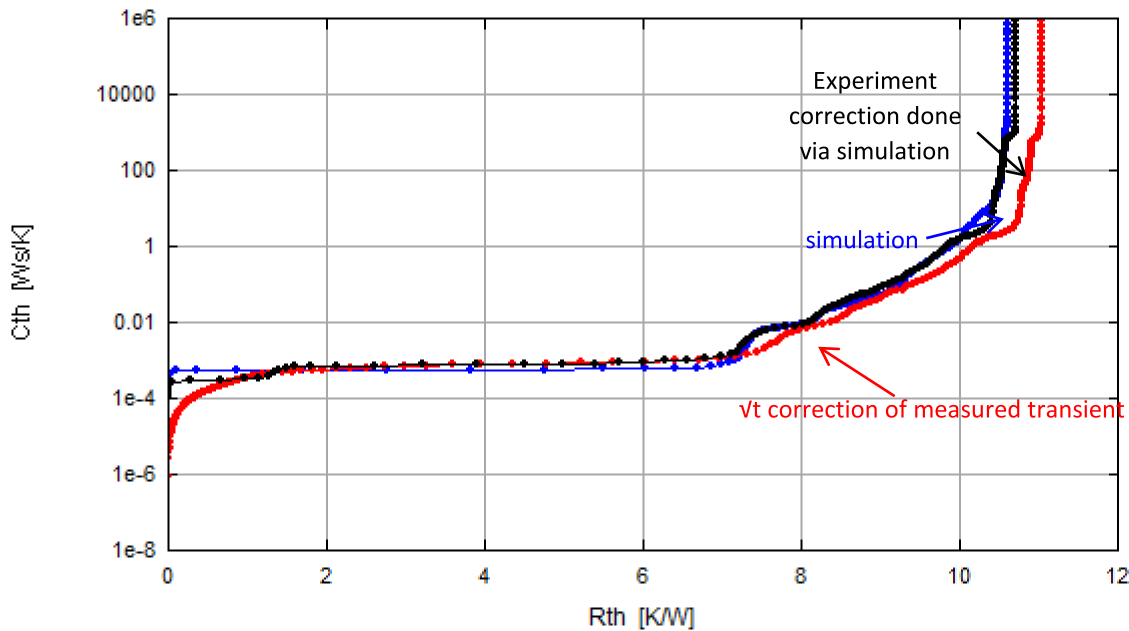

Figure 76: Cumulative structure function of the simulation and the experiment with two different electrical transient corrections

6.2 Results of the validation flow

The structure function is a very useful tool for comparison. This property is used to compare and adjust the simulation to an experiment. With the aid of the iterative calibration it is also possible to identify the source of the difference between the two curves. The source of the observed difference can be assigned to a structure in the LED. This would make analyzing simulated and measured thermal transients more difficult. It can be seen that the shape of the transient is similar, but the origin of the difference cannot be found out. The methodology to use the structure function has been working well as long as correlations between features of the curve and physical objects can be made.

It has been shown that LED, where the die chip is coated with a filler has a more complex heat flow path. There, its structure function does not follow sequentially the terms of the physical structure of the device. The layers occur on the curve in order in which the heat conducts them after the power step. However, there is still the correspondence between thermal properties of a structure in the device and a feature in the structure function (see Figure 77). The calibration process in the validation flow shows that in the detailed model the thermal behavior of the active layer, the die substrate, the die attach glue, the filler and the Al-Base are important parameters of the structure function.

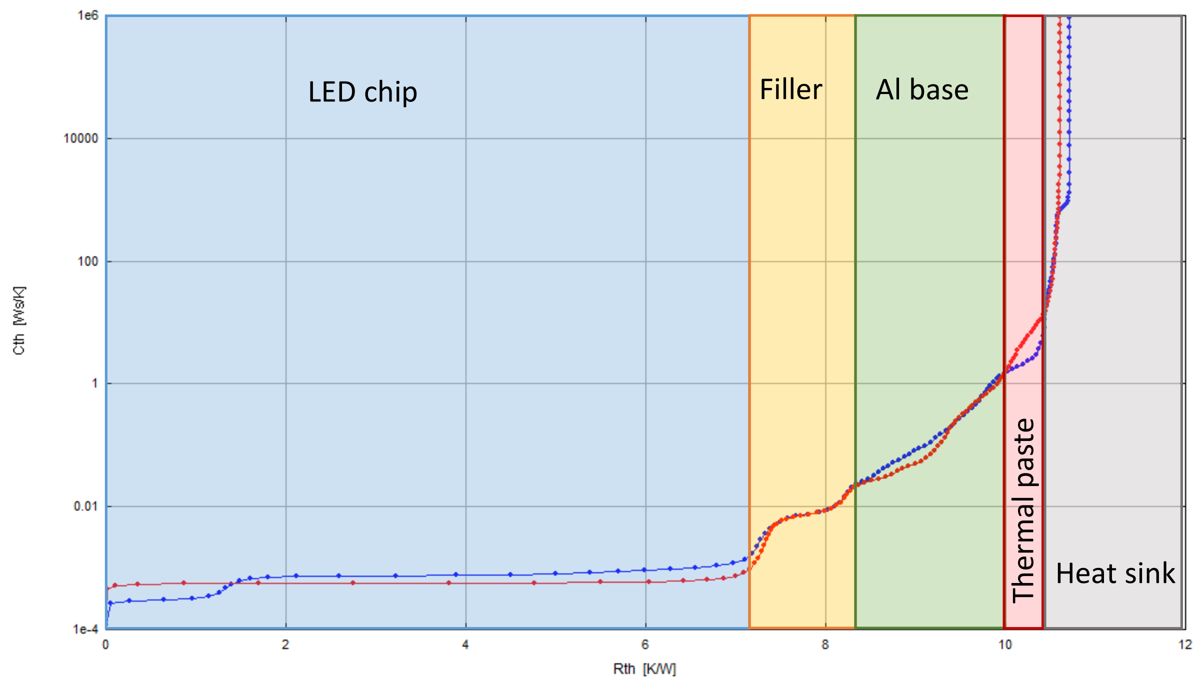

Figure 77: Measured (blue) and simulated (red) cumulative structure function with its correspondance to physical objects

The small differences between simulation and measurement can have different reasons. One reason can be that the thermal conductivity and heat capacity are temperature dependent. Another reason can be that some parameters are strongly correlated, e.g. the boundary conditions of the simulations can differ from those of the real measurement, or the thermal paste has not dispersed perfectly on the Al base. Further small details in the model, like the reflector layers, cause abrupt changes in the heat flow but cannot be seen in the structure function. However, the essential heat flow path is reflected by the structure function.

7 Summary

This thesis represents the basic idea of the structure function. The heat flow path of a device can presented by the structure function. That's the reason why the structure function is an important tool of the thermal management of an LED. It offers the possibility of locating either material transitions or changes of the cross sectional area of the material in the heat flow path.

The structure function can be calculated through the thermal transient, which is the time-dependent temperature change after a power change. The thermal transient can be obtained from both experiment and simulation. The measurement requires an accurate equipment which is able to sample data points right after the power step to get all structure-caused temperature changes. The recorded thermal transient includes the electrical transient which has no information about the heat flow path in LED. Therefore, it has to be corrected. The correction of the electrical transient is a $\sqrt{t}$-based substitution which comes from the assumption of the temperature change of an infinite large and uniform material's surface.

It is important that the recorded thermal transient is as free from noise as possible due to the sensitivity of the mathematical transformation into the structure function. A compensation of the noise can also be achieved by performing 100 measurements of the thermal transient and averaging them. The averaged curve has an improved signal to noise ratio, hence the further processing is done with a less noisy signal. The construction of the structure function for all measured curves can also provide an estimation of standard deviation of the further calculation.

The calculation of the structure function starting from the transient is implemented in SCILAB to get a deeper understanding. The transformation of the thermal transient is based on the simplification that a heat flow path can be represented as a thermal circuit. There are some calculation steps necessary to obtain the thermal network corresponding to physical reality. The calculation steps are very sensitive. For example, the derivative and the deconvolution steps enhance the noise. In addition, the transformation into a physical thermal network requires high precision. Otherwise numerical oscillations dominate the result and it becomes useless.

The "structure function algorithm" which is written in SCILAB is now ready to be used. It can be implemented on the Red Pitaya. Hence, the algorithm can be used externally to investigate reliability issues of LEDs. The Red Pitaya offers a measurement setup which is smaller and more compact than the T3ster setup. Furthermore, the Red Pitaya does not demand a laboratory environment.

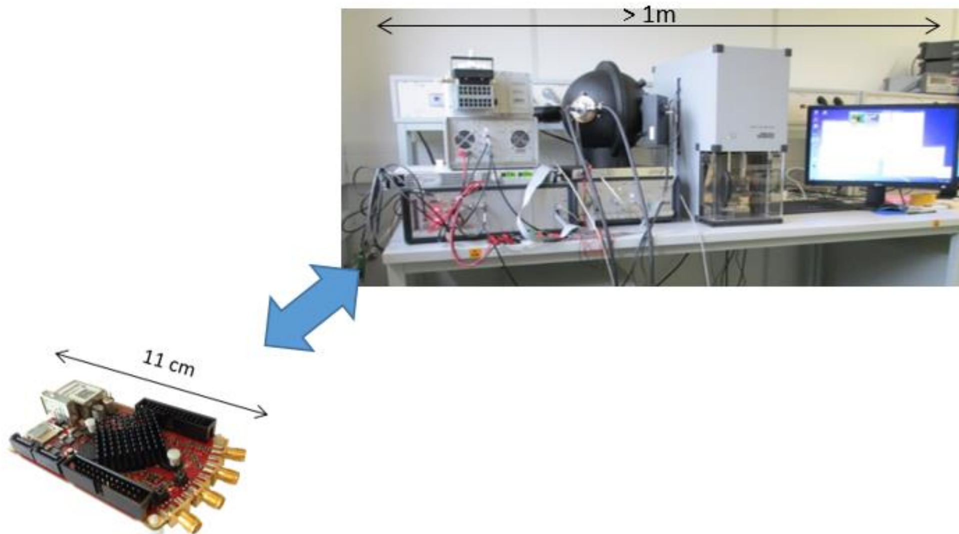

Figure 78: Red Pitaya versus T3ster

The thermal transient can also be received by a simulation. In this thesis, a CFD-simulation is used. There geometrical data and material properties are the required input data. The created LED model offers the possibility to generate a calibrated model with the help of a developed "validation flow". The "validation flow" contains comparison studies between measurement and simulations which allows correlating features of the structure function to real physical objects. The simulation of the thermal transient has the further advantages that it is noisefree. In the scope of this master thesis, the investigation of the LED module (described in chapter 4 to 6) focuses on one special type of an LED. The simulated values of each material (thermal conductivity, density, and specific heat) of the LED model present one of many solutions. Due to that, a generalization of these material values for other LED designs would be deceptive.

In addition, no substitution of the electrical transient is needed which causes mathematical artifacts. Therefore, the early section of the measured thermal transient can not only be corrected by extrapolation but also by replacing it with the initial part of the simulation. This new type of correction leads to no misinterpretation any longer.

The "validation flow" offers a good option to get a better understanding of the features of the structure function. Furthermore, the validated structure function gives a deeper insight into the heat flow path of the inner structure of an LED.

8 References

[1] J. Li, J. Wang, Z. Liu, and A. Poppe, “Solid-State Physics Fundamentals of LED thermal Behavior,” in *Thermal Management for LED Applications*, vol. 2, Springer, 2014, p. 551.

[2] M.-H. Chang, D. Das, P. V. Varde, and M. Pecht, “Light emitting diodes reliability review,” *Microelectron. Reliab.*, vol. 52, no. 5, pp. 762–782, May 2012.

[3] Opto Osram Semiconductors (Ed.), “Reliability and Lifetime of LEDs Application Note,” pp. 1–14, 2013.

[4] V. Székely, “Identification of RC networks by deconvolution: chances and limits,” *Circuits Syst. I Fundam. Theory …*, vol. 45, no. 3, pp. 244–258, 1998.

[5] M. Carmona, S. Marco, J. Palac, and J. Samitier, “A Time-Domain Method for the Analysis of Thermal Impedance Response Preserving the Convolution Form,” *Components Packag. Technol. IEEE Trans.*, vol. 22, no. 2, pp. 238–244, 1999.

[6] M. Sen, “Analytical Heat Transfer,” *Book*, p. 231, 2008.

[7] A. Vass-Varnai, V. Szekely, Z. Sarkany, and M. Rencz, “New level of accuracy in TIM measurements,” in *Semiconductor Thermal Measurement and Management Symposium (SEMI-THERM), 2011 27th Annual IEEE*, 2011, pp. 317–324.

[8] P. Szabó and V. Székely, “Investigation of parallel heat flow path in electro-thermal microsystems,” *Microsyst. Technol.*, 2011.

[9] V. Székely, M. Rencz, and V. Szekely, “Thermal dynamics and the time constant domain,” *Components Packag. Technol. IEEE Trans.*, vol. 23, no. 3, pp. 587–594, 2000.

[10] P. Szabó, M. Renez, and V. Szekely, “Thermal modelling of multiple die packages,” *… , 2005. EPTC 2005. …*, 2005.

[11] V. Székely, S. Török, É. Nikodemusz, G. Farkas, and M. Rencz, “Measurement and evaluation of thermal transients,” in *Instrumentation and Measurement Technology Conference, 2001. IMTC 2001. Proceedings of the 18th IEEE*, 2001, pp. 210–215.

[12] V. Székely, M. Rencz, A. Poppe, and B. Courtois, “THERMODEL: A tool for thermal model generation, and application for MEMS,” *Analog Integr. Circuits …*, no. 1, pp. 49–59, 2001.

[13] M. Rencz, A. Poppe, and E. Kollar, “Increasing the accuracy of structure function based evaluation of thermal transient measurements,” *… , 2004. ITHERM’04. …*, pp. 85–90, 2004.

[14] *Transient Dual Interface Test Method for the Measurement of the Thermal Resistance Junction to Case of Semiconductor Devices with Heat Flow Trough a Single Path, JEDEC Standard, JESD 51-1 14*, no. November. 2010.

[15] *Integrated Circuits Thermal Measurement Method - Electrical Test Method (Single Semiconductor Device), JEDEC Standard, JESD 51-1 1*. 1995.

[16] V. Székely, “A new evaluation method of thermal transient measurement results,” *Microelectronics J.*, vol. 28, pp. 277–292, 1997.

[17] JULABO GmbH (Ed.), “http://www.julabo.com/de/produkte/kaeltethermostate/kaelte-umwaelzthermostate/f25-me-kaelte-umwaelzthermostat,” *(1.6.2015)*. .

[18] Mentor Graphics Corporation (Ed.), *POWER BOOSTER UNITS for T3Ster*. 2009, p. 1.

[19] Mentor Graphics Corporation (Ed.), *T3Ster Thermal Transient Tester*. 2009.

[20] K. Han, M. Liu, S. Fan, and H. Shen, “Improved electrical measurement method for junction temperature of light emitting diodes,” *Przegląd Elektrotechniczny*, no. 3, pp. 180–184, 2012.

[21] D. B. ; S. H. S. Utermohlen, F. ; Herrmann, I. ; Etter, “Temperature sensitivity modeling of pn-junction diodes for microbolometer-based thermal imaging applications,” in *Semiconductor Conference Dresden-Grenoble (ISCDG), 2013 International*, 2013, pp. 1–4.

[22] M. Mansoor, I. Haneef, and S. Akhtar, “Silicon diode temperature sensors–A review of applications,” *Sensors Actuators A …*, vol. 232, pp. 63–74, 2015.

[23] B. Siegl, “An introduction to Diode Thermal Measurements,” *Therm. Eng. Assoc. Inc., St. Clara, CA. USA*, 2009.

[24] M. Glavanovics and H. Zitta, “Thermal Destruction Testing : an Indirect Approach to a Simple Dynamic Thermal Model of Smart Power Switches,” vol. 2, pp. 2–5.

[25] R. Bornoff, “Using T3Ster Measurements to Calibrate Simulation Models.” .

[26] Red Pitaya Team, “http://wiki.redpitaya.com/index.php?title=User_Manual.” .

[27] V. Székely and A. Szalai, “Measurement of the time-constant spectrum: Systematic errors, correction,” *Microelectronics J.*, vol. 43, no. 11, pp. 904–907, 2012.

[28] T. J. Kennett, A. Robertson, and W. V Prestwich, “Bayesian Deconvolution I: Convergent Properties,” *Nucl. Instruments Methods*, vol. 151, no. 1, pp. 285–292, 1978.

[29] W. Richardson, “Bayesian-based iterative method of image restoration,” *JOSA*, vol. 62, no. I, 1972.

[30] N. Dey, L. Blanc-f, C. Zimmer, P. Roux, Z. Kam, and J. Zerubia, “3D Microscopy Deconvolution using Richardson-Lucy Algorithm with Total Variation Regularization To cite

this version : 3D Microscopy Deconvolution using Richardson-Lucy Algorithm with Total Variation Regularization," 2006.

[31] M. S. Freixes, "Thermal Modeling of Microsystems and Electronic Components: Model Order Reduction," Universitat de Barcelona, 2007.

[32] Y. C. Gerstenmaier, W. Kiffe, and G. Wachutka, "Combination of thermal subsystems modeled by rapid circuit transformation," *Therm. Investig. …*, no. September, pp. 17–19, 2007.

[33] Mentor Graphics Corporation (Ed.), "FloTHERM ® User Guide," 2012.

[34] Mentor Graphics, "http://s3-blogs.mentor.com/robinbornoff/files/2014/09/FloTHERM-10-splashscreen.png," *(12.7.2015)*. .

[35] Mentor Graphics Corporation (Ed.), "FloTHERM ® Background Theory," 2012.

[36] C. Mion, "Investigation of the Thermal Properties of Gallium Nitride Using the Three Omega Technique," North Carolina State University, 2005.

[37] Valley Design (Ed.), "http://www.valleydesign.com/sappprop.htm," *(1.7.2015)*. .

[38] A. Vass-Varnai and Z. Sarkany, "Simulation based method to eliminate the effect of electrical transients from thermal transient measurements," in *Electronics Packaging (…*, 2014, pp. 591–595.

9 Table of Figures

Figure 1: The electric energy (P_{el}) in a light emitting diode, which is a function of the induced current (I_f) and voltage (U_f), becomes rather heat (P_{diss}) than light (P_{opt}) 2

Figure 2: Schematic drawing of thermal resistance 5

Figure 3: Graphical representation of Fourier's law 7

Figure 4: Analogy between thermal and electrical resistance 8

Figure 5: Thermal model of a homogenous rod a length of L, a thermal conductivity of λ and a specific heat of c_v and its one-dimensional thermal equivalent 9

Figure 6: The RC model of the heat flow path of a sliced ideal rod 10

Figure 7: The cooling transient of an LED 11

Figure 8: Cumulative and differential structure function of a homogenous rod 12

Figure 9: RC model of a non-ideal rod which consists of two types of RC pairs 13

Figure 10: Cumulative and differential structure function of a two materials rod 13

Figure 11: Schematic presentation of the structure function 14

Figure 12: Diagram of the measurement setup of the DUT – device under test 16

Figure 13: Actual test setup – LED on a liquid cooled cold plate 17

Figure 14: Illustration of the heat flow resulting from the junction of an LED 17

Figure 15: Refrigerated and heating circulator – for the cold plate [17] 18

Figure 16: T3ster Booster – power switching unit [18] 18

Figure 17: Measurement scheme of the thermal characterization of an LED, which is the device under test (DUT) 19

Figure 18: T3ster – measurement unit [19] 19

Figure 19: Diode characteristic (representation of the diode conduction equation) for different temperatures 20

Figure 20: The nearly linear dependency between voltage and temperature, where V_g = 3.47 V, IF = 0.01 A, r = 2 and C = 0,084 A/K^{-2} like in GaN 22

Figure 21: Calibration curve of one LED with two different I_m (10 mA and 20 mA) – almost no deviations of the linear fit delivering the K-Factors 23

Figure 22: Thermal transient shown in the diode characteristic 24

Figure 23: Applying driving (I_{drive}) and measurement current on a diode – reaching a hot steady state level & applying only measurement current – reaching a cool steady state level 25

Figure 24: Recorded transient – starting from the measured increasing voltage (left) to the calculated temperature drop (right) 26

Figure 25: Power change at the cooling measurement on an LED 26
Figure 26: Electrical transient shown in the diode characteristic 27
Figure 27: Recorded transient of an LED module (voltage change) and calculated temperature change with extrapolation 29
Figure 28: Measured thermal transient 30
Figure 29: Summary of the calculation steps of the structure function 31
Figure 30: Thermal impedance curve – linear time scale 32
Figure 31: Thermal impedance curve – logarithmic time scale 33
Figure 32: The simplest thermal model: a parallel resistance and capacitance and its discrete time constant representation 34
Figure 33: Schematic drawing of a black box model.. 35
Figure 34: Distributed infinite RC systems represented as the time constant spectrum 36
Figure 35: The derivative of a(z) 37
Figure 36: Shape of the weighting function wzz 38
Figure 37: The derivative of the unprocessed signal and its time constant spectrum 39
Figure 38: Comparing the time constant spectrum of a noisy and smooth derivative of thermal impedance 39
Figure 39: Time constant spectrum – calculated with the Fourier-domain inverse filtering .. 41
Figure 40: Time constant spectrum – calculated with the Bayes iteration 43
Figure 41: Drawing of the time constant spectrum and its relationship with a thermal RC circuit 44
Figure 42: Worst-case error of the direct discretization dependent on the distances of the lines (in the case where R(z) is constant)[4] 45
Figure 43: Drawing of a Foster network and their RC values 46
Figure 44: Basic element in the Cauer network 47
Figure 45: Chain of RC ports in the Foster Network 48
Figure 46: Profile of the structure function calculation 49
Figure 47: Cumulative structure function (CSF) 53
Figure 48: Cumulative and differential structure function calculated with double precision. 55
Figure 49: Cumulative and differential structure function calculated with quad-precision ... 55
Figure 50: Cumulative structure function with different number of time constants – regarding 101 RCs as best solution 56

Figure 51: Differential structure function with different numbers of time constants- referring 101 RCs as best compromise 57

Figure 52: Cumulative structure function with different measurement rates 58

Figure 53: Differential structure function with different measurement rates 58

Figure 54: Splashscreen of FloTHERM® [34] 60

Figure 55: Schematic of finite volume method – Determination of the middle-cube's temperature (T) and the influence of its neighbors........ 61

Figure 56: Picture of the investigated one chip - LED module, which has an outer measurement of 13 mm x 13mm and a filler´s diameter of 9 mm 62

Figure 57: LED cross section investigation at the place of the LED chip via light microscope. 63

Figure 58: LED cross section investigation with SEM concentrating on the region of the LED chip 64

Figure 59: Investigation of the left part of the dam at the cross section 65

Figure 60: Schematic buildup of the investigated LED........ 66

Figure 61: Appearance of the simulated LED 67

Figure 62: Hot steady state of LED model -the active layer has a power of 307mW (lower picture: top view; upperpicture: side view) 69

Figure 63: Schematic representation of the validation flow........ 70

Figure 64: Thermal transient (upper picture), CSF (left lower picture) and DSF (right lower picture) of measured one Chip-LED-module........ 71

Figure 65: Structure functions of measurement – one with thermal paste, other without thermal paste 72

Figure 66: Cumulative (left) and differential (right) structure function of the simulated thermal transient (upper picture)........ 73

Figure 67: Comparison of the differential structure function of experiment and simulation – assure the correct number of objects in the model 74

Figure 68: Correlation of the active layer; starting the iteration from a to b to c 75

Figure 69: Modification of the die substrate – simulations have different thermal conductivities 75

Figure 70: Modification of the die attach glue – different thermal conductivities 76

Figure 71: Filler calibration – the lines have different specific heat values, line b shows the best fit to the experiment 77

Figure 72: Influence of the filler's thermal conductivity........ 77

Figure 73: First iterative adjustment of the structure function 78

Figure 74: Correlation of the simulated (red) to the measured (blue) structure function with the help of modification of the properties of the Al base 79

Figure 75: Replacement of the early sections of the measured thermal transient................. 80

Figure 76: Cumulative structure function of the simulation and the experiment with two different electrical transient corrections 81

Figure 77: Measured (blue) and simulated (red) cumulative structure function with its correspondance to physical objects.. 82

Figure 78: Red Pitaya versus T3ster 84

10 List of tables

Table 1: Failure sites, causes, effects, modes and mechanisms of LEDs [2] 4

Table 2: Thermal- electrical analogy 7

Table 3: Values of the worst case error as a function of the distance between the poles 45

Table 4: Measured dimensions of the investigated cross section of the LED module (all the measurements have a relative error of 5% which comes from the inaccuracy of measuring) 65

Table 5: Material properties (density, specific heat and thermal conductivity) of each region in the chosen LED 67